An Investigation into Manganese(2+) Interferences and Retrospective Dose Assessment of Shelled Species using EPR Spectroscopy

by

Eden Gough

A Thesis Submitted in Partial Fulfillment of
the Requirements for the Degree of

Master of Applied Science
in
Nuclear Engineering

The Faculty of Engineering and Applied Science

University of Ontario Institute of Technology
(Ontario Tech University)

Oshawa, Ontario, Canada

May 2023

An Investigation into Manganese(2+) Interferences and Retrospective Dose Assessment of Shelled Species using EPR Spectroscopy

Submitted by Eden Gough

An oral defense of this thesis took place on May 10, 2023 in front of the following examining committee:

Examining Committee

Chair of Examining Committee	Dr. Igor Pioro
Research Supervisor	Dr. Edward Waller
Examining Committee Member	Dr. Kirk Atkinson
Thesis examiner	Dr. Robert Bailey, Faculty of Science

The above committee determined that the thesis is acceptable in form and content and that a satisfactory knowledge of the field covered by the thesis was demonstrated by the candidate during an oral examination. A signed copy of the Certificate of Approval is available from the School of Graduate and Postdoctoral Studies.

Abstract

High intensity Mn^{2+} peaks in calcified tissues of shells are known to impact the lower dose detection limit in retrospective electron paramagnetic resonance (EPR) studies. This thesis investigates the factors causing Mn^{2+} accumulation in shells including crystalline structure and animal habitat. Inductively coupled plasma - optical emission spectroscopy (ICP-OES) was used to determine the Mn^{2+} concentrations in shells of thirteen species. A methodology to quantitatively compare Mn^{2+} concentrations with Mn^{2+} EPR peak intensity in calcified shells was developed as a potential indicator tool for selecting shelled species for EPR dosimetry. This comparison found that shells of zebra mussels, grove snails, and heath snails were best suited as environmental dosimeters due to their low Mn^{2+} concentrations and Mn^{2+} EPR peaks. Dose-response curves for grove and heath snails were developed by irradiating shells to 2, 3, 5, 7, and 10 Gy. Both species had minimum detectable doses of 2 Gy.

Keywords: calcified shells, Mn^{2+}, EPR dosimetry, ICP-OES

Declaration of Authorship

- I hereby declare that this thesis consists of original work of which I have authored. This is a true copy of the thesis, including any required final revisions, as accepted by my examiners.
- I authorize the University of Ontario Institute of Technology to lend this thesis to other institutions or individuals for the purpose of scholarly research. I further authorize University of Ontario Institute of Technology to reproduce this thesis by photocopying or by other means, in total or in part, at the request of other institutions or individuals for the purpose of scholarly research. I understand that my thesis will be made electronically available to the public.

Signed: Eden Gough

Date: May 29, 2023

Statement of Contributions

Contributing individuals to the work in this thesis:

- Amna Hassan, Ontario Tech University, for providing the background and framework for many of the experiments in this thesis work.
- Dr. Margarita Tzivaki, Ontario Tech University, for providing information and troubleshooting relating to the EPR spectrometer.

Acknowledgements

I would first like to extend my most sincere gratitude to my supervisor Dr. Ed Waller for his invaluable guidance, and continuous support and encouragement (and healthy helping of memes) throughout my master's program.

I am also endlessly grateful to Amna Hassan, Marta Kocemba, and Margarita Tzivaki for being sounding boards throughout my research process, for providing multitudes of information and encouragement (and comic relief), and for keeping me on track when I needed it most.

Lastly, thank you to my family, friends, and fiancé for their kindness, love, encouragement, and for keeping me fed and watered.

The research work presented in this thesis has been funded by the Natural Sciences and Engineering Research Council of Canada (NSERC) and the University Network of Excellence in Nuclear Engineering (UNENE).

Contents

List of Figures

List of Tables

Chapter 1

Introduction

1.1 Background and Motivation

There is mounting global interest in nuclear processes, and with this interest comes a responsibility to investigate the effects of ionizing radiation and protect the environment from any negative impacts. The International Commission on Radiological Protection (ICRP), International Atomic Energy Agency (IAEA) and the Canadian Nuclear Safety Commission (CNSC) have all highlighted the necessity of protecting the environment from radiation exposure [1] [2] [3]. Also, in 2022, the IAEA announced that it was launching a research project intending to improve the current system of assessing the radiological impact on terrestrial biota [4]. This drive to understand and assess the environmental impacts of radiation to non-human biota is the motivation behind this thesis work.

The United Nations (UN), in its 17 Sustainable Development Goals (SDGs), has highlighted the need to protect life below water (Goal 14) and life on land (Goal 15) [5]. The IAEA realizes the important role that nuclear science and technology can play in achieving these goals - isotopes can be used to monitor and track ocean acidification and contamination as well as soil contamination. The protection of the environment from radiation contamination during a radiological accident for example, is another concern for the IAEA. An essential aspect of environmental protection after an accident is determining how much dose was received in the affected area, which will be further elaborated on in this chapter.

1.1.1 Environmental Exposure to Radiation and Retrospective Dosimetry

Environmental radiation exposure can occur through many pathways, including nuclear power and isotope generation, radioactive waste transportation and disposal, nuclear accidents and nuclear weapons testing [6]. The scale of the impact that a radiological release has on the environment depends on the amount and type of radionuclides deposited in the environment [6]. In the event of an unplanned radiological release into the environment, prompt dose assessments are required for the surrounding natural environment. Knowing the dose to the environment after an accident can inform the response and remediation measures that are taken in the aftermath of the exposure.

It is not guaranteed that synthetic dosimeters will be in place at the time of a release [7]. As such, a retrospective dose assessment must be completed using samples from the environment where the release occurred. This process is called retrospective dosimetry. Materials such as bricks, quartz, porcelain, cotton and phone screens have been studied extensively and used for retrospective dosimetry [8]. There has also been an emphasis on using aquatic and terrestrial species as retrospective dosimeters [9] [10]. The samples selected for dose assessments must possess the property of being able to preserve information about the release between the time of exposure and when the sample is measured.

Throughout history, there have been incidents where large amounts of radiation have been released into the environment, such as the Chernobyl and Fukushima nuclear disasters. A radiological release will lead to an accumulation of radionuclides in the soil, sediment, and water in which organisms inhabit [11]. When an accident occurs, many radionuclides are potentially released into the environment. Two radionuclides, cesium-137 and strontium-90, are of particular concern to the environment after a release due to their long-half lives and ability to accumulate in the soil, sediment, and water for many years [11]. Cesium-137 follows similar absorption pathways as potassium in organic material, and strontium accumulates in bones [12] [13]. Retrospective dose studies were also performed after these accidents to determine the dose to the environment. For example, after the Chernobyl nuclear accident, the needles of pine trees in forests near the accident were used for retrospective dosimetry, and the absorbed gamma dose was calculated as 80-100 Gy [14].

There is also a particular interest in resolving doses using natural dosimeters in the 'low-dose' range, generally defined as $<$100 mGy. This range is relevant in dosimetry, as there is evidence that doses in the low-dose range can have severe adverse health impacts on humans. So as not to confuse the definition, in this work, doses that are still relatively

low (2-10Gy) but not <100 mGy will be referred to as being in the 'lower-dose' range.

1.2 Retrospective Dosimetry and Elemental Analysis on Shelled Species

When selecting objects or species from the natural environment to use after a radiological release, the calcified tissues of shelled species have been suggested [10] [15]. It is believed that, using the appropriate dosimetry techniques, the cumulative radiation dose to an environment can be detected by collecting and analyzing aquatic and terrestrial shelled animals near a radiological release [16]. This is due to the solid crystalline structure, composed primarily of calcium carbonate ($CaCO_3$), that makes up the shell. Many materials with crystalline structures can act as fortuitous dosimeters as the free electrons formed after exposure to ionizing radiation become trapped in their crystal lattice [17]. For this reason, materials such as bricks, quartz, porcelain, and tooth enamel have also been used as fortuitous dosimeters due to their crystalline structure [8]. In some crystalline materials, the amount of free electrons formed is proportional to the radiation dose they were exposed to. The shells of molluscs and crustacea have proven to be effective materials for dosimetry [10]. An appropriate retrospective dosimetry technique must be used to identify the free radicals formed in a crystalline structure after irradiation. Electron paramagnetic resonance (EPR) spectroscopy is a technique frequently used to detect free radicals, and its applicability will be explored further in this thesis.

The shelled species investigated in this work are mainly molluscs and crustacea. The most common application of shelled species in research is currently related to their use as biomonitors and indicators of metal pollution in the environment. Various species of crustacea, bivalves, and gastropods have been studied for these purposes. Bivalves and gastropods inhabit the soil and sediments where radionuclides and heavy metals accumulate [18] [19] [20]. One metal that accumulates in shelled species that is of particular interest to this work is manganese. Manganese, in its +2 oxidation state, is incorporated into calcified shells. When studying shells using EPR, interferences caused by Mn^{2+} can inhibit the detection of low radiation doses [21] [10]. As such, this report investigates the Mn^{2+} concentrations in fourteen shelled species from terrestrial, marine, and aquatic environments and the various factors that can affect Mn^{2+} accumulation into shells. Elemental analysis techniques suitable for detecting Mn^{2+} are also explored in this work.

1.3 Research Objectives and Statement of Work

This work aims to investigate the manganese(2+) effects on shelled species from a retrospective dosimetry perspective. A review of the species' environmental factors and shell compositions that cause elevated Mn^{2+} contents will be conducted to describe which species, in general, may be more suitable for retrospective dosimetry. As EPR is highly species-dependent, it is beneficial to have an idea of which types of species may be most beneficial to use in retrospective EPR analyses. Following this, the correlation between manganese(2+) concentrations in the calcified tissues of shelled species and its effect on EPR spectra will be determined. To confirm the results of this comparative study, an investigation into the dose-response of species showing good dosimetric potential will be irradiated, and their dose-response will be quantified. The results of this experiment could help provide a basis for determining which samples are good dosimeters. This work, in particular, is focused on the potential use of calcified tissues of molluscan, crustacean, and reptilian species as retrospective dosimeters. The applicability of EPR as a dosimetry technique and ICP-OES as an elemental analysis technique will also be discussed.

This thesis work was in part a continuation of experimental work conducted by A. Hassan [21]. Experiments conducted based off this work include improving the inductively coupled plasma-optical emission spectroscopy (ICP-OES) methodology and creating a refined grove snail (*Cepaea nemoralis*) dose-response curve.

The objectives of this work can be summarized as follows:

1. Selecting various shelled species to use for ICP-OES and EPR analysis, and identifying the limitations posed by Mn^{2+} presence in samples with respect to low-dose EPR spectroscopy measurements.
2. Identifying factors that affect Mn^{2+} abundance in calcified tissues of shelled species.
3. Developing sample preparation and analysis methods for ICP-OES and EPR experiments. This includes selecting appropriate EPR measurement parameters.
4. Determining the correlation between manganese(2+) concentrations and EPR peak intensities in shell samples and establishing a linear dose-response relationship at lower doses (2 Gy to 10 Gy) in species identified as having low Mn^{2+} concentrations and low Mn^{2+} EPR peak intensities.
5. Performing a novel investigation into the potential dose-response of turtle shells at low doses (2 Gy to 19 Gy).

Chapter 2

Theoretical Background and Literature Review

Pertaining to the use of electron paramagnetic resonance (EPR) spectroscopy as a retrospective dosimetry technique using shelled species, and the effects that manganese(2+) (Mn^{2+}) can have on EPR spectra, this literature review will consider previous work relevant to these topics. The literature explored for the following chapter has been grouped into four topics:

1. A review of the fundamental principles of EPR spectroscopy, which provides the basis for its applicability as a retrospective dose assessment tool within this work. Additional retrospective dosimetry techniques will be reviewed and compared against EPR with reference to dose detection limits and applicability.

2. A review of Mn^{2+} in the context of shelled species and the environment, its incorporation into the crystalline structure of shells, and its effect on dose detection in EPR spectra.

3. A review of the applicability of shelled species using EPR dosimetry in the context of their shell structure and Mn^{2+} concentrations, including a review of the different animal groups whose shells will be analyzed in this work. Shelled species' habitats, shell structure, and other contributing factors to Mn^{2+} concentrations will be reviewed, as well as dose detection limits in said species using EPR. The effects of ionizing radiation on shelled species and their suitability as fortuitous dosimeters will also be discussed.

4. A review of the fundamental principles of inductively coupled plasma-optical emission spectroscopy (ICP-OES) as an elemental analysis technique. Various other

elemental analysis techniques will be reviewed, and detection limits will be compared.

2.1 Fundamentals of Electron Paramagnetic Resonance

Electron paramagnetic resonance (EPR) spectroscopy is a method used to analyze materials with unpaired electrons, also called paramagnetic materials. This technique refers to the absorption of electromagnetic radiation by a paramagnetic sample within an applied magnetic field, causing the unpaired electrons to transition from a lower to a higher energy state [17].

The unpaired electrons in paramagnetic materials belong to one of two spin states (m_s), α ($m_s = +\frac{1}{2}$) and β ($m_s = -\frac{1}{2}$), when there is no applied magnetic field [17]. When an external magnetic field, B_0, is applied, the energy states of the electrons will separate proportionally to the strength of the magnetic field. This is known as the Zeeman effect and is seen in Figure 2.1. In the presence of the magnetic field, the lower energy state (β) is more energetically favoured than the higher energy state (α) [17]. In EPR, electromagnetic radiation energy in the form of microwave energy is also applied. Electrons in the lower energy state can absorb the microwave energy and transition to the higher energy state when the applied electromagnetic energy is equal to the applied magnetic field. This condition is known as resonance (Equation 2.1):

$$h\nu = g\mu_B B_0 \tag{2.1}$$

Where:
h: Planck's constant, $6.62607015 \times 10^{-34}$ J/Hz
ν: frequency of the electromagnetic radiation [Hz]
g: g-value or spectroscopic splitting factor
μ_B: Bohr magneton, 9.274×10^{-24} J/T
B_0 : applied magnetic field [T]

At resonance condition, the electrons undergo spin-flip transitions, and the number of unpaired spins in the paramagnetic material is proportional to the intensity of these transitions [22]. The applied magnetic field oscillates while the electromagnetic radiation field is kept constant, which causes the absorption of energy and spin-flip transition between energy states. The resultant EPR spectrum is the first derivative of the absorption curve with respect to the magnetic field. The absorption spectra, an example of which

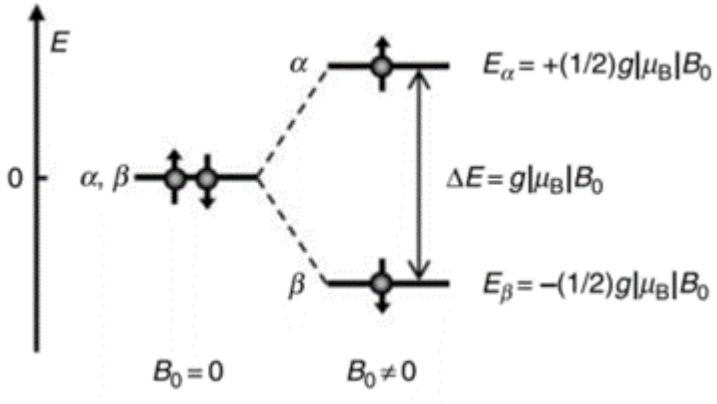

FIGURE 2.1: The Zeeman effect, the splitting of electrons between two energy states in the presence of a magnetic field, B_0. [17]

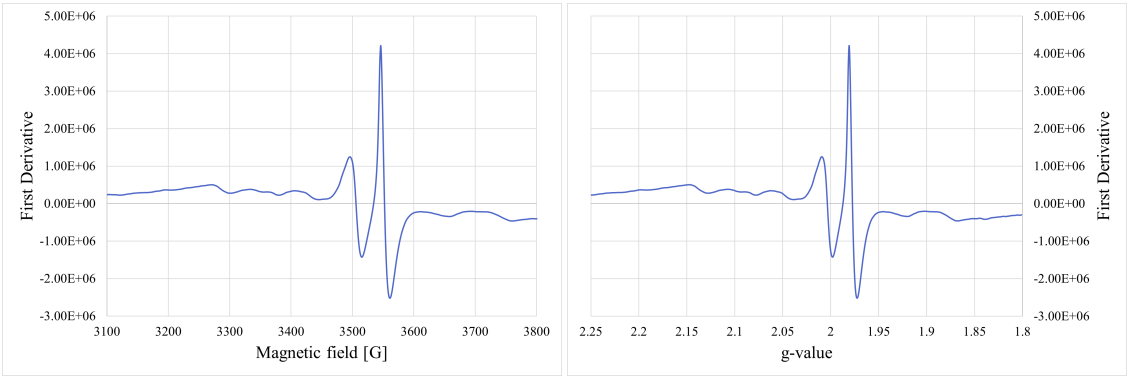

(A) (B)

FIGURE 2.2: Example EPR absorption spectrum showing the first derivative of the absorption in relation to (A) the magnetic field [G] and (B) the g-factor.

can be seen in Figure 2.2, are characterized by their shape, width, intensity, and g-factors [17].

The g-factor, known as the spectroscopic splitting factor, is characteristic of every sample [23]. EPR spectra can also be presented with respect to the g-value or the magnetic field value 2.2. The g-values shown in the EPR spectra provide insight into a sample's electronic structure and provide a valuable means of identifying and quantifying the short-lived radicals in a reaction [24]. For instance, it can aid in identifying a specific metal ion, its oxidation and spin states, and its coordination environment [23]. The g-factor of a sample determines the magnetic field position where an EPR spin-flip transition will

occur at a given microwave frequency. Most organic radicals have a g-value of about 2 [17], and metal ions have ranging g-values [24].

The free electrons, otherwise known as free radicals, required for EPR studies can be found in various samples. A free radical is a type of paramagnetic center, a lattice defect characterized by an unpaired electron trapped in the crystalline structure of the materials that causes a permanent magnetic dipole with a random orientation [17]. Types of paramagnetic centers include organic free radicals, paramagnetic transition metal complexes (such as $MnCO_3$), triplet species, defect centers in solids, and radiation-induced radicals [17]. EPR spectroscopy is typically used to determine the radiation dose to a sample by detecting the radiation-induced paramagnetic centers, since the number of centers formed can be proportional to the absorbed radiation dose [25]. The dose can be assessed with relation to the peak-to-peak amplitude of the first derivative of the absorption spectra [25]. The following subsection will go into further detail about using EPR spectroscopy as a dosimetry technique.

2.1.1 Electron Paramagnetic Resonance Spectroscopy as a Retrospective Dosimetry Technique

As discussed in Chapter 1, retrospective dosimetry is a tool used following an accidental exposure to ionizing radiation when conventional dosimeters are unavailable to assess and reconstruct the radiation dose to an affected area or object [26]. This technique can involve using man-made objects, biological, and biogenic samples from the affected area as natural dosimeters. A material's qualifying property for retrospective dosimetry using EPR is that it must form stable, long-lived free radicals in quantities proportional to the absorbed dose when exposed to ionizing radiation [10]. Other typical applications of EPR dosimetry include the identification of irradiated foodstuffs and archaeological dating [22]. The absorbed radiation dose is measured in a unit called the gray (Gy), and 1 Gy is equivalent to 1 joule of energy deposited in 1 kilogram of material.

Many materials with crystalline structures, both naturally occurring (tooth enamel and quartz) or man-made (bricks and porcelain), can act as fortuitous dosimeters as they form stable, long-lived, dose-dependent quantities of free radicals when exposed to ionizing radiation [8]. Ionizing radiation is a type of radiation with sufficient energy to remove electrons from atoms which they pass through. Ionizing radiation comes in the form of alpha particles (α), which are positively charged particles composed of two protons and two neutrons; beta particles (β-) and positrons (β+), which are negatively and positively charged electrons; and gamma rays (γ) and X-rays, which are massless,

uncharged photons. When crystalline materials are exposed to ionizing radiation, the free electrons are captured in the material's crystal lattice and can remain there for several years [27].

Radiation-induced free radicals are molecules with unpaired electrons, formed when certain crystalline materials such as hydroxyapatite [$Ca_{10}(PO_4)_6(OH)_2$] found in bones and teeth, calcium carbonate [$CaCO_3$] in shelled species, and the amino acid alanine [$CH_3{-}CH(NH_2){-}COOH$] are exposed to ionizing radiation [28]. Calcified tissues, such as those found in shells, bones, and tooth enamel, are particularly effective environmental and biodosimetric materials due to the radiation-induced radicals formed in the hydroxyapatite and calcium carbonate structures [22]. The approach to using calcified tissues in retrospective EPR dosimetry is based on the dose-dependent formation of carbonate radical centers that can be evaluated using EPR. The lowest detectable dose in the calcified tissues of shells was identified as 0.2 Gy [10] [29]. The free radicals formed in irradiated carbonates can remain stable for thousands of years at stable temperatures [30].

The most common applications of EPR dosimetry are in tooth enamel and alanine [31] [32]. The free radical formed is primarily CO_2^- in irradiated tooth enamel [33] and $(CH_3)CHCO_2^-$ in irradiated alanine [34]. Alanine has proven to be a very effective dosimeter due to its low dose detection limit, and the formation of long-lived stable free radicals when irradiated [35]. It is frequently used as a reference dosimeter in irradiation experiments. Alanine reference dosimetry will be carried out in experiments in this work, which will be discussed further in Section 3.4.2. Dosimetry in tooth enamel has been performed primarily for dose reconstruction in the teeth of people who have been exposed to ionizing radiation, including atomic bomb survivors and Chernobyl cleanup workers [31]. EPR studies of tooth enamel have shown a detectable dose dependence from 30 mGy to above 100 kGy [22] [36] [37].

Most common EPR experiments for dosimetry purposes use X-band microwaves between 9.0-9.6 GHz as the applied electromagnetic radiation [38]. Using higher frequency bands (Q- and W-bands) results in higher sensitivity, but measurements at these bands are negatively impacted by water content in the sample [36]. Lower frequency bands (L- and S-bands) are used for samples with higher water content but provide reduced sensitivity levels [36]. The X-band is the most extensively used frequency band in EPR dosimetry, as it delivers a high level of sensitivity in EPR measurements while not being overly influenced by sample size and water content [36]. Water content in EPR samples can cause a decrease in EPR signal intensity and increase noise [39]. Steps are taken during EPR sample preparation to limit the moisture content.

By quantifying the radiation-induced centers in materials, there is a potential to

reconstruct the dose to the sample. At resonance condition, the electrons in irradiated samples undergo spin-flip transitions, and the intensity of these transitions is proportional to the number of electrons in the sample, which is proportional to the absorbed radiation dose [22]. EPR is a preferred method for dose reconstruction, as the spectra can be read non-destructively. When the magnetic field is removed, the sample reverts to its degenerate state, where the electron's spin state is indistinguishable. The EPR method does not physically alter the sample permanently, lending to the non-destructive nature of EPR analyses. Another feature of EPR is that it only measures the cumulative dose to a sample, meaning that any doses accumulated from background radiation will also be included in the dose reconstruction.

The applicability of EPR is not limited to radiation studies. The detection of free radicals also has applications in medicine, biology, cosmetology, and biotechnology [40]. Fundamentally, EPR spectroscopy aims to study free radicals and other paramagnetic centers in suitable materials. This report will focus on the radiation-induced free radicals formed in the calcified tissues of shelled species. The applicability of shelled species as fortuitous dosimeters using EPR will be explored further in Section 2.3.

To retrospectively assess the dose to a sample using EPR, the dose to the sample is reconstructed. This is done by measuring the peak-to-peak intensity of the radiation-induced peaks assessed in EPR spectra. There are two main methods of calibrating these signal-to-dose correlations: the calibration curve and additive dose methods [37] [22]. In the calibration curve method, using a calibrated radiation source, many identical samples are irradiated to known dose points, and their EPR spectra intensities are measured and averaged at each dose. A calibration curve is produced as the best linear fit of absorbed doses versus EPR signal intensities. Alternatively, the additive dose method relies on incrementally irradiating one sample to known doses and measuring the increase in EPR signal intensity after every irradiation. Based on this, a radiation response curve as in Figure 2.3 can be constructed, and the unknown accidental or initial dose can be back extrapolated. The calibration curve method is better suited to large sample groups, while the additive method is better suited to individual samples.

2.1.2 Other Retrospective Dosimetry Techniques

Other methods of physical retrospective dosimetry in addition to EPR will be briefly summarized in this section to compare measurement techniques and dose detection limits.

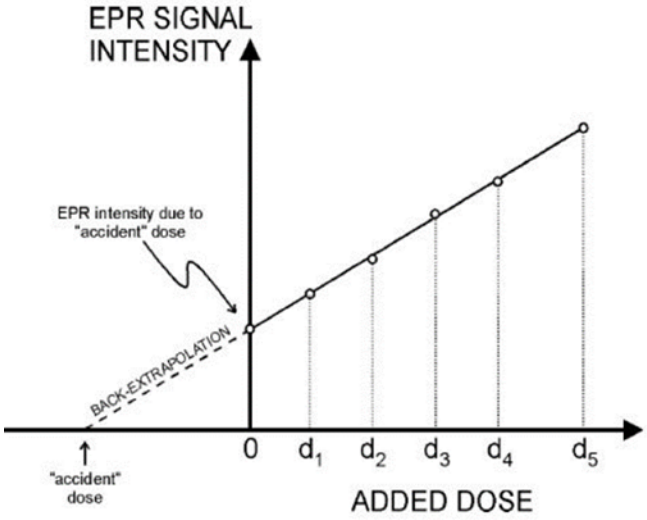

FIGURE 2.3: Dose reconstruction based on the additive irradiation method [22].

Thermoluminescent Dosimetry (TLD)

The principle of thermoluminescent dosimetry relies on the emission of light from an irradiated material activated by heat. This method is commonly used to measure absorbed radiation dose. Commercial thermoluminescent dosimeters are used in medical, personal, and environmental applications [41]. Good quality thermoluminescent materials require certain properties including high dose sensitivity, low dose fading over time, and a linear dose-response [42]. Like dosimetric materials for EPR, materials suitable for TLD are crystalline solids [43]. When these thermoluminescent materials are exposed to ionizing radiation at room temperature, electrons are removed from the atom or molecule and trapped within the material's crystal lattice. The material is then heated, which causes the crystal lattice to vibrate and release the trapped electrons, which return to ground state and release energy, in the form of light, in the process. The quantity of light emitted will be proportional to the cumulative absorbed dose. Unlike EPR, this method reads the dose destructively since the excited electrons have been returned to ground state.

The principles of thermoluminescent dosimetry are typically applied to prefabricated dosimeters that have low detectable doses and are used for personal dosimetry. However, these luminescent techniques can also be applied to accident dosimetry of existing materials such as mobile phone screen glass [44], chip cards [45], dental ceramics [46], bricks, and tiles [47], with minimum detection doses as low as a few mGy in some of these

materials.

Dose detection limits of 0.5 Gy have been reported in the biogenic calcium carbonate of mollusc shells using the TL method [48]. However, one disadvantage of the TL process is that samples can experience signal fading due to thermal influence, which can reduce the accuracy of the dose-response readings and generate significant errors. Signal fading of up to 60% has been reported in biogenic calcite [48].

Optically Stimulated Luminescence (OSL) Dosimetry

Optically stimulated luminescence (OSL) dosimetry is a physical dosimetry technique typically used as an alternative to TLD and relies on optical stimulation in the form of light to release electrons trapped in the lattice of an irradiated crystalline material. When those electrons return to ground state, energy in the form of light is released, and the quantity of light emitted is studied. Like TLD, the readout in OSL measurements is destructive. OSL has been used in dating, as well as in measuring the accumulated radiation dose in building materials [49], quartz [50], and resistors in mobile phones [51], with detection limits as low as 20 mGy being reported in some of these materials. Dose detection limits in biogenic calcium carbonate using OSL have not been reported in the literature; however, a dose detection limit of 4 Gy was reported in natural calcite [52].

2.1.3 Summary

Retrospective dosimetry is an essential tool of accident dosimetry. It aims to retroactively determine the absorbed dose to a person or environment after an unplanned radiation exposure when no conventional dosimeters are present. Retrospective dosimetry techniques can be used to determine the doses in a multitude of samples with crystalline structures, including man-made materials such as bricks and phone screens, biological material such as teeth, and biogenic materials such as the calcified tissues (shells) of molluscs. Of particular interest to this thesis are the dose detection limits in the calcified tissues of shelled invertebrates.

Electron paramagnetic resonance (EPR) dosimetry was discussed in Section 2.1.1 and is the preferred retrospective dosimetry method used in this work due to its non-destructive nature and low detection limits. Like EPR, crystalline solids are used for TLD and OSL because these techniques rely on electrons being trapped in the crystal lattice defects of the material after being ionized by radiation. A downside of these techniques is that the doses are read destructively because the excited electron has been moved back to ground state. Dose detection limits of 0.2 Gy [10] [29] and 0.5 Gy [48] in

biogenic calcium carbonate have been reported for EPR dosimetry and TLD respectively and are unreported using OSL.

2.2 Manganese(2+) Abundance and Effects

This section will detail information about Mn^{2+}, its abundance in the environment, its incorporation into shelled species, and its effects on the lower limit of detection in EPR spectra. The purpose of this literature review of Mn^{2+} is that this element in its particular oxidation state has limiting effects on the lower limit of detection using EPR in shelled species, so an analysis of it must be completed.

2.2.1 Manganese(2+) In The Environment

Manganese is an element naturally occurring in rocks, soil, and water. It is found abundantly in the Earth's crust and in other natural sources such as ocean spray, vegetation, and volcanic ash [53]. The majority of manganese in soils comes from crustal sources, with some other sources coming from deposition from the atmosphere, wash-off from various surfaces, leaching and excretion from plants, and from dead plant and animal materials. Manganese can also be found in anthropogenic (non-environmental) sources consisting mainly of sewage and wastewater discharges, mining activity and metal production emissions, and fossil fuel combustion [53]. It is also a vital nutrient for animals, plants, and microorganisms, however, it can be toxic at extreme levels.

While manganese is quite abundant on Earth, it always exists with other compounds and never in its native form. Manganese-55 is the only stable isotope of manganese, and it can exist in 11 different oxidation states, ranging from (-3) to (+7), but the most common oxidation states are +2 (e.g., manganese carbonate [$MnCO_3$] - Figure 2.4a), +4 (e.g., manganese dioxide [MnO_2] - Figure 2.4b), and +7 (e.g., potassium permanganate [$KMnO_4$] - Figure 2.4c) [53]. Most manganese compounds can exist in soil as solids or as small particles in water, and exists exist in aquatic environments as Mn^{2+} and Mn^{4+} ions [53].

Table 2.1 summarizes the average manganese concentrations in different environmental media. The most common oxidation state for manganese in saltwater, freshwater, and soil is +2 [53]. It is worth noting that the values presented in this table are averages, and that concentrations can vary in locations depending on nearby sources.

The manganese oxidation state of particular interest in this work is the +2 state, which has five unpaired electrons. The presence of manganese(2+) ions causes problems

(A) (B) (C)

FIGURE 2.4: (A) manganese sulfate powder, (B) manganese dioxide powder, (C) potassium permanganate crystals.

TABLE 2.1: Average manganese concentrations in different environmental media.

Environmental Media	Concentration
Seawater	0.4-10 μg/L, average of 2 μg/L [54]
Freshwater	1-200 μg/L [54]
Surface water	16 μg/L (median level) [54]
Ground water	5 μg/L (median level) [54]
Soil	300-600 mg/kg [53]
Air	40 ng/m^3 (rural areas) [53]
River sediment	410-6700 mg/kg (dry weight) [53]
Interstitial water of marine sediments	1.5-5000 μg/kg [55]

when studying the EPR spectra of shelled species. High-intensity manganese(2+) peaks have been shown to impact the lower limit of detection in low-dose EPR spectroscopy studies [21] [10]. Manganese is taken up into the calcite and aragonite crystal structure that primarily make up mollusc and crustacean shells by replacing the calcium atom [56]. Methods of manganese incorporation into shelled species will be explored in further detail in the following subsection.

2.2.2 Manganese(2+) Incorporation Into Shelled Species

To understand how manganese is incorporated into shells, their mineralogy must first be explained. The calcified shells of species such as molluscs are composed mainly (95-99%) of calcium carbonate ($CaCO_3$), with small amounts of protein and other trace elements such as manganese, iron, magnesium, and strontium, to name a few [57] [58]. The calcified

shells of crustaceans are up to 75% $CaCO_3$, with smaller amounts of protein, chitin and trace elements [59]. Calcium carbonate exists in three different polymorphic forms with varying stabilities - calcite, aragonite, and vaterite (in order of decreasing stability) [60]. Within shells, there exist two calcium carbonate forms - calcite and aragonite, as biogenic vaterite is very rare due to its instability [56]. Figure 2.5 below shows that the crystalline structures of calcite and aragonite vary. Aragonite has orthorhombic symmetry and is nine-fold coordinated by oxygen, while calcite has trigonal symmetry and is octahedrally coordinated by oxygen.

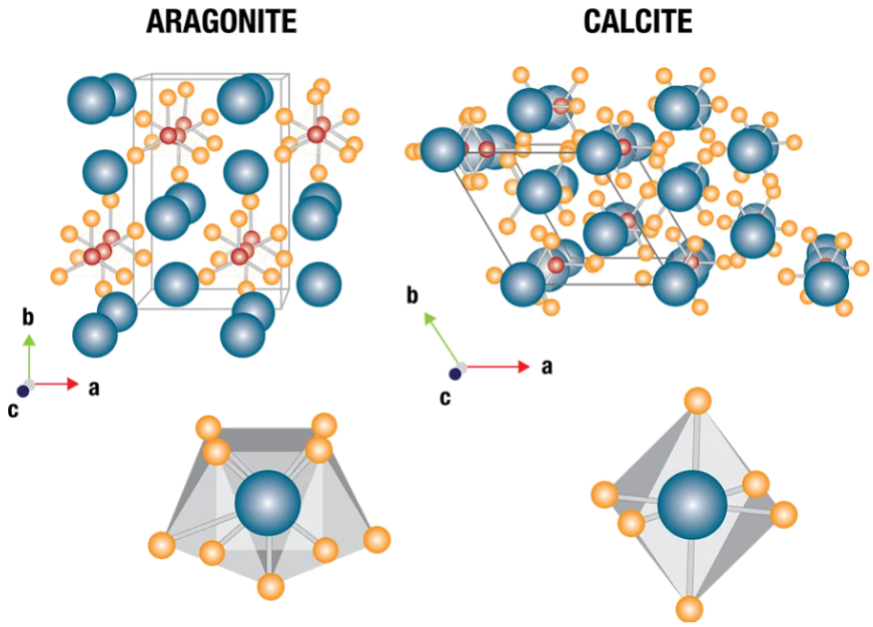

FIGURE 2.5: The crystalline structures of aragonite and calcite. Calcite holds a trigonal shape while aragonite holds an orthorhombic shape. The calcium site is nine-fold coordinated by oxygen in aragonite, whereas it is six-fold (octahedrally) coordinated in calcite [56].

Manganese is always incorporated into shelled species as high-spin Mn^{2+}, and its accumulation in a shell depends mainly on the shell's crystal structure [56]. Most mollusc and crustacean shells are composed primarily of calcium carbonate in its calcitic and aragonitic forms [56] [61]. Mn^{2+} ions are incorporated into the crystal structure of calcite and aragonite by entering and replacing the Ca^{2+} sites [62]. Mn^{2+} is always coordinated by an octahedron of CO_3 complexes, which is isostructural to calcite [56]. This structural similarity means Mn^{2+} is more chemically stable in the octahedral calcitic environment than in the nine-fold coordinated aragonitic environment [56]. It follows that shells with

higher amounts of the calcite polymorph will contain more Mn^{2+} than aragonitic shells [56]. Mn^{2+} cannot be taken up in the crystal structure of non-biogenic aragonite, yet bivalves with aragonitic shells can incorporate Mn^{2+} in concentrations above 400 μg/g [63]. This is reportedly due to the formation mechanisms of calcium carbonate in biological species, where Mn^{2+} is incorporated into the shell's initial amorphous calcium carbonate phase prior to crystallization [56]. When the shell crystallizes into aragonite, Mn^{2+} ions are present in an octahedral coordination similar to calcite, within the nine-fold coordination of the shell [56].

The dominating $CaCO_3$ polymorph within a shell is largely species-dependent and affected by factors such as the animal's environment. The shells of freshwater and terrestrial molluscs are mainly composed of aragonite [56], while the shells of crustacea and marine molluscs are primarily composed of calcite [61]. Typical mollusc shells are predominantly composed of either calcite or aragonite, but some shells, such as the marine bivalves *Mytilus californialis* and *Mytilus edulis* can contain both polymorphs in more equal parts depending on the temperature and salinity of the seawater that the species inhabit [64] [65]. The percent aragonite in a shell with mixed mineralogy can increase with water temperature and decrease with salinity [64].

Molluscs and crustacea accumulate Mn^{2+} into their atomic structures over their lifetime, resulting in identifiable amounts in many species' shells. In aquatic biota, Mn^{2+} is increasingly bioconcentrated by species at lower trophic levels [53]. The Mn^{2+} absorption into aquatic specimen also tends to increase with decreasing salinity [53]. As a result, shells of species with saltwater habitats will contain less Mn^{2+}. The uptake of Mn^{2+} by aquatic invertebrates can also decrease with water pH and increase with water temperature [53]. The concentrations of Mn^{2+} in the aquatic environment surrounding the shells are said to have little effect on the Mn^{2+} concentrations within the shells. Instead the Mn^{2+} concentrations at the sediment-water interface in aquatic environments are the primary factor in determining Mn^{2+} uptake into aquatic biota, where they accumulate the metals through filter-feeding activities and absorption [66] [67]. Manganese is also accumulated in terrestrial molluscs via their diet and absorption from the environment [68] [69]. Shell colour and thickness can also be related to the amounts of Mn^{2+} within a shell. Darker shell colours have been attributed to higher Mn^{2+} concentrations within mollusc shells [10]. Shell thickness is also said to be correlated to Mn^{2+} contents in shells, with thicker shells containing higher Mn^{2+} concentrations [20]. Species-specific habitats and mechanisms of Mn^{2+} incorporation into shells will be further detailed in Section 2.3.

Most of the literature related to the analyses of Mn^{2+} incorporation into shelled species surrounds their use as biomonitors. Other heavy metals and transition metals (including

Zn, Fe, Cr, Pb, Cu, Cd, As, Pb, and Hg), in addition to Mn^{2+}, are easily bioaccumulated through feeding activities and absorption into the tissues and shells of molluscs and crustacea [70] [19]. The metals are incorporated into shells through biomineralization, following the same pathways as calcium [60]. As such, shelled species are commonly used as biomonitors and indicators of metal pollution and changes in environmental conditions [71] [72] [73].

2.2.3 The Effects of Manganese(2+) on EPR Spectra

Identifying the lower limit of detection (LLOD) when measuring samples using EPR is imperative, as it dictates the lowest level of radiation detectable in that sample in the event of an unplanned exposure. Many factors can affect the LLOD of a sample in low-dose EPR dosimetry. For example, some samples have very complex native signals, meaning that dose reconstruction below a certain dose point is not always feasible [27]. Regarding shelled species, crustacean and mollusc shells are composed mainly of $CaCO_3$ but also contain other components, such as proteins and trace metals, that combine to create a unique species-dependent EPR spectrum. In particular, the presence of Mn^{2+} in shell samples can cause a characteristic sextet of high-intensity Mn^{2+} peaks in EPR spectra that can impact the lower limit of detection. Several studies on the EPR spectra of shelled species have noted the interference of Mn^{2+} signals when performing dose reconstructions [21] [10] [74]. Figure 2.6 shows the six Mn^{2+} peaks clearly labelled in the background EPR spectrum of an ocean snail (*Littorina littorea*) sample. When evaluating the Mn^{2+} signal in EPR spectra, Sheng et al. suggest measuring the peak-to-peak amplitude of just the first Mn^{2+} peak [75].

In order to explain the presence of the six Mn^{2+} peaks, the nuclear spin of atoms must be explored. The nuclear spin of an atomic nucleus, defined by the symbol "I", is a property of the atom. It represents the overall spin and resulting magnetic moment of the atom and is associated with the reactivity of the nucleus to the effects of an external magnetic field [76]. The principle of nuclear spin can be explained as follows. Subatomic particles spin on their axes, and these spins are paired against each other, resulting in a net spin value of the nuclei. In the presence of this net nuclear spin, the free electrons (paramagnetic centers) in the atom will experience an additional magnetic field. This interaction of the electron spin with the magnetic nuclei of the sample is called a hyperfine interaction. If the individual numbers of neutrons and the number of protons in a nucleus are both even, then the net spin is zero. If the sum of neutrons and protons in a nucleus is odd, then the net spin is a half-integer spin (i.e. 1/2, 3/2, 5/2). When a

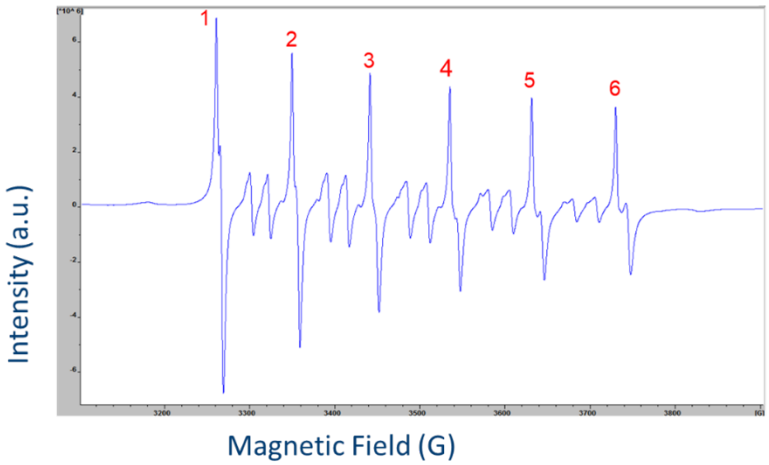

FIGURE 2.6: Six characteristic Mn^{2+} peaks in the background EPR spectrum of a *Littorina littorea* sample.

particle with a half-integer spin is placed in a magnetic field, the particle can either align with or against the magnetic field [17]. The nuclear spin of Mn^{2+} is $I = 5/2$. According to the laws of quantum mechanics, a nucleus with a spin I has $2I+1$ possible orientations and will split a single EPR peak into $2I+1$ peaks. Therefore, six orientations ($2I+1 = 6$) are possible for Mn^{2+}, resulting in six characteristic peaks in EPR spectra that can be attributed to Mn^{2+} when the atom is in the presence of an external magnetic field.

The presence of Mn^{2+} peaks of differing intensities in the EPR spectra of various shelled species has prompted the need to examine if there is a correlation between the concentrations of Mn^{2+} in shells and the intensity of the Mn^{2+} peaks in the EPR spectra of a species. These effects will be explored further in Chapter 4.

2.3 The Applicability of EPR Dosimetry on Shelled Species

A large portion of the research surrounding the EPR response of molluscs and crustacea is regarding the detection of irradiated foodstuffs and the dating of natural carbonates in fossilized mollusc shells for archaeological purposes. Aquatic animals like molluscs and crustacea are carriers of pathogenic germs that can cause harm to humans if ingested. An appropriate method of decontaminating these foodstuffs is irradiation with high-energy gamma rays, which also causes the formation of free radicals in their calcified tissues. The doses used for food irradiation generally range from 0.1-10 kGy [77]. Although these doses

are too high for the applications of this thesis, important information can be obtained from these studies, such as g-values, and the linearity of the dose-response of calcified tissues in shelled species at high doses, which is reported to be from 0.5-2 kGy [78] [79].

However, a study by Sadło et al. was conducted to determine the lower limit of detection in various freshwater and marine mollusc shells using EPR [10]. This study concluded that detection limits for marine shells were predominantly better out of eight freshwater and seventeen marine mollusc shells. Some of the freshwater molluscs displayed no radiation response at doses of 10 Gy, while the lowest detectable dose limit for this group was in zebra mussels (*Dreissena polymorpha*) at 2 Gy. Since that study, M. Tzivaki resolved the lowest detectable dose in zebra mussels to 0.2 Gy [29]. On the other hand, all marine molluscs in this study displayed a radiation response at 4 Gy or below, with many showing dose detection limits below 1 Gy. An investigation by A. Hassan showed that some species of freshwater and marine molluscs showed no dose-response at doses of 10 Gy [21]. However, in both studies, lower detection limits were obscured by Mn^{2+} peaks. The difference in detection limits presented in both studies shows that shell structure and animal habitat relating to Mn^{2+} uptake can significantly affect detection limits.

In order to analyze crustacean and mollusc shells with EPR, they must first be prepared. Sample preparation methodologies do not vary significantly throughout the literature and are as follows. The sample is purchased or collected from the environment, and any soft tissues are separated and discarded [80]. The remaining debris is washed away, and the samples are frozen or air dried [81] [82]. The shells are then ground into a fine powder for EPR analysis, which can be done using a mortar and pestle or a mill [83] [82]. The sample can either be irradiated prior to cleaning [82] [81], or after cleaning, drying, and grinding [83]. Grinding the samples into a powder prior to irradiation allows the unirradiated background spectrum to be measured using EPR. Additional signals due to excessive grinding during sample preparation have been reported in EPR spectra and can be mitigated through chemical etching of a sample with phosphoric acid [84]. However, the etching process on ground mollusc shells was found to have no impact on spectra intensity [21]. Irradiations are carried out using cobalt-60 [82], or cesium-137 [81] gamma sources. Following careful preparation procedures is vital to ensure the accuracy and reproducibility of EPR results.

2.3.1 The Effects of Ionizing Radiation on Shelled Species

Ionizing radiation interacts with the calcium carbonate in calcified tissues by influencing the creation of radical centers. Radical centers have different g-values in EPR spectra. In

EPR spectra, the g-values are the locations within the spectra where a spin-flip transition will occur due to a particular free radical, and the identity of free radical can be determined based on the g-value.

When shelled species are exposed to ionizing radiation, excited electrons can be captured in the lattice defects of the shell. Specifically, in irradiated mollusc shells, radical centers that can be attributed to CO_2^-, CO_3^-, $CO_3^{(3-)}$, SO_2^-, SO_3^-, O_3^-, and O^- are formed [30] [85]. These free radicals have g-values within the range of 2.0006-2.0062 in EPR spectra [30] [86]. Some of these free radicals, such as the CO_3^- radical, are not used for dose detection as they are unstable. The $CO_3^{(3-)}$, CO_2^-, and SO_3^- radicals are commonly used for dose detection in carbonates due to their stability [87] [88]. However, the dose-response of the SO_3^- radical is not proportional to a dose between 0.18-10 Gy, making it unreliable for dose detection at low doses [87]. The CO_3^- and CO_2^- radicals are therefore used for radiation detection at lower doses, and correspond to g-values of 2.0012, and 2.0016 respectively [89] [90]. CO_2^- centers in particular remain stable and can be tracked for decades ,and often occur in carbonates of marine origin [85] [91]. The concentrations of these radiation-induced radicals will increase with increasing dose, and the measurements of the radiation-induced EPR peaks attributed to these radicals can be used to determine an absorbed radiation dose.

A concern when analyzing irradiated samples is that the radiation-induced free radicals will be short-lasting. However, this is not a concern in the calcified tissues of molluscs and crustacea, as the free radicals formed are reported to last for years due to electrons getting trapped in the crystal lattice of the shell [30].

2.3.2 Molluscs

The Mollusca phylum comprises many classes of animals including gastropods (e.g. snails, slugs), bivalves (e.g. scallops, mussels, clams), cephalopods (e.g. squids, octopuses, ammonites), and polyplacophora (chitons). Among invertebrates, mollusc shells have the most diverse variation of microstructures [92]. The mineral part of molluscan shells are composed almost entirely of highly ordered aggregates of calcium carbonate in its calcitic and aragonitic polymorphous forms [92]. The key feature of most molluscan bodies is their calcareous (consisting mainly of calcium carbonate) shell, which can be singular (gastropods), twofold (bivalves), or eightfold (chitons). The mineral portion of the shell comprises 95-99% of the shell weight, and the organic portion constitutes 0.1-5% [92].

Mollusc shells consist of 3 main layers as seen in Figure 2.7; the periostracum, which is uncalcified; the ostracum or peristaltic layer, which is calcified and the thickest layer;

and the hypostracum or nacre, which is also calcified and contains stacks of calcite and aragonite [93] [92].

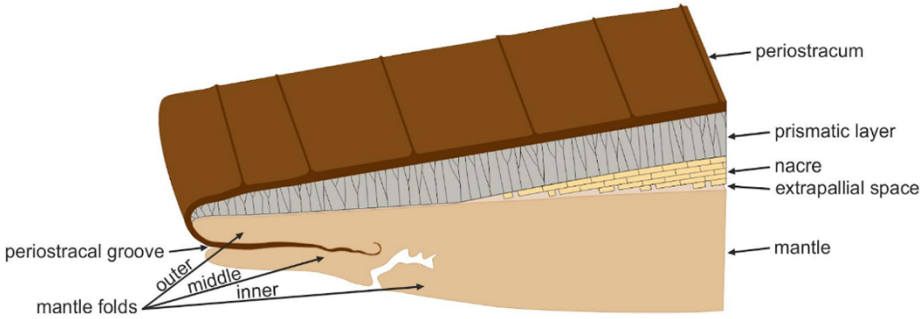

FIGURE 2.7: The layers of a mollusc shell, specifically the periostracum, prismatic layer, and nacre [92].

The shell's main calcium carbonate polymorph (aragonite or calcite) differs depending on the species. In general, the shells of terrestrial and freshwater molluscs are composed primarily of aragonite, while the shells of marine molluscs are composed primarily of calcite [56] [94]. The mantle is an organ located between the shell and body of a mollusc, and is responsible for secreting the proteins and minerals necessary for shell formation [92]. It was found that the soluble molluscan shell proteins that make up only 0.03-0.05% of shell weight, have been proven to control the calcium carbonate polymorph [92]. The polymorph secretion is dictated by proteins associated with either aragonitic or calcitic shell layers, and is specific to the species and its environment [92].

Molluscs absorb minerals and essential nutrients for shell formation from their diet and surrounding environment. Calcium is an essential mineral for all mollusc shell formation and is ingested and absorbed into the mollusc body [95]. Metals such as Fe, Mn, Cu, and Zn are also absorbed via the same pathways as calcium [69]. Manganese is particularly interesting, as high concentrations of manganese in shells can cause high-intensity peaks in EPR spectra that affect the lower dose detection limit [21].

In bivalves, the bioaccumulation of trace metals happens through filter-feeding of solutions and suspended materials [69]. In gastropods, the accumulation of trace metals has been said not to be directly affected by concentrations in water and sediment, but more tied to the animal's feeding habits, age, and growth rate [96]. However, other studies have suggested that the bioaccumulation of trace heavy metals in snail tissues was proportional to the metal concentrations in the water that the snails inhabit [18].

Gastropods

Gastropods are a class of molluscs, comprising snails, which are of interest in EPR dosimetry studies. Snails are the largest group of molluscs and cover many habitats including terrestrial, saltwater, and freshwater environments.

Many EPR studies have been conducted on snail shells, and dose detection limits of 2 Gy have been realized for terrestrial snails *Cepaea nemoralis* and *Cepaea homoralis* [21] [10]. In a study conducted by A. Hassan a preliminary dose-response curve from 2-20 Gy was created for *Cepaea nemoralis* using the radiation-induced free radical CO_2^- identified at g=2.0016 in the EPR spectra [21]. The methodology used for creating this curve will be refined in this thesis to determine if the dose detection limit can be improved. Regarding aquatic snails, this same study by A. Hassan identified that freshwater pond snails (*Lymnaea stagnalis*) displayed no dose-response at doses of 10 Gy, due to high-intensity Mn^{2+} peaks in the EPR spectra. However, a dose detection limit of 3 Gy has been determined in the shells of the freshwater snail *Viviparus conectus*, showing that detection limits can vary greatly even between freshwater gastropods [10]. Furthermore, a detection limit of 0.3 Gy was identified in the shell of the marine snail *Tonna galea* [10].

Many gastropod shells display the characteristic Mn^{2+} sextet in their EPR spectra [21] [10]. The accumulation of trace metals in gastropods can be related to the animal's feeding habits, age, and growth rate [96] or due to metal concentrations in the snail's environment [18]. Regarding the crystalline structure of gastropod shells, although the dominant $CaCO_3$ polymorph in freshwater molluscs is aragonite, the main polymorph in freshwater gastropods can be species-dependent, and in some cases, is calcite instead of aragonite [89] [97]. Terrestrial gastropods show less species-dependence on the main polymorph and are consistently reported to be composed primarily of aragonite [98] [99]. The main carbonate polymorph in marine gastropod shells depends on environmental conditions [100].

The diet of gastropods varies from species to species: freshwater snails are mainly considered herbivores, consuming algae and decaying plants [101]; terrestrial gastropods can be herbivorous and omnivorous, consuming living and decaying plants, fungi, soil and animal matter, and in rare cases are predatory, consuming earthworms and slugs [102] [103]; and marine gastropods can be herbivores, omnivores, or carnivores depending on the species, consuming algae, small fish and molluscs, seaweed, and worms amongst other things [104].

The habitats of gastropods and subsequent environmental exposure also vary depending on the species. Terrestrial snails live in dark, moist areas, such as gardens and forests,

and come into contact with soils containing Mn^{2+} through cutaneous contact, egg-laying, and feeding [68]. Freshwater and marine snails prefer living in shallow water and are typically found along the shorelines, living in the sediment. These snails come into contact with Mn^{2+} through the water and sediment that they inhabit [68] [104].

Grove snails (*Cepaea nemoralis*) and their applicability as retrospective dosimeters using EPR will be a specific focus of this thesis, due to their relatively low detection limits (2 Gy [21])and global abundance. This species is native to central and western Europe and is found in many locations worldwide, including in eastern Europe and North America, specifically Virginia, New York, Ontario, and Massachusetts [105]. The snail is active in the spring through autumn, particularly in rainy weather. From late autumn to early spring, the snails hibernate under layers of plant and soil. The snail is abundant in various habitats, including gardens, parks, and forests [105]. Its diet consists mainly of dead and living plant material, fungi, carrion, peat and algae [106]. Grove snails have highly polymorphic shell patterns, with a shell of a brown, orange, red, yellow, or olive colour, and exhibit between 1 and 5 black or dark brown spiral stripes [107]. Shell colour in *Cepaea nemoralis* is genetically predetermined [105].

Bivalves

Bivalves are a class of molluscs characterized by a two-fold shell. Many bivalves live in benthic environments, meaning they dwell on sediment at the bottom of water bodies. They are filter feeders, uptaking food, inorganic particulates, and heavy elements from water [108].

As discussed in Section 2.2.2, bivalves are typically used as biological indicators for metal pollution [109]. Shells of freshwater bivalves are predominately made of aragonite, while marine bivalves are made of calcite [94], and dose detection limits in marine mollusc shells are generally lower than those of freshwater molluscs [10]. The EPR spectra of bivalves typically display the characteristic set of six Mn^{2+} peaks [21]. Reportedly, shells of freshwater bivalves can contain Mn^{2+} concentrations above 1000 μg/g [56]. Mn^{2+} accumulates into the bivalves via filter feeding and substitutes for Ca^{2+} during biomineralization [110].

Dose detection limits in the EPR spectra of bivalve shells have been reported as low as 0.2 Gy in the marine molluscan shell *Arcidae* sp. [10] and 0.2 Gy in the shells of freshwater zebra mussels (*Dreissena polymorpha*) [29]. In a study of zebra mussels by M. Tzivaki, a radiation-induced peak at g=2.0034 was used for dosimetry, and a linear

dose-response due to the irradiation and free radical formation within its calcified shell was created from 0.2-32 Gy [29].

2.3.3 Crustacea

Crustacea (comprising crab, lobster, and shrimp) are one subphylum of the Arthropod phylum. The distinguishing characteristic of arthropods is the existence of a jointed skeletal covering composed partly of chitin bound to protein. Specifically, crab, lobster, and shrimp all fall within the Decapoda order of crustaceans and are commonly referred to as decapods. The principal components of crustacean shells are chitin (15-40%), protein (20-40%), calcium and magnesium carbonate (20-50%), and other minor components [111]. Species with harder exoskeletons, such as crabs and lobsters, contain higher amounts of $CaCo_3$ (up to 75%), which adds rigidity to the crustacean cuticle [112]. Lobster shells reportedly contain less calcium carbonate than hard-shelled crabs [113].

Regarding the physical structure of crustacea, they have a rigid exoskeleton composed of a layered cuticle. The cuticle is composed of four layers; the epicuticle, exocuticle, endocuticle, and membranous layer [114]. In order to grow, crustacea must undergo a process of shedding their shells, known as moulting. Before moulting, a new exoskeleton is formed under the old exoskeleton. Underneath the calcified cuticle is a cellular hypodermis that enables the synthesis of the exoskeleton [114]. During this cuticle synthesis, trace metals such as manganese are incorporated into the shell structure [112].

According to the literature, the shells of decapod crustacea are composed mainly of the calcite polymorph of calcium carbonate [61]. As previously mentioned, Mn^{2+} ions are more stable in calcite than aragonite [56], so it can be assumed that the calcified tissues of these species will contain considerable amounts of Mn^{2+}. Mn^{2+} is incorporated into the shells of different species depending on many factors, including environment, diet, and shell formation mechanism.

Like molluscs, lobsters [115] and crabs [116] have proven to be effective biomonitors for trace metals and pollution. They are also benthic organisms and inhabit the sediment layer in saltwater bodies. As previously mentioned, it has been reported that the Mn^{2+} concentration at the sediment-water interface in aquatic environments is the primary factor in determining Mn^{2+} uptake into aquatic biota, where it is accumulated through feeding and absorption [66]. Mn^{2+} is bioavailable and concentrated in benthic fauna, which is a food source for crustacea [53]. Crustacea also accumulate metals through direct absorption into their exoskeletons and gills in addition to feeding [117] [118].

Crab and lobster shells display strong Mn^{2+} signals in EPR spectra [25] [82]. Alternatively, shrimp shells have been reported to show much lower intensity Mn^{2+} peaks [21] [119]. This was suspected to be due to the shrimp's environment, assuming it was farmed instead of harvested from the wild, thus impacting its exposure to Mn^{2+}. A study performed by A. Hassan also determined that shrimp shells do not display any radiation-induced peaks at doses of 10 Gy, due to the more significant amounts of chitin (15-30%) and smaller amounts of $CaCO_3$ (13-40%) contained in the shell, resulting in the formation of fewer carbonate radicals for dose detection [21] [111].

Lobster

The EPR spectra of lobster shells, specifically the Norway lobster (*Nephrops norvegicus*) [82] and American lobster (*Homarus americanus*) [21] have the distinct Mn^{2+} sextet. Irradiation experiments have been carried out on lobster shells in the high dose (1 kGy-5 kGy) range, and a radiation-induced peak at g=2.0009 was identified [82]. Lobsters are omnivorous, consuming animals and plants, including fish, other crustaceans, molluscs, algae and sea plants [120].

Crab

Unlike lobsters, crab species can inhabit saltwater, freshwater and terrestrial environments [121]. This means that the pathways of Mn^{2+} accumulation in crab samples largely depend on the species and habitat. Crabs are typically omnivorous, consuming algae, molluscs, plant material, and fungi, amongst other things [122].

The EPR spectra of crab shells show the six characteristic Mn^{2+} peaks [25]. A study by S. Abdou and N. El-Faramawy on the EPR sensitivity of various crab exoskeleton parts revealed that the crab dactyl (the moveable finger of the claw) was the most sensitive to gamma irradiation, and should be used for dose-response studies [123]. This same study showed that the CO_2^- induced free radical in crab dactyl at approximately g=2.003 was used as a dosimetric signal and linear from 0.5 to 15 kGy [123].

Dungeness crabs (*Metacarcinus magister*) are a commonly farmed and consumed marine crab species that inhabit North America's western coastline. According to the literature, no irradiation or EPR studies have been carried out on the shells of Dungeness crabs, however, it is assumed they will contain Mn^{2+} due to the calcitic structure of the crustacean cuticle.

2.3.4 Turtle

Turtles are reptiles falling under the phylum Chordata and are of the order Testudines and are characterized by an outer covering of horny scales. The turtle shell is composed of two main sections; the carapace (top section) and plastron (bottom section) which are fused together. The carapace and plastron are usually composed of overlapping scutes and bony plates, which provide the shell with structural integrity and are joined by an area called the bridge. The carapace and plastron are covered by a keratinized epithelium [124].

The carapace and plastron are composed mainly of phosphates and carbonates of calcium and magnesium in the form of hydroxyapatite and calcium carbonate, and collagen, although the percent composition of each component is inconclusive in the literature [125]. However, hydroxyapatite is assumed to be the main component in the shell, as it is the main mineral component of bones. Turtles are aquatic animals living in both freshwater and marine habitats. The midland painted turtle (*Chrysemis picta marginata*) is of particular interest in this thesis and is a species of turtle native to Ontario, listed as a specially protected reptile under the Ontario Fish and Wildlife Conservation Act. It is an omnivorous freshwater turtle inhabiting shallow wetlands, consuming algae, plants, insects, frogs, fish, and snails, amongst other things [126].

There is little in the way of literature related to the use of turtles for retrospective dosimetry studies. The most similar research has been the study of thermoluminescence in turtle shell fossils by Ovhal et al. [41]. This study describes the first thermoluminescent characterization of a turtle shell fossil. The shell fossil was irradiated using a cobalt-60 gamma source, and the researchers successfully generated a linear dose-response curve for doses in the range of 0.79-28.5 kGy. The work performed in this thesis will focus on lower doses, those typically in the range of 2 Gy to 10 Gy.

2.3.5 The Effects of Temperature and Shell Grain Size

The temperature at which a sample is analyzed using EPR can affect its spectra. The temperature of an EPR sample can be modified during irradiation, storage, or measurement. EPR has a higher sensitivity at low temperatures, as lower temperatures lead to a longer relaxation time of the paramagnetic centers, thus limiting signal fading [127]. One study found that a storage temperature of approximately 45 degrees C can limit signal fading in clam and cycline shells [9], while another study found that storage of irradiated Norway lobster samples stored at -20 degrees C showed less EPR signal fading [82]. In another study, calcium carbonate samples were gamma-irradiated to doses between

0-109 kGy at temperatures ranging from 77 K to 298 K, and the samples irradiated at 77 K showed much lower EPR signal intensity [85], indicating that irradiation at lower temperatures causes less free radical formation.

The sample grain size at which samples are analyzed can also affect the spectra. A grain size between 0.1 and 1 mm is typically recommended for optimal sensitivity [128] in this text. Grain sizes below 0.1 mm have a lower sensitivity, leading to more variation in EPR spectra and results of lower accuracy, and are not recommended for use in EPR studies [9]. The sensitivity of EPR spectra to dose increases with grain size until saturation is reached [129]. However, at larger grain sizes, the orientation effects of the sample grains become dominant, and the effect of sample anisotropy on EPR spectra becomes a concern [27]. Thus, grain sizes of sufficiently small and homogenous size must be used to generate isotropic EPR spectra. A goniometer installed on an EPR spectrometer can reduce the error associated with sample anisotropy at larger grain sizes. The sample is rotated to precise angles between EPR measurements, and the resulting spectra are subsequently averaged.

2.4 ICP-OES Elemental Analysis

In the past sections, it has been made clear that Mn^{2+} signals in the irradiated calcified tissues of shelled species pose a problem when resolving the lower limit of detection using EPR. As such, there is an interest in determining if the Mn^{2+} concentrations in shells are related to the intensity of Mn^{2+} peaks in EPR spectra. To determine the manganese concentrations in the various shelled species, a method of elemental analysis is required.

ICP-OES is an analytical technique that measures the wavelengths of light emitted from excited atoms and uses this information to calculate the concentration of an element in a sample. The principle of this process relies on the fact that when ions and atoms absorb energy, electrons can move from a ground state to an excited state. When the electrons return from their excited state to a lower energy level, they release light at specific wavelengths. The wavelength of the emitted light is unique to each element. For example, light emission at a wavelength of 257.610 nm corresponds to Mn^{2+}. The amount of released light at a specific wavelength is proportional to the number of atoms of a specific element, and can be translated to an elemental concentration within the sample [130].

The ICP-OES instrument works using the principle outlined above. A liquid sample is aerosolized via a nebulizer and then atomized and ionized using an argon plasma operating at $>$ 5000K [130]. In this state, the electrons are excited and move to higher

energy levels. As the electrons return to ground state, light at specific wavelengths is released, and measured by a detector. The operating system then converts the amount of light into an elemental concentration. For an ICP-OES to accurately determine elemental concentrations within a sample, it needs to be calibrated using solutions with known concentrations of the element of interest, from which a calibration curve can be made.

Samples analyzed using ICP-OES must be in a liquid form. If the sample to be analyzed is solid (such as mollusc shells), it must be dissolved into a solution. This is achieved through open vessel digestion of the sample. Open-vessel digestion yields a controlled environment with minimum contamination and improved detection limits for analytical chemistry analysis [131]. Standard solutions must also be prepared to compute ICP-OES results. Standard solutions contain known concentrations of a substance and are essential when investigating the elemental analysis of a sample, as they are used to generate a calibration curve to determine the unknown elemental concentration in the sample. The range of concentrations in the calibrating solutions is selected to include the presumed element concentration in the sample solutions.

Sample preparation methods for ICP-OES analysis of solid samples are consistent across the literature. Solid samples are dissolved through open-vessel, microwave, or direct digestion with acid and are diluted with water after dissolution [132] [133]. Calibration standards are prepared from standard solutions of the elements of interest [134]. Detection limits of 12 ppb have been reported for Mn^{2+} [135]. ICP-OES is a destructive technique, as the sample cannot be recovered after processing and analysis. ICP-OES has a variety of applications, including elemental analysis in geological samples and crude oil, and is generally used for its low detection limits and capability to measure more than one element at once [136].

2.4.1 Other Analytical Techniques and Methods of Elemental Analysis

Elemental analysis is a method of determining the quantities of particular elements in a material. There are many different elemental analysis techniques. The inductively coupled plasma-optical emission spectroscopy (ICP-OES) method was described above, as it successfully determines Mn^{2+} concentrations in samples. Other elemental analysis techniques, including atomic absorption spectroscopy (AAS), neutron activation analysis (NAA), and inductively coupled plasma-mass spectrometry (ICP-MS), and X-ray fluorescence (XRF), will be compared and summarized based on detection limits.

Atomic Absorption Spectroscopy (AAS)

AAS is used in various applications including determining chemical element concentrations in waters, glass, food, pharmaceuticals, industrial wastes and environmental and biological samples [137]. This technique uses a high-intensity atomic emission light source, such as a hollow cathode lamp, to excite the atoms in a sample by absorbing ultraviolet or visible light [137]. Like ICP-OES, the sample must be atomized prior to analysis to measure its elements. Each element absorbs a specific wavelength of electromagnetic radiation, and the light source will emit light at a wavelength specific to the element being analyzed. When that energy is absorbed in an element, the electrons are excited and move to a more energetic state. The amount of light that is absorbed by the sample is measured, and the concentration of the element of interest in the sample can be calculated, as the amount of light absorbed is proportional to the number of excited atoms of the specific element.

AAS differs from ICP-OES in that AAS can only measure one element at a time, while ICP-OES can measure multiple elements simultaneously. Detection limits of 0.3 ng/mL have been reported for using this technique [138]. AAS also cannot measure non-metals, while ICP-OES can detect a range of non-metals. It is also a destructive technique, as the sample must be atomized to be analyzed.

Inductively Coupled Plasma - Mass Spectrometry (ICP-MS)

Inductively coupled plasma-mass spectrometry (ICP-MS) is an analytical technique similar to ICP-OES in that it utilizes an inductively coupled plasma to ionize the sample, but instead of measuring the light emitted from the excited elements, it measures their mass directly [139]. The mass of the various ions is determined via a mass spectrometer, which filters ions according to their mass/charge ratio. Detection limits of 0.2 ng/L for Mn^{2+} have been reported [140].

Some characteristics of this technique are that it is destructive and capable of multi-element analysis. It is also more costly than an ICP-OES system but boasts lower detection limits.

Neutron activation analysis (NAA)

Neutron activation analysis (NAA) is another elemental analysis method that has its basis in nuclear reactions. Neutrons irradiate the sample to be analyzed, and the resulting radionuclides formed via neutron capture within the sample emit gamma rays with

energies corresponding to specific elements as they decay [141]. When bombarded with neutrons, neutron activation products are formed specific to the various elements in the sample. The amount of a given activation product is proportional to the concentration of its parent isotope in the original sample. The intensity of the emitted gamma rays at specific energies is proportional to the concentration of the corresponding element within the sample.

Unlike the aforementioned analytical techniques, NAA is a non-destructive method. It is, however, a more limiting technique as access to a research reactor is required to irradiate the samples. NAA has applications in the analysis of construction materials, environmental samples, and biological materials, and due to its non-destructive nature it also has applications in archaeology and forensics [142]. Detection limits of 0.64 µg/g (ppm) of Mn^{2+} using NAA have been reported [143]. It also has the capability of simultaneously determining the concentrations of multiple elements.

X-Ray Fluorescence (XRF)

X-ray fluorescence (XRF) is a non-destructive, multi-elemental analysis method with applications in oil and gas, metal recycling, mining, and automotive and aerospace [144]. The atoms in a sample are excited by high-energy X-rays, and electrons in the innermost orbitals are ejected from the atoms. To return the atom to ground state, the electrons from outer orbitals drop down to fill the inner shells, and in doing so, secondary (or fluorescent) X-rays are emitted [145]. Every element has a set of X-rays with discrete energies unique to that element. These energies are measured, and the output from XRF analyses are spectra with peaks corresponding to various elements, and the peak intensities are indicative of the element's concentration within the sample. Detection limits of 2.6 µg/g for manganese(2+) have been reported in the literature [146]. When comparing ICP-OES and XRF, ICP-OES exhibits lower detection limits and less error than XRF. XRF is also limited in the number of elements that can be detected - light elements ($z<11$) cannot be detected using conventional XRF methods due to their low fluorescence yield [145].

X-Ray Diffraction (XRD)

X-ray diffraction (XRD) is an analytical technique commonly used in conjunction with elemental analysis methods to determine a crystalline sample's crystal structure, phase composition, and orientation.

This method can be used to distinguish between the different phases of molecules in a crystalline solid. For example, in a sample such as a shell composed primarily of $CaCO_3$, it would be able to determine the amounts of calcite, aragonite and vaterite within the sample.

2.4.2 Summary

In summary, many different elemental analysis techniques with a wide range of applications and detection limits are available for determining elemental composition in a sample. One application relevant to this thesis is determining the element concentrations in biological samples such as calcified tissues. Element detection limits for each technique discussed above are summarized in Table 2.2. ICP-OES was selected as the preferred elemental analysis method in this thesis due to its low detection limits and availability.

TABLE 2.2: Mn^{2+} detection limits identified in various elemental analysis techniques.

Analysis technique	Detection limit (μg/g)
ICP-OES	0.012
AAS	0.3×10^{-4}
ICP-MS	0.2×10^{-7}
NAA	0.64
XRF	2.6

Chapter 3

Experimental Work and Methodology

This chapter details the experimental work and methodologies used in this thesis. The methods used in this work are based on and adapted from the literature. Many of the experimental methods used in this thesis are based on A. Hassan's work into mollusc and crustacean shell dosimetry [21]. The experiments are divided into four different stages:

1. Shell sample selection, collection, cleaning, and grinding for all experiments.
2. Detailing sample preparation and measurement procedures for the inductively coupled plasma - optical emission spectroscopy (ICP-OES) analysis of manganese(2+) concentrations in shelled samples.
3. Determining electron paramagnetic resonance (EPR) spectroscopy measurement procedures, including sample preparation and irradiation methodologies, and equipment operation parameters.
4. Detailing the procedures followed in the experiments using EPR analysis, which include determining the Mn^{2+} intensity in the spectra of various shelled species, measuring the dose-response in EPR spectra of terrestrial snails and turtle shells, and the methodology involved in creating dose-response curves.

These different stages will aid in achieving the three main experimental goals of this thesis which are:

- Investigating the effects of manganese(2+) concentrations in various shelled species using ICP-OES and EPR spectroscopy.

- Evaluating the radiation dose-response of two terrestrial snail species and generating dose-response curves.
- Exploring the dose-response in turtle shells.

3.1 Shell Sample Selection, Collection, Cleaning, and Grinding

This section will detail the shell sample selection, collection, cleaning, and grinding procedures for the various shelled species used in this work. Some of the species used in this work had previously been obtained and cleaned by A. Hassan and M. Tzivaki [21] [29].

3.1.1 Sample Selection

The shells of fourteen species were used to achieve this thesis's three main experimental goals as listed above. The selected species represent a variety of biomes. Shells of freshwater, marine, and terrestrial molluscs; crustacea; and one reptile were selected as samples for this work. The number of individual shells collected per species varied based on the size of the shell. As snail shells are smaller in size, dozens of shells were collected for one species, whereas only one crab and lobster shell were used as the animals are much larger. The species name, its procurement location, and the experiment(s) in which it was used are listed in Table 3.1.

TABLE 3.1: Summary of shelled species procurement locations and applicable experiments in this thesis. Samples marked with an asterisk (*) were obtained and prepared by A. Hassan and M. Tzivaki [21] [29].

Samples	Procurement Location	Experiment
Lobster (*Homarus americanus*)*	Grocery store	Mn^{2+} investigation
Dungeness crab (*Metacarcinus magister*)	Grocery store	Mn^{2+} investigation
Shrimp (*Penaeus monodon*)*	Grocery store	Mn^{2+} investigation
Grove snail (*Cepaea nemoralis*)	Ontario Tech University campus grounds	Mn^{2+} investigation and dose-response
Heath snail (*Xerolenta obvia*)	Forest in Peterborough, Ontario	Mn^{2+} investigations and dose-response
Freshwater snail (*Viviparus georgianus*)	Paudash Lake, Ontario	Mn^{2+} investigation
Pond snail (*Lymnaea stagnalis*)*	Storm pond at Ontario Tech University	Mn^{2+} investigation
Blue mussel (*Mytilus edulis*)*	Grocery store	Mn^{2+} investigation
Eastern oyster (*Crassostrea virginica*)*	grocery store	Mn^{2+} investigation
Pond mussel (*Elliptio complanata*)*	Prince Edward County, Ontario	Mn^{2+} investigation
Zebra mussel (*Dreissena polymorpha*)*	Sandbanks Provincial Park, Ontario	Mn^{2+} investigation
Scallop (*Pecten* sp.)	Grocery store	Mn^{2+} investigation
Ocean snail (*Littorina littorea*)	Beach at St Andrews, New Brunswick	Mn^{2+} investigation
Turtle (*Chrysemys picta marginata*)	Kincardine, Ontario	Dose-response

3.1.2 Sample Collection

Samples were collected from various locations, as summarized in Table 3.1 above. The shells of Grove snail (*Cepaea nemoralis*) were gathered from the Ontario Tech University campus near the storm pond. The empty shells were found mainly on top of the soil in the tall grass bordering the pond. Snail shells can be found empty due to predation or the snails dying and decaying, leaving the shell behind. Samples were placed in a plastic bag and taken to the lab for cleaning. Care was taken to collect only the empty snail shells. On rare occasions, a living snail was accidentally collected, but they were always promptly returned unharmed to their habitats.

Ocean snails (*Littorina littorea*) were collected in St. Andrews, New Brunswick from the sandy saltwater beachfront during low-tide. The empty snail shells were found mixed in with rocks and shells from other species on the sediment. Freshwater snail (*Viviparus georgianus*) shells were collected from shorelines areas at Paudash Lake, Ontario, and terrestrial heath snails (*Xerolenta obvia*) were collected by a colleague in Peterborough, Ontario.

3.1.3 Sample Cleaning

Shell samples must be cleaned of all dirt, soft tissue, and organic matter before grinding. Many of the species used for experimentation had organic matter attached that was removed. The sample cleaning procedures are based on methods developed by A. Hassan and M. Tzivaki from their dosimetry work using shelled species [21] [29].

Crab

A whole, fresh Dungeness crab (*Metacarcinus magister*) was purchased from the grocery store (Figure 3.1). The crab shell was broken down using dissection tools and physical force. As the shells were broken down, the organic material was removed using tools and discarded. Once all organic material that could be physically removed was discarded, the remaining shells were soaked in a solution of 1.2% sodium hypochlorite (household bleach) for 24 hours to loosen any residual organic matter, decontaminate and remove any odours from the shell. The sodium hypochlorite solution was prepared by 5-fold diluting 6% bleach with tap water. The shell pieces were then rinsed with reverse osmosis (RO) water, and any residual organic material was removed using appropriate tools. Shells were rinsed repeatedly until no soft tissue remained. Shell pieces were then set to dry in a desiccator for approximately two weeks before ICP-OES and EPR sample preparation.

As previously stated, the crab dactyl (the moveable finger of the claw) is the most sensitive to gamma irradiation and will be used in these experiments [123]. The lobster and shrimp shells used in this work had been prepared similarly, but were previously cleaned by A. Hassan [21].

FIGURE 3.1: Dungeness crab sample.

Scallop

Scallops were purchased frozen from the grocery store. The shells were already very clean, and no physical removal of organic material was required. Shell samples were placed in a 1.2% sodium hypochlorite solution for 24 hours to remove odours and then placed in a desiccator to dry for approximately two weeks. Other bivalve samples (blue mussel, oyster, pond mussel, zebra mussel) were obtained, already prepared, from lab colleagues. Sample preparation for these involved the removal of organic material and debris using dissection tools and soaking them in a 1.2% sodium hypochlorite solution for 24 hours. Samples were then rinsed with RO water, and care was taken to ensure no debris remained before drying in a desiccator for at least two weeks.

Snails

As seen in Table 3.1 above, empty snail shells were collected from various locations. Most shells contained no organic material. Preliminary cleaning of the shells was done by rinsing them under tap water to remove any surface debris. Next, a large beaker was filled with RO water, and snail shells were placed in the water to soak for 1-2 days to loosen any solidified dirt. Snails were rinsed again using tap water, and dissection tools

were used to clean out hard-to-reach debris. Given the conical shape of the snail shells, extra care had to be taken to clean the whole interior of the shell. To do this, a wash bottle was filled with RO water, and the nozzle inserted into the shell opening to flush out any dirt. Pipe cleaners were also inserted gently into the shells to remove any debris. The process of flushing with water and using a pipe cleaner was repeated until no more dirt was observed. Shell samples were then placed in a desiccator to dry for approximately two weeks.

Turtle

A turtle (Figure 3.2) was retrieved from Kincardine, Ontario near the Bruce Power site. The turtle was identified as a midland painted turtle (*Chrysemys picta marginata*). It is unknown how the turtle died or how long it was deceased before collection, but it is assumed to have been hit by a vehicle in late summer 2022.

FIGURE 3.2: Midland painted turtle collected from Kincardine, Ontario.

The turtle sample was prepared in accordance with biosafety procedures submitted to the Ontario Tech Biosafety Officer. This procedure was established to ensure safe preparation and proper disinfection of the sample. The turtle carcass was placed in a freezer before preparation and removed and thawed slightly before cleaning. To clean the turtle shell, its carcass had to first be broken open. This was done by double bagging the carcass in plastic zip bags and placing it horizontally in a desktop vise grip, which was slowly cranked and the sample readjusted until the turtle carapace separated from

the plastron. Next, precision tools were used to cut and scrape out the soft tissues and remove the elastic membrane from the inner surface of the shell.

Before sample preparation, the plastron and carapace were placed, covered, in a 1.5% hydrogen peroxide solution (a mix of 3% drugstore hydrogen peroxide, diluted twofold with deionized water) for at least 24 hours to disinfect the sample and loosen any remaining soft tissues. Afterwards, the sample was removed from the solution, and tools were used to remove any residual soft tissues. Then the shell pieces were then rinsed with DI water and placed in the fume hood to dry for two weeks.

3.1.4 Sample Grinding

Shells in powder form were required for all experiments in this work. As mentioned in Chapter 2, shells in a fine powdered form are required for ICP-OES sample preparation, and using homogenous powdered shells for irradiation and EPR measurements allows for more accurate results.

Samples must be dry, as moisture can affect EPR spectra by affecting spectra intensity [39]. As seen in Figure 3.3a, a mortar and pestle were used to break the shell sample into smaller pieces and grind them into a fine powder. The top of the mortar was covered with a layer of parafilm, with a hole for the pestle, to minimize particulate escape while grinding (Figure 3.3b). The finely ground shells were placed in Avantech stainless steel mesh sieves and gently shaken to separate shell powder into the desired grain sizes, ranging from <0.1mm to 1mm (Figure 3.4). The nominal opening sizes of the sieves were 1mm (#18), 0.5mm (#35), and 0.1mm (#140). Samples were repeatedly ground and sieved until the desired amount of shell powder was achieved for the desired grain size. Shell samples for different species were all ground separately, and the mortar and pestle were wiped clean with a dry cloth between grinding each species. Shell powder was stored in a desiccator until use.

3.2 ICP-OES Procedures

This section outlines the ICP-OES sample preparation and measurement methodology. Sample preparation methods were developed based on standard EPR sample preparation methods for shelled species [21]. Sample procurement locations are summarized in Table 3.1, and sample collection processes are expanded on in Section 3.2.1 below.

ICP-OES was selected as the elemental analysis method for determining Mn^{2+} concentrations in the various shelled species, as this method has a low detection limit and

(A) (B)

FIGURE 3.3: (A) Shell sample in mortar and pestle, (B) Mortar and pestle covered in parafilm.

FIGURE 3.4: Shell powder of various sizes (From L-R: 1-0.5mm grain size, 0.5-0.1mm grain size, >0.1mm grain size).

is widely used for determining Mn^{2+} concentrations in biological materials [53]. This technique also has the capability of measuring multiple elements simultaneously. A multi-element analysis was not necessary for these experiments, however it could be advantageous in the future if other elemental concentrations need to be determined.

3.2.1 Sample Preparation

The individual ICP-OES samples were prepared by grinding each shell sample into a fine powder (<0.1 mm grain size) following the procedure detailed in Section 3.1. Shell powders of such a small grain size were necessary as the shell had to be dissolved in nitric acid. Two different ICP-OES experiments were performed with similar sample preparation methodologies. The samples for the first experiment were prepared by A. Hassan in 2020 but were not analyzed due to delays caused by the Covid-19 pandemic [21]. Samples used were pond mussel, lobster, pond snail, oyster, zebra mussel, blue mussel, shrimp, and grove snail shells. A. Hassan developed the methodology below used to prepare ICP-OES samples for the first experiment.

Each powdered sample was weighed to 200 mg for the first experiment and then deposited in a 50 mL beaker. Appropriate PPE (lab coat, safety glasses, nitrile gloves) was donned. The beakers were placed on a hot plate inside a fume hood, and 1 mL of 67% concentration nitric acid was added to each beaker. The hot plate was turned on at 60 degrees C to begin the open-vessel digestion process. The samples were heated for approximately 30 minutes or until the powdered sample had dissolved in the acid. The solution was then filtered into a 50 mL volumetric flask using Whatman #42 filter paper. The filter paper was used to separate any solid residue left from open-vessel digestion. After the liquid was filtered, the volumetric flask was filled to mark with deionized water.

Additionally, calibration standard solutions were created using a manganese standard stock solution of 100 mg/L. A blank solution (no manganese) and five calibration standard solutions (0.5, 3, 9, 15, and 20 mg/L) were prepared by diluting the standard stock solution with the appropriate amount of deionized water to reach 50 mL. 1 mL of nitric acid was also added to each standard solution and the blank solution to match the acid concentration used in open-vessel digestion. For example, the 15 mg/L stock solution was prepared by combining 7.5 mL of stock solution with 34 mL of deionized water and 1 mL of nitric acid. Samples were stored in the fume hood until use.

After measuring the samples in the first experiment, many concentrations were below the calibrated range, so it was necessary to carry out a second round of ICP-OES experiments, this time with samples with higher shell, and lower calibration standard concentrations. The range of the calibration standards was also modified, and concentrations were selected based on the first experiment's results. The sample preparation method was modified to prepare samples for the second experiment. In this experiment, the mass of the powdered shell was doubled to 400 mg, and the total volume of the sample was halved, theoretically quadrupling the amount of manganese in the original samples.

Samples used in this experiment were heath snail, grove snail, ocean snail, freshwater snail, pond mussel, zebra mussel, blue mussel, lobster, crab, scallop, and oyster shells. A shrimp sample was not prepared for this experiment, as shrimp had proven ineffective as a candidate species for EPR dosimetry due to its lack of dose-response [21]. To facilitate the dissolution of the shell sample in the acid, three modifications to the methodology were made; the hot plate was heated to 90 degrees C (Figure 3.5) instead of 60 degrees C, 1.1 mL of nitric acid mixture was added instead of 1 mL, and in some cases 1 mL of deionized water was added to the beaker to help the sample dissolve. Instead of 50 mL volumetric flasks, 25 mL flasks were used.

FIGURE 3.5: Samples undergoing the open-vessel digestion process on a hot plate in the fume hood.

Samples were again filtered into the volumetric flasks using Whatman #42 filter paper (Figure 3.6) and filled up to mark (Figure 3.7). Standard solutions with concentrations of 0.1, 0.3, 0.7, 1.5, 3, and 8 mg/L were prepared by diluting the standard stock solution with deionized water and 1.1 mL nitric acid to reach the 25 mL mark. Clean filter papers were weighed before use. After all the samples had fully filtered and the filter paper had dried (Figure 3.8), the papers were weighed again to determine the actual shell mass dissolved in each ICP-OES sample solution. Determining the mass of the remaining sample aided in resolving the actual amount of shell that dissolved into each sample, enabling the mass-averaged Mn^{2+} concentrations to be calculated, leading to more precise results. The results of ICP-OES measurements will be discussed in Chapter 4 of this report.

FIGURE 3.6: Samples filtering into volumetric flasks through filter paper.

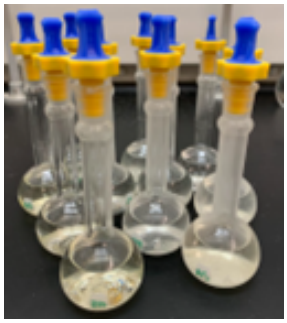

FIGURE 3.7: Prepared ICP-OES samples.

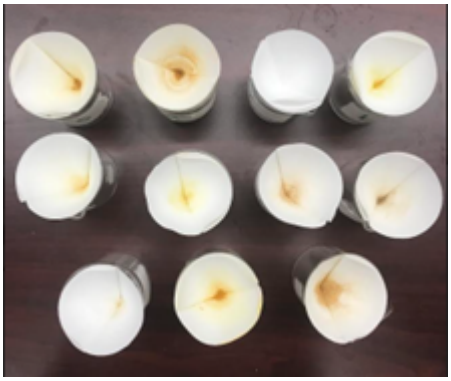

FIGURE 3.8: Dried filter papers with leftover shell residue to be weighed.

3.2.2 ICP-OES Measurements

Samples were analyzed using the Vista-MPX Simultaneous ICP-OES seen in Figure 3.9 Samples were all mixed prior to analysis by inverting the flasks approximately twenty times. The blank sample and calibration standards were analyzed first so that the instrument could develop a calibration curve. The range of concentrations in the calibrating solutions was selected to include the presumed element concentration in the sample solutions. Samples were introduced into the instrument through a small sipper tube placed in the sample solution. The spectrometer analyzed each sample three times, and the processing system averaged the concentrations to output one final elemental concentration value. The sipper tube was placed in water between samples to remove traces of the previous sample from the system. Appendix A discusses an additional experiment that was commenced which involved breeding grove snails with the goal of controlling Mn^{2+} concentrations in their shells.

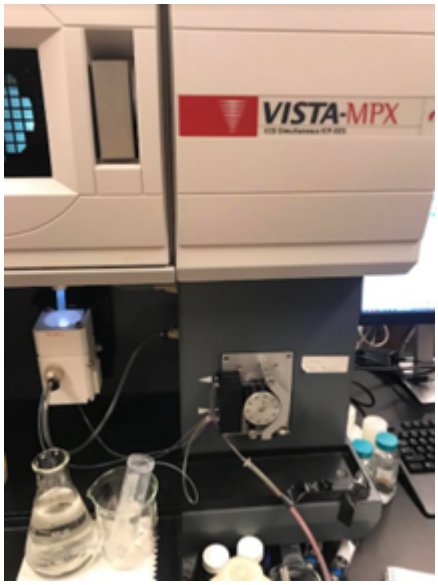

FIGURE 3.9: Sample being analyzed with the Vista-MPX ICP-OES.

The samples were also briefly analyzed with X-ray fluorescence (XRF) to determine if their elemental composition could be resolved. However, due to the higher detection limits of XRF compared to other analytical chemistry techniques, no discernible XRF patterns were observed. The detection limits of the specific instrument could also have been too high to calculate Mn^{2+} concentrations within the sample reasonably.

3.3 EPR Measurement Procedures

EPR is the preferred dosimetry technique for this work and was used to analyze both manganese(2+) peaks in EPR spectra for the Mn^{2+} investigation and to assess the dose-response in terrestrial snail and turtle shells. This section will detail the steps involved in preparing and irradiating samples for EPR analysis, and determining EPR measurement parameters. Sample preparation methods for shelled species were adapted based on processes developed by A. Hassan and M. Tzivaki [21] [29].

3.3.1 EPR Sample Preparation and Irradiation

The Bruker EMX-Micro X-band EPR spectrometer was used for all EPR measurements. The Hopewell Design G10 cesium-137 gamma source was used for all irradiations, with an approximate dose rate of 0.189 Gy/hr. The following methodology applies to all shell samples used in this work.

Powdered shell samples were prepared using the methods outlined in Section 3.1. Grain sizes of 0.1-0.5mm were selected based on the literature, as grain sizes below 0.1 mm have a lower sensitivity, resulting in more variation in the EPR spectrum [9]. At the same time, the orientation effects become dominant at larger grain sizes, and sample anisotropy becomes a concern [27]. The shell samples needed to be dry, as moisture can affect EPR spectra by affecting spectra intensity.

Wilmad LabGlass Quartz EPR tubes (710-SQ-100M) with an inner diameter of 4mm and outer diameter of 5mm were used to hold the shell samples for EPR measurements. The process of preparing an EPR sample is as follows:

- Empty tubes were marked at heights of 8.3 cm and 3.4 cm from the bottom of the tube using digital calipers (Figure 3.10) A small piece of masking tape was placed around the tube right above the 8.3 cm mark for labeling the sample (Figure 3.11).
- The empty tube was weighed using a digital balance, and its mass was recorded.
- Using a funnel, the sample was then filled and packed into the EPR tubes up to approximately the 3.4 cm line. Samples were filled to just slightly over the 3.4 cm line to account for any sample loss during transfer between microcentrifuge tubes and EPR tubes. The EPR tubes were gently tapped against a hard surface about 30 times to ensure that the sample was compacted within the tubes. The samples were filled to a height of 3.4cm, as that is the active height of the resonator within the EPR.

FIGURE 3.10: Using digital calipers to mark EPR tubes at heights of 8.3 cm and 3.4 cm.

FIGURE 3.11: EPR tubes with masking tape marking the 8.3 cm height.

- The sample tube was weighed again using a digital balance, and its mass was recorded. The unirradiated sample mass can be calculated by subtracting the filled tube's mass from the empty tube's mass.

- Wearing gloves, the filled EPR tubes were cleaned using Kimtech™ Kimwipes and ethanol, taking care to remove the marking at 3.4 cm. Kimwipes were used as they do not leave residue on the tubes that can cause unwanted signals in the EPR spectra. Samples were set down on a dry Kimwipe to dry for 2-3 minutes and were then carefully inserted into the EPR cavity up to the 8.3 cm mark. The placement of 8.3 cm was chosen as it positions the sample in the EPR cavity at the active resonator, and also ensures the exact placement of every sample to ensure consistency with EPR measurements.

- Tubes were inserted into the EPR up to the 8.3 cm mark, and background spectra of the samples were taken by measuring unirradiated samples using the desired parameters. Measurements of each unirradiated sample were always taken prior to

irradiation as a control background. Measurement parameters will be discussed in the next section. EPR spectra were obtained using the Bruker WinEPR Acquisition software.

- To prepare the samples for irradiation, they were carefully transferred into 0.6 mL microcentrifuge tubes and weighed again before being attached to a 3D printed sample holder as seen in Figure 3.12.

FIGURE 3.12: Prepared samples in the 3D sample holder.

- At least one alanine dosimeter was included in the sample holder as a reference dosimeter. Alanine reference dosimetry will be discussed further in Section 3.4.2.
- Samples in the holder were placed 34 cm from the center of the Hopewell G10 cesium-137 source (Figure 3.13 located on campus at Ontario Tech U and were irradiated to the desired dose. Samples were placed at this location as it was the distance at which the alanine calibration curve was created [21].
- After irradiation, samples were transferred back into the same EPR tube used for background measurements and weighed again.
- Tubes were then cleaned with Kimwipes and ethanol, and samples were measured again using the same parameters used to take background measurements.
- All EPR spectra were processed using the Bruker WinEPR Processing software.

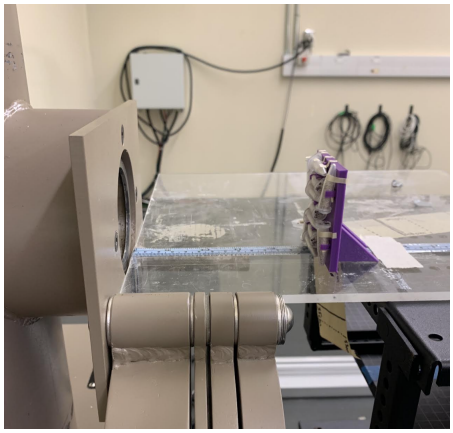

FIGURE 3.13: Sample holder placed 34 cm from the center of the gamma source.

3.3.2 EPR Measurement Parameters

The Bruker EMX-Micro X-band EPR spectrometer was used for all EPR measurements. The EPR parameters at which samples are analyzed can significantly affect the resulting spectra. Specific measurement parameters were developed for analyzing different shell samples, which will be discussed in Sections 3.4.1 and 3.4.4. This section will explain the general purpose of various EPR parameters and how they are determined. Parameters explored in this section are the modulation amplitude, modulation frequency, time constant, microwave power, conversion time, receiver gain, time constant, number of scans, resolution, sweep width, and sweep time.

Choosing the most suitable modulation amplitude, modulation frequency, and time constant must be done carefully, as each parameter can distort the EPR signal, making spectra analysis complicated [24]. Increasing the modulation amplitude results in an increased EPR signal intensity. However, if the modulation amplitude is too large, the signal can become distorted, as seen in Figure 3.14 [24]. Therefore the literature suggests it is best to keep the modulation amplitude as approximately 1/10 of the narrowest signal in the EPR spectrum for optimal sensitivity [24] [29]. The modulation frequency, which, if too high, can broaden and dilute signals, is commonly chosen to be 100 kHz which the literature suggests should be used for optimal sensitivity [24].

The time constant is used to filter out noise by slowing the response time of the spectrometer to improve the signal-to-noise ratio [24]. If the chosen time constant is too long, then the signal can become distorted or even disappear entirely, as seen in Figure 3.15 [24]. The literature suggests that the time constant should be set to less than 1/10

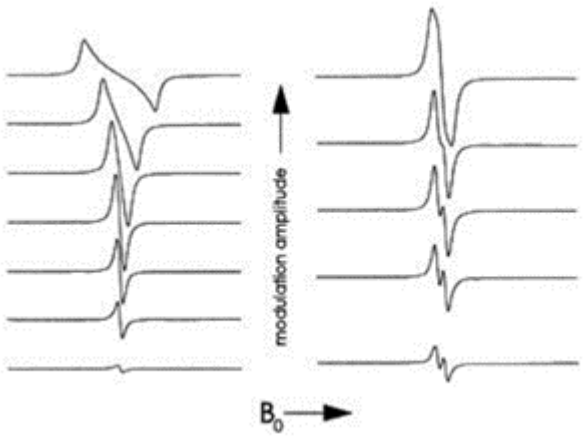

FIGURE 3.14: The effects on the signal shape and intensity with increased modulation amplitude [147].

of the time taken to scan the narrowest line in the spectrum [147]. Equation 3.1 enables the time constant to be determined:

$$\frac{\text{spectrum width [G]}}{\text{narrowest line width [G]}} \times \frac{\text{time constant [s]}}{\text{sweep time [s]}} < 0.1 \tag{3.1}$$

This equation will be applied when defining parameters for different shell samples.

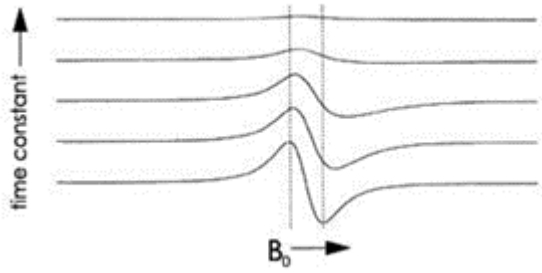

FIGURE 3.15: The effect on the signal shape and intensity with an increasing time constant [147].

Microwave power is another parameter that must be determined. The intensity of the EPR signal grows with the square root of the power, but at higher powers the signal diminishes in an effect called saturation [147]. When determining optimal parameters for EPR operation, it is suggested to perform a power saturation study to ensure that the microwave power is not saturated [147]. A power saturation study is conducted by measuring a sample at different microwave powers, and measuring the corresponding

peak-to-peak intensity of the spectra. The spectrum intensity will increase linearly with microwave power up to a certain point when the intensity will begin to deviate. The signal becomes saturated at this point, and the corresponding microwave power should be used for EPR measurements. It is also worth noting that the anisotropy of a sample is increased as the microwave power increases [148].

The conversion time is the time it takes for the analog-to-digital converter to accumulate the signal at each data point [147]. If a conversion time is too long, the spectrum will decrease in resolution. A time constant longer than the conversion time will improve the signal-to-noise ratio; however, if it is considerably longer than the conversion time, the lineshape and position will be distorted [147].

The number of data points is the number of channels where data is accumulated over the width of the spectrum, also called the resolution, and represents the number of steps taken along the width of the magnetic field. As a rule, at least 10 data points should be taken over the narrowest line in the spectrum [147].

The sweep time is the time it takes to acquire the data at every data point and is calculated as the product of the number of data points and the conversion time [147].

The number of scans is the number of times the spectrum is amassed across the magnetic field. The spectra are signal-averaged when there are multiple scans, and in doing so, the random noise will decrease as the square root of the number of scans averaged, and the signal-to-noise ratio will improve [24].

The sweep width and the center field determine which magnetic field region the signal is measured over. Many of the radiation-induced peaks of interest occur at magnetic field values around 3500 G (g=2), so the EPR studies in this work will be focused on that region of the magnetic field [17].

Lastly, the gain is increased or decreased to adjust the display size of the spectra within the processing system [147]. The gain must be large enough that the signal does not get clipped but not too small that important peaks cannot be identified.

3.4 Experimental Studies Using EPR

This section will detail the various experiments performed using the Bruker EPR spectrometer. This includes the methodology for assessing the Mn^{2+} peaks in the EPR spectra of various shelled species outlined earlier. This section will also detail the use of alanine reference dosimetry, and the methodology used when measuring spectra for the terrestrial snail dose-response curves.

3.4.1 Manganese(2+) Study

This section will detail the EPR parameter selection process for the manganese(2+) investigation of shelled species and the sample measurement process.

Optimal EPR parameters can vary depending on sample composition. As crustacean and mollusc species have slightly different shell compositions (mollusc shells are 95-99% $CaCO_3$, while crustacean shells are up to 75% $CaCO_3$ [92][112], it was presumed that their optimal parameters would vary. As the objective of the Mn^{2+} investigation into shelled species is to be able to quantitatively compare all of the spectra, it was necessary to confirm that the same parameters could be used for measuring both the mollusc and crustacean shells without resulting in over-saturation of the EPR signal for one sample group.

This was achieved by experimentally determining the optimal microwave power for molluscs and crustacea and selecting the lowest of the two, which would result in no over-saturation for either sample group. The basis behind performing a power saturation study, as explained in Section 3.3.1, is to ensure that the microwave power selected does not result in oversaturation of the EPR signal.

An unirradiated terrestrial grove snail (*Cepaea nemoralis*) shell sample was used to conduct the power saturation study on molluscs, and an unirradiated American lobster (*Homarus americanus*) shell was used to conduct the power saturation study on crustacea. All other parameters except the microwave power were held constant to perform the power saturation study. The microwave power was increased in small increments from 0.2 to 2 mW, and the increase in the intensity of the native central peaks in the resulting EPR spectra were measured to assess the effects of increasing microwave power. The optimal microwave power for the species was the point at which the square root of the power began to deviate from linearity. The power saturation curves are shown as the square root of the microwave power vs the signal amplitude since the signal amplitude increases with the square root of the microwave power [147]. Results of the power saturation study for molluscs are shown in Figure 3.16, and the power saturation point was identified at 0.94 mW.

The power saturation curve for the American lobster shell sample is seen in Figure 3.17, where an ideal microwave power of 1.8 mW was identified based on measuring spectra at powers between 0.4 and 4 mW. The peak-to-peak intensity increase of the first Mn^{2+} peak was measured for this study.

Since the spectra of mollusc shells become saturated at 0.94 mW while crustacean shells become saturated at 1.8 mW, a microwave power of 0.94 mW was selected as that

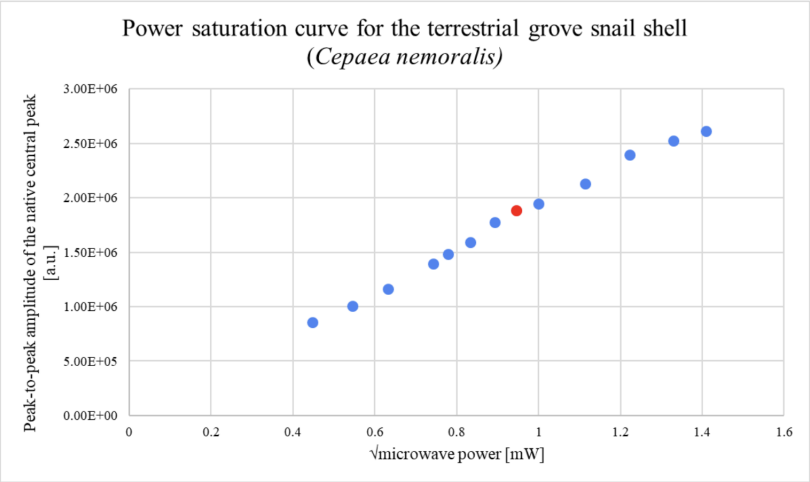

FIGURE 3.16: Power saturation curve for an unirradiated grove snail sample. The optimal microwave power occurs at 0.9 mW where a slight deviation from linearity occurs.

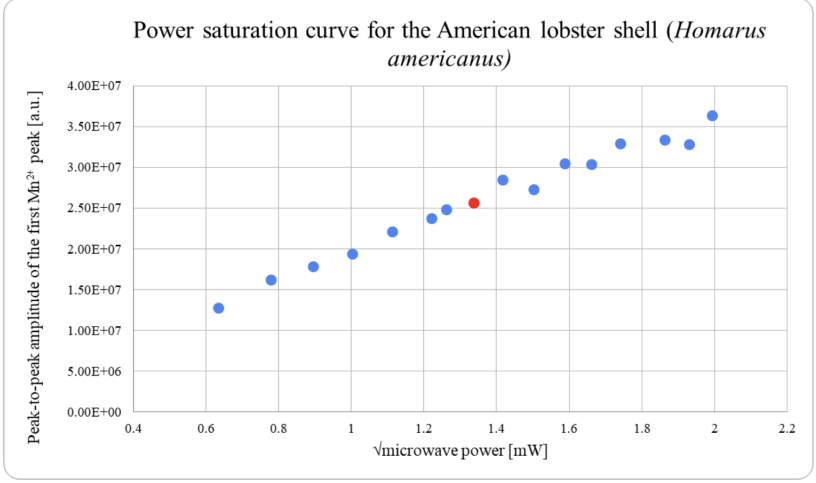

FIGURE 3.17: Power saturation curve for an unirradiated lobster sample. The optimal microwave power occurs at 1.8 mW.

would result in no oversaturation for either sample group.

Along with the microwave power, the modulation amplitude is another parameter that can greatly impact the shape and intensity of the EPR spectra. The signal will become distorted if the modulation amplitude is too large [24]. The ideal modulation amplitude is found at the largest amplitude at which the signal linewidth stays stable [29]. The central native peak on the grove snail EPR spectrum was used to measure the change in linewidth. The literature also suggests keeping the modulation amplitude as

approximately 1/10 of the narrowest signal in the EPR spectrum [29]. The narrowest signal linewidth in the EPR spectrum for terrestrial grove snails was identified as 5.3 G. Measurements of the signal linewidth versus modulation amplitude for grove snails are shown in Figure 3.18 The modulation amplitude was selected at 0.4 G as it fell within the region of stable linewidth and was less than 1/10 of the narrowest signal in the EPR spectrum.

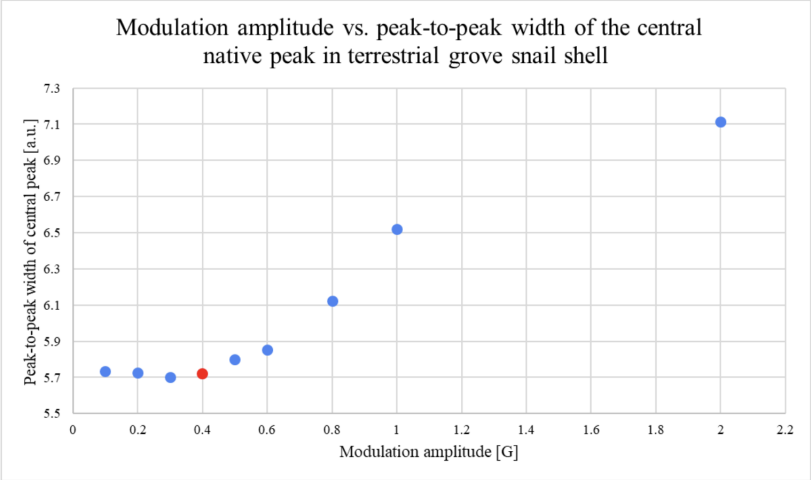

FIGURE 3.18: Peak-top-peak width of the central peak dependent vs modulation amplitude. A modulation amplitude of 0.4 G was selected as it is less than 1/10 the narrowest signal in the EPR spectrum and it falls within a region of stable linewidth.

A modulation frequency of 100 kHz was selected as that is what the literature suggests [24]. The receiver gain was selected as 1×10^4, as that resulted in a spectrum that was not clipped off, nor had a large S/N ratio. The sweep width was selected as 800 G and the center field at 3500 G in order to capture all six Mn^{2+} peaks on the spectra. The number of scans was set to 5, and the resolution was selected as 8000 data points to lessen the noise in the spectra and increase the signal-to-noise ratios. A conversion time of 10 ms was selected to not cause a decrease in signal resolution. The resultant sweep time was 80 s, based on the product of the scan time and resolution (10 ms $\times$ 80 data points = 80 s).

In order to select a proper time constant, Equation 3.1 was used. The narrowest line width in the background spectrum of the grove snail shell was 5.3 G, the total spectrum width was 800 G, and the sweep time was 80 s. Using this data, a time constant of 20.48 ms was chosen based on the calculation below.

$$\frac{800 \text{ G}}{5.3 \text{ G}} \times \frac{20.48 \text{ ms}}{80 \text{ s}} = 0.038 < 0.1$$

All of the selected EPR parameters are seen in Table 3.2 below. Saturation tests using these parameters were briefly conducted on every other shell sample in the Mn^{2+} investigation, and it was determined that these parameters were suitable for measuring the rest of the shell samples.

TABLE 3.2: EPR parameters for measuring Mn^{2+} signal intensity in shelled species.

Parameter	Value
Microwave Power	0.9 mW
Modulation Amplitude	0.4 G
Modulation Frequency	100 kHz
Receiver Gain	$1.00 \cdot 10^4$
Conversion Time	10.0 ms
Time Constant	20.48 ms
Number of Scans	5
Center Field	3500 G
Sweep Width	800 G
Sweep Time	80 s
Resolution	8000

Once the ideal parameters were determined, all mollusc and crustacean shell samples were measured following the EPR sample measurement process outlined in Section 3.3.1. According to the literature, the peak-to-peak intensity of the first Mn^{2+} peak, as seen in Figure 2.6, should be used for assessing the effects of Mn^{2+} on spectra [75]. Each shell sample was measured three times, and the intensity of the first manganese peak was averaged. As each shell sample had different densities, the spectra intensities were density-averaged. Manganese(2+) signal intensities were qualitatively compared between species, and the results of this experiment will be discussed in Section 4.2.

3.4.2 Alanine Powder Reference Dosimetry

Using a material that can function as a reference dosimeter when performing EPR experiments is crucial to achieving accurate results. Alanine powder is one such material. Determining the proportionality of the peak-to-peak intensity of the EPR spectra to the absorbed dose allows for materials such as alanine to be used as dosimeters. Reference dosimeters and calibration curves are very helpful in laboratory settings as they allow for samples of unknown doses to be measured. According to the International Atomic

Energy Agency (IAEA), accuracy, consistency, and traceability are all essential characteristics of radiation dosimeters [149]. Alanine powder is an excellent candidate as a reference dosimeter using EPR as it satisfies these conditions. It is also sensitive to ionizing radiation, and forms stable, long-lived free radicals in proportion to the dose [150].

Alanine is an amino acid that comes as a white crystalline powder. When alanine powder [$CH_3-CH(NH_2)-COOH$] is exposed to ionizing radiation, it is deaminated into the stable radical [$CH_3-CH-COOH^-$], which can be measured using EPR. The concentration of free radicals present in the alanine sample should show a linear response to the applied radiation dose [35]. The alanine spectra show three distinct peaks, as seen in Figure 3.19, with the central peak frequently used for the peak-to-peak measurements [25].

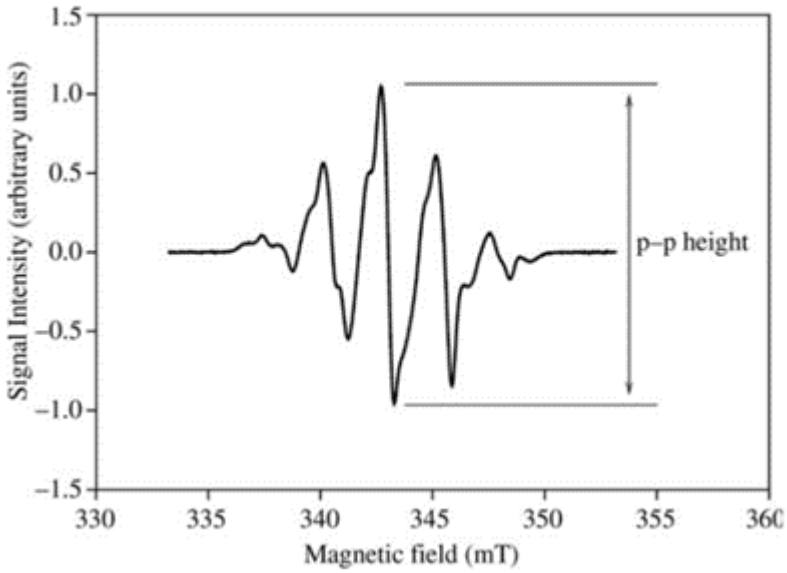

FIGURE 3.19: Example of an irradiated alanine spectrum with three distinct peaks [151].

Alanine powder was used as a reference dosimeter in this work. An alanine calibration curve developed by A. Hassan for EPR dosimetry (seen in Figure 3.20) was specifically used in this thesis. Reference dosimetry work using alanine involved including at least one alanine sample in each batch of samples to be irradiated to determine the dose that the samples received.

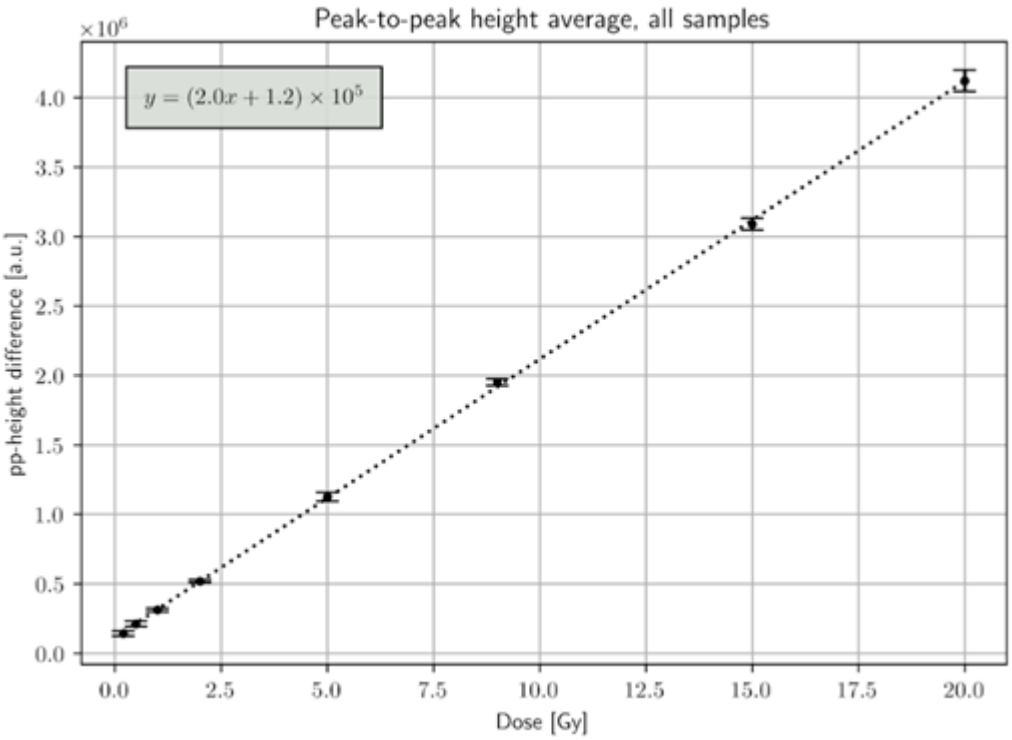

FIGURE 3.20: Alanine dose-response calibration curve [152].

3.4.3 Terrestrial Snail Shell Irradiation Measurements

This section will describe the process of measuring the dose-response grove snail and heath snail shells.

Grove Snail

It was deemed necessary to create a refined dose-response curve for grove snail (*Cepaea nemoralis*) shells based on recommendations from A. Hassan's previous work, and results from the manganese(2+) investigation. In A. Hassan's preliminary work into determining the dose-response of terrestrial grove snails, a dose-response curve was created using one sample per dose group, irradiated to 2, 10, and 20 Gy. Linearity was observed between the dose and the intensity of the radiation-induced peak [21]. It was suggested that a refined dose-response curve be generated using more samples to allow for statistical evaluation of the peak-to-peak intensities at each dose group. Further suggestions include modifying the EPR parameters by increasing the number of scans and the modulation amplitude to attempt to resolve the minimum detectable dose below 2 Gy. This experiment aimed

to make a feasible dose-response curve for *Cepaea nemoralis* that can be used in case of large (high-dose) environmental exposures. Also, based on observations from the Mn^{2+} study/investigation, grove snail shells had low-intensity Mn^{2+} peaks and low Mn^{2+} concentrations, so this irradiation study was used to confirm a dose-response in the sample due to this correlation.

To create the dose-response curve, first, the dose points to which the shells should be irradiated were determined. Dose points of 2, 3, 5, 7, and 10 Gy were selected as 2 Gy was the minimum detectable dose identified in this species. Each dose group consisted of ten shell samples ground to grain sizes between 0.5 mm to 0.1 mm, and one alanine dosimeter was included for reference dosimetry. Another two samples were irradiated to 1.5 Gy to determine if a lower detectable dose could be resolved. The shells were ground following the same methodology in Section 3.1. The samples were then measured using EPR at the parameters listed in Table 3.2, following the method outlined in Section 3.3.1. These parameters take into account the suggestions by A. Hassan for lowering the dose detection limit; the number of scans was increased from 1 to 5, and the modulation amplitude was increased from 0.3 G to 0.4 G. Each sample was measured three times, and the peak-to-peak intensities of the radiation-induced peak were averaged per sample.

Additionally, samples were rotated at 90-degree increments within the EPR cavity to explore the effects of grain size on EPR spectra and to confirm sample isotropy. It is suggested in the literature that if sample grain sizes are too large, the effects of anisotropy will be seen, affecting the accuracy of EPR results [27]. The samples were rotated by hand as a goniometer was not available at the time. Each 10 Gy dose group shell sample was rotated within the shell cavity at 90-degree increments between runs. It was determined that the effects of grain size were negligible on EPR spectra after measuring and comparing the spectrum intensities of each sample at different rotations. This confirms that the selected grain size (0.1 - 0.5 mm) results in sample isotropy. Therefore, subsequent EPR measurements were not taken at different rotations for the rest of the dose groups.

For ease of reference within this thesis, the samples were numbered according to dose group and sample number within the group. The numbering follows a format of "GSx-y" where x is the dose group and y is the sample number within the dose group. For example, GS5-9 represents the ninth sample within the 5 Gy dose group of grove snails.

Alanine dosimetry was also performed in each dose group using the alanine dosimeter and the alanine calibration curve developed by A. Hassan for the G10 source (Figure 3.20). Reference dosimetry using alanine was carried out to confirm the dose to each sample group, and the results are seen in Table 3.3 below. Each alanine sample was measured three times. The dose-response curve will be generated by plotting the measured doses

versus radiation-induced peak intensities. Results from this dose-response experiment are discussed in Chapter 4.

TABLE 3.3: Alanine reference dosimetry measured dose results for each *Cepaea nemoralis* dose group.

Intended Dose [Gy]	Measured Dose [Gy]
2	2.11 ± 0.04
3	3.22 ± 0.06
5	4.94 ± 0.05
7	6.87 ± 0.03
10	9.93 ± 0.03

Heath Snail

After identifying a linear dose-response within the shell of one terrestrial gastropod species, it was deemed necessary to determine if other terrestrial gastropod shells can also function as natural fortuitous dosimeters. As such, an experiment was conducted on the dose-response of the shell of another terrestrial snail species, the heath snail (*Xerolenta obvia*).

The heath snail shell, similar to the grove snail (*Cepaea nemoralis*) shell, showed low Mn^{2+} concentrations and low Mn^{2+} spectra intensities in the Mn^{2+} study, so it was deemed necessary to determine if the species also showed a dose-response at low doses. The shells were ground and measured using the methods in Section 3.2 and 3.3.1, and the EPR parameters in Table 3.2 Heath snail shell samples were irradiated to doses of 2, 3, 5, 7, and 10 Gy, and each dose group consisted of two shell samples and one alanine dosimeter. It was not possible to measure ten shell samples per dose group due to limited sample availability. Additionally, in this experiment, the snail shells were irradiated additively. This approach was more efficient than irradiating each sample group individually. A numbering format similar to the one used for grove snails was used to identify the different heath snail samples. Alanine reference dosimetry was conducted after each irradiation, and the results are in Table 3.4. Results from this experiment are discussed in Chapter 5.

3.4.4 Turtle Shell Irradiation Measurements

It was deemed necessary to investigate the EPR dose response of turtle shells in the low-dose range, as no previous literature has been reported on the subject.

TABLE 3.4: Alanine reference dosimetry measured dose results for each *Xerolenta obvia* dose group.

Intended Dose [Gy]	Measured Dose [Gy]
2	2.317 ± 0.005
3	3.453 ± 0.025
5	5.664 ± 0.065
7	7.946 ± 0.085
10	11.105 ± 0.0095

In total, ten turtle shell samples, comprising seven carapace and three plastron samples, were prepared. The carapace and plastron samples were prepared and measured separately as it was unknown whether the two parts would differ in spectra or radiation sensitivities. Before irradiation, background measurements were taken for both the carapace and plastron samples, and the resulting spectra were identical, indicating similar compositions of both shell parts.

In order to analyze the turtle shells using EPR, the operational parameters had to be determined. Optimal EPR parameters are species-dependent and vary based on the sample's composition. As little is known about the ratios of different molecules composing turtle shells, various parameter sets were tested to measure the unirradiated background signal of the shell samples (Parameter Set 1). Parameters used in this thesis to measure the mollusc and crustacean shells were used. Additionally, parameters that have been used to measure rainbow trout bones [29] (Parameter Set 2), human teeth [153] (Parameter Set 3), and human bones [154] (Parameter Set 4) were all tested as well. The four parameter sets are listed in Table 3.5. Figure 3.21 shows the background spectra taken using these parameter sets. In each spectrum the internal standard marker is seen at a magnetic field value of 3550 G and a native, and one native peak is seen at a magnetic field value of 3490 G.

After measuring the background spectra, the shell samples were irradiated to doses of 2, 3, 6, 9.5, and 19 Gy following the same procedure as in Section 3.3. Shell samples were additively irradiated, and after each irradiation, every sample was measured using EPR to determine if there was a dose-response. Results of this experiment will be discussed in Chapter 5.

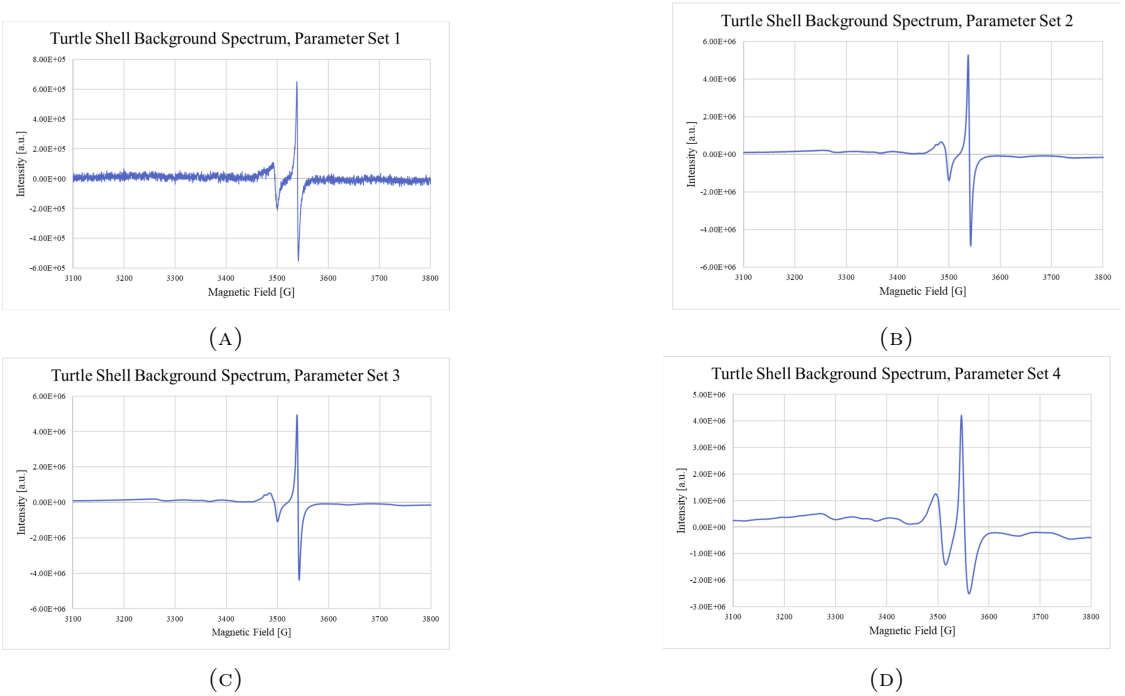

FIGURE 3.21: Resulting background spectra of turtle shells being measured using the four parameter sets listed in Table 3.5.

TABLE 3.5: EPR parameters for measuring Mn^{2+} signal intensity in shelled species.

Parameter	Set 1 (mollusc)	Set 2 (trout)	Set 3 (teeth)	Set 4 (bone)
Microwave Power [mW]	0.9	9.87	24.22	13.03
Modulation Amplitude G	0.4 G	6	4	2.5
Modulation Frequency [kHz]	100	100	100	100
Receiver Gain	$1.00 \cdot 10^4$	$1.00 \cdot 10^4$	$1.00 \cdot 10^4$	$1.00 \cdot 10^4$
Conversion Time [ms]	10.0	50	41	10.24
Time Constant [ms]	20.48	10.24	327.68	81.92
Number of Scans	5	1	1	6
Center Field [G]	3500	3500	3500	3500
Sweep Width [G]	800	800	800	800
Sweep Time [s]	80	100	328	5.243
Resolution	8000	2000	8000	512

Summary

This chapter discusses the methods of shell sample selection, collection, and cleaning. Sample preparation techniques for ICP-OES and EPR analysis were detailed, and sample measurement methodologies were also discussed. The experiments in this thesis were divided into three main sections. First, an investigation into the effects of manganese(2+) in shelled species was conducted, to determine if there was a correlation between the concentrations of Mn^{2+} in the shells and Mn^{2+} peak intensity in the EPR spectra. It is hypothesized that identifying shells with low correlations between these two factors could indicate their suitability as materials for low-dose EPR studies. Second, based on results obtained from the manganese(2+) investigation, the dose-responses of shelled species identified as having low-intensity Mn^{2+} peaks and low Mn^{2+} concentrations ware investigated. The two species that met these criteria were terrestrial grove snails (*Cepaea nemoralis*) and heath snails (*Xerolenta obvia*). Lastly, an experiment examining the potential dose-response of turtle shells was performed.

Chapter 4

Results and Discussion - Manganese(2+) Study

The presence of Mn^{2+} peaks of differing intensities in the EPR spectra of various shelled species has prompted the need to examine if there is a correlation between the concentrations of Mn^{2+} in shells and the intensity of the Mn^{2+} peaks in the EPR spectra of a species.

Inductively coupled plasma-optical emission spectroscopy (ICP-OES) is an analytical method for determining the elemental composition of a sample. This technique relies on the emission of light at various wavelengths for analysis. For this technique to work, a solution containing the dissolved shell sample to be analyzed is aerosolized via a pump and then injected into an extremely high-heat (5000 K) argon plasma. The sample is atomized and ionized in this plasma because of the high thermal energy. When the excited electrons drop back to ground state, energy in the form of light is released. This ICP-OES process looks for light emissions at a wavelength of 257.10 nm which corresponds to the emission wavelength of Mn^{2+}. High-intensity Mn^{2+} peaks in EPR spectra can obstruct the radiation-induced peaks at low doses, so Mn^{2+} concentrations were analyzed in various shell samples using ICP-OES. It was hypothesized that the shells displaying higher-intensity Mn^{2+} peaks in their EPR spectra should also reflect a higher concentration of Mn^{2+} within the shells.

The objective of this study was first to determine the Mn^{2+} concentration in shell samples using ICP-OES and then compare those concentrations with the intensity of the Mn^{2+} peaks from each species using EPR. The desired result is to observe that species with low Mn^{2+} concentrations also have low Mn^{2+} EPR intensities. If samples identified as having this correlation also have a radiation dose-response at lower doses, then this method of investigating the Mn^{2+} concentrations and peaks in a sample could be used as a tool for selecting suitable shelled species for EPR dosimetry. Shell samples

of marine, freshwater, and terrestrial molluscs were analyzed. Two ICP-OES experiments were performed, with ten and eleven shell samples in each experiment respectively.

4.1 ICP-OES Results

The first ICP-OES analysis was done on ten shell samples previously prepared in March 2020 by A. Hassan [21]. The calibration standards used for the first experiment were 0.5, 3, 9, 15, and 20 mg/L. These calibration standard concentrations were chosen using educated guesses, as it was unknown what the Mn^{2+} concentrations would be in the samples. For ICP-OES results to be accurate, the ion concentrations must fall within the calibrated range. The Mn^{2+} concentrations found in the first round of ICP-OES experiments are presented in Table 4.1 and fall mainly outside the calibrated concentrations, indicating that in the second experiment, the standard solution and sample concentrations should be adjusted to fall better within the calibrated range and improve accuracy.

TABLE 4.1: First experiment results: Manganese(2+) ion concentrations for shelled mollusc and crustacean species. Highlighted results fell within the calibrated range, unhighlighted results did not.

Sample	Mn^{2+} Concentration (mg/L)
Pond Mussel	1.274
Lobster	0.539
Pond Snail	0.311
Oyster	0.195
Zebra Mussel-2	0.098
Zebra Mussel-3	0.086
Blue Mussel	0.078
Shrimp	0.078
Grove Snail	0.074
Zebra Mussel-1	0.063

Standard solutions of 0.1, 0.3, 0.7, 1.5, 3, and 8 mg/L were prepared in the second experiment. Results for this experiment are presented in Table 4.2. Mn^{2+} concentrations in eight of the eleven samples fall within the calibrated range. The scallop, zebra mussel, and blue mussel Mn^{2+} concentrations are below the range, indicating that the concentration of Mn^{2+} in these shells is <0.1 mg/L.

The samples yielded similar Mn^{2+} concentration versus peak-to-peak intensity of Mn^{2+} peaks in both experiments. However, in the first experiment, most of the results were inaccurate due to the concentrations falling outside the calibrated range.

TABLE 4.2: Second experiment results: Manganese(2+) ion concentrations shelled mollusc and crustacean species. Concentrations were mass-corrected. Highlighted results fell within the calibrated range, unhighlighted results did not.

Sample	Mn^{2+} Concentration (mg/L)
Pond Mussel	3.869
Freshwater Snail	2.128
Lobster	1.609
Oyster	0.783
Ocean Snail	0.488
Grove Snail	0.199
Heath Snail	0.181
Crab	0.153
Scallop	0.089
Zebra Mussel	0.065
Blue Mussel	0.028

Table 4.3 summarizes the factors that can affect the Mn^{2+} concentration in a shelled species, such as its dominant calcium carbonate polymorph, the type of animal and habitat, and its colour. Based on the literature review, it is known that species made of aragonite are reported to contain less manganese [56]. Species living in saltwater are also said to contain less manganese, as saltwater has less Mn^{2+} than freshwater [53]. Shells of marine animals are said to be composed mainly of calcite, with some shells showing mixed morphology [61]. Freshwater shells are said to be composed mainly of aragonite [56]. Terrestrial molluscs are mainly composed of aragonite, and the amount of Mn^{2+} in their environment largely depends on their location [99]. Shell colour is also hypothesized to play a role in Mn^{2+} concentrations, where darker shells are said to contain less manganese [10].

TABLE 4.3: Summary of dominant $CaCO_3$ polymorph and habitat for all species involved in the Mn^{2+} investigation.

Samples	Dominant $CaCO_3$ polymorph	Type
Shrimp (*Penaeus monodon*)	Calcite[1]	Marine crustacean
Lobster (*Homarus americanus*)	Calcite[1]	Marine crustacean
Dungeness crab (*Metacarcinus magister*)	Calcite[1]	Marine crustacean
Eastern oyster (*Crassostrea virginica*)	Calcite[2]	Marine bivalve
Blue mussel (*Mytilus edulis*)	Calcite and aragonite[3]	Marine bivalve
Scallop (*Pecten* sp.)	Calcite[4]	Marine bivalve
Ocean snail (*Littorina littorea*)	Calcite and aragonite[5]	Marine gastropod
Pond mussel (*Elliptio complanata*)	Aragonite[6]	Freshwater bivalve
Zebra mussel (*Dreissena polymorpha*)	Aragonite[6]	Freshwater bivalve
Pond snail (*Lymnaea stagnalis*)	Aragonite or calcite[7]	Freshwater gastropod
Freshwater snail (*Viviparus georgianus*)	Aragonite or calcite[7]	Freshwater gastropod
Grove snail (*Cepaea nemoralis*)	Aragonite[8]	Terrestrial gastropod
Heath snail (*Xerolenta obvia*)	Aragonite[8]	Terrestrial gastropod

1. Shells of decapod crustaceans have calcite as their main $CaCO_3$ polymorph [61].
2. Oyster shells are composed mainly of calcite [155].
3. *Mytilus edulis* shells are reported to contain both calcite and aragonite in more equal ratios [64][156].
4. Shells of marine bivalves are primarily composed of calcite [94].
5. Shells of *Littorina littorea* are composed of calcite and aragonite in more equal parts [157] [158].
6. Freshwater bivalve shells are reported to be composed of aragonite [56].
7. While most freshwater mollusc shells are composed primarily of aragonite, some freshwater gastropod species have calcite as their main polymorph [89]. The dominating $CaCO_3$ polymorph in freshwater gastropods can be species-specific [97].
8. Terrestrial gastropods are mainly composed of aragonite [99].

Based on the predominant calcium carbonate polymorph and habitat of each of the samples analyzed (as summarized in Table 4.3), it is expected that shells composed of calcite (marine species) and shells of freshwater animals will have the highest Mn^{2+} concentrations. Based on this assumption, the Mn^{2+} concentrations identified in the pond mussel, pond snail, and freshwater snail samples are consistent with the assumption that their freshwater environments and sediment habitats contribute significantly to Mn^{2+} uptake. The Mn^{2+} concentrations identified in the blue mussel, zebra mussel, scallop, crab and shrimp shells are lower than expected.

Due to their calcitic composition, the blue mussel, scallop, and shrimp shells were expected to contain much higher concentrations of Mn^{2+}. The low Mn^{2+} concentration in the blue mussel is especially surprising given its dark colour. These discrepancies could be because these particular samples were all farmed instead of harvested from the wild. Their origins are unknown as they were all purchased from the grocery store. Farmed molluscs are typically seeded on ropes and rafts and suspended in the water instead of on the ocean floor sediment where most of the Mn^{2+} is bioaccumulated [159].

Zebra mussels also show very low Mn^{2+} concentrations, which is surprising given that they are freshwater molluscs, and other freshwater molluscs in this study show much higher Mn^{2+} concentrations. On the other hand, these results align with the literature, as very low-intensity Mn^{2+} peaks and low detection limits (0.2 Gy) have been reported in zebra mussels, which implies that the Mn^{2+} concentrations in their shells are not very high.

The bioaccumulation of metals into zebra mussel shells is reported to be very dependent on the site where the sample was collected [160], which could explain the limited amounts of Mn^{2+} in these samples. The low Mn^{2+} concentration in the crab sample is also assumed to be due to the specific animal's habitat. The unexpectedly low Mn^{2+} concentrations in some species emphasizes the importance of knowing where the animal was collected from, in order to assess their predicted Mn^{2+} levels.

4.2 EPR Results

The intensity of the first Mn^{2+} EPR peak of each sample from the second ICP-OES experiment is presented in Table 4.4 below. In a typical EPR spectrum of shelled species containing Mn^{2+}, there are six distinct characteristic Mn^{2+} peaks (Figure 2.6). The first Mn^{2+} peak was used in all EPR spectra for the intensity comparison between shell samples, as suggested in the literature [75]. Following the parameter selection process in Section 3.4.1, a set of parameters was developed to measure the spectra of all shell samples. Since every sample was measured using the same EPR parameters (Table 3.2), the spectrum intensities are quantitatively compared. Each sample in this investigation shows the characteristic Mn^{2+} spectrum at varying intensities.

The oyster sample displays the highest Mn^{2+} peak at an intensity of 1.05×10^8. Samples that show the lowest-intensity Mn^{2+} peaks are the heath snail, zebra mussel, grove snail, and freshwater snail shells. Based on these results, it should be assumed that the oyster sample would contain the highest Mn^{2+} concentrations, and the samples with the lowest-intensity Mn^{2+} peaks would contain the lowest Mn^{2+} concentrations. This

TABLE 4.4: The peak-to-peak intensity of the first manganese peak in the EPR spectra of the listed samples.

Sample	Peak-to-Peak Intensity of First Mn^{2+} Peak [a.u.]
Oyster	1.05×10^8
Ocean Snail	6.72×10^7
Lobster	1.72×10^7
Scallop	1.26×10^7
Crab	2.36×10^6
Pond Mussel	1.78×10^6
Blue Mussel	1.23×10^6
Freshwater Snail	7.60×10^5
Grove Snail	7.58×10^5
Zebra Mussel	2.90×10^5
Heath Snail	2.09×10^5

potential correlation between Mn^{2+} peak-to-peak intensity and Mn^{2+} concentration is explored in the following section. Additionally, it must be noted that the samples with the highest peak intensities all have calcite as their predominant $CaCO_3$ polymorph, which could indicate that shells with calcitic structures produce higher-intensity EPR spectra.

4.3 ICP-OES and EPR Comparative Results

The results from Tables 4.2 and 4.4 were combined and visually represented in Figure 4.1. Peak-to-peak spectra intensities for the first Mn^{2+} peak are along the x-axis, and Mn^{2+} concentrations are along the y-axis. This comparison aims to determine which species contain both low-intensity Mn^{2+} peaks and low Mn^{2+} concentrations, as high-intensity Mn^{2+} peaks can obscure the radiation-induced signals in EPR spectra at low doses [21]. It was hypothesized that this Mn^{2+} investigation method could be used as a tool for selecting species for low-dose EPR studies based on selecting samples with comparatively low results for both variables. After identifying potentially suitable species, their shells must be irradiated to determine their dose-response characteristics and lower limit of detection. The problem posed by high-intensity Mn^{2+} peaks in EPR spectra is unique to low-dose studies because at higher doses (in the kGy range), the intensity of the radiation-induced peaks are high enough that Mn^{2+} interferences do not pose an issue.

Results of the quantitative comparison show that zebra mussel, heath snail, and grove snail shells (circled in red in Figure 4.1) have the lowest Mn^{2+} concentrations and Mn^{2+}

EPR peak intensities. This result indicates that these species may be desirable to use as natural dosimeters for retrospective EPR dosimetry. It is essential to consider the various characteristics of shells that can impact their Mn^{2+} concentrations and subsequent effectiveness as dosimeters, including shell structure, animal habitat, and diet. The zebra mussel, heath snail, and grove snail shells may be particularly effective due to a combination of factors, including the polymorphic form of $CaCO_3$ that makes up their shells and their environmental exposure to Mn^{2+}. All three shells are primarily composed of aragonite, and the two snails are both terrestrial species, indicating that gastropod species with aragonitic shell contents living in terrestrial environments could be particularly good candidates for reference dosimetry. Previous experiments by A. Hassan and M. Tzivaki showed that grove snails had a dose-detection limit of 2 Gy [21], and zebra mussels had a dose-detection limit of 0.2 Gy [29]. The dose-response of *Cepaea nemoralis* and *Xerolenta obvia* is further explored in Chapter 5 to confirm their efficacy as dosimetric materials.

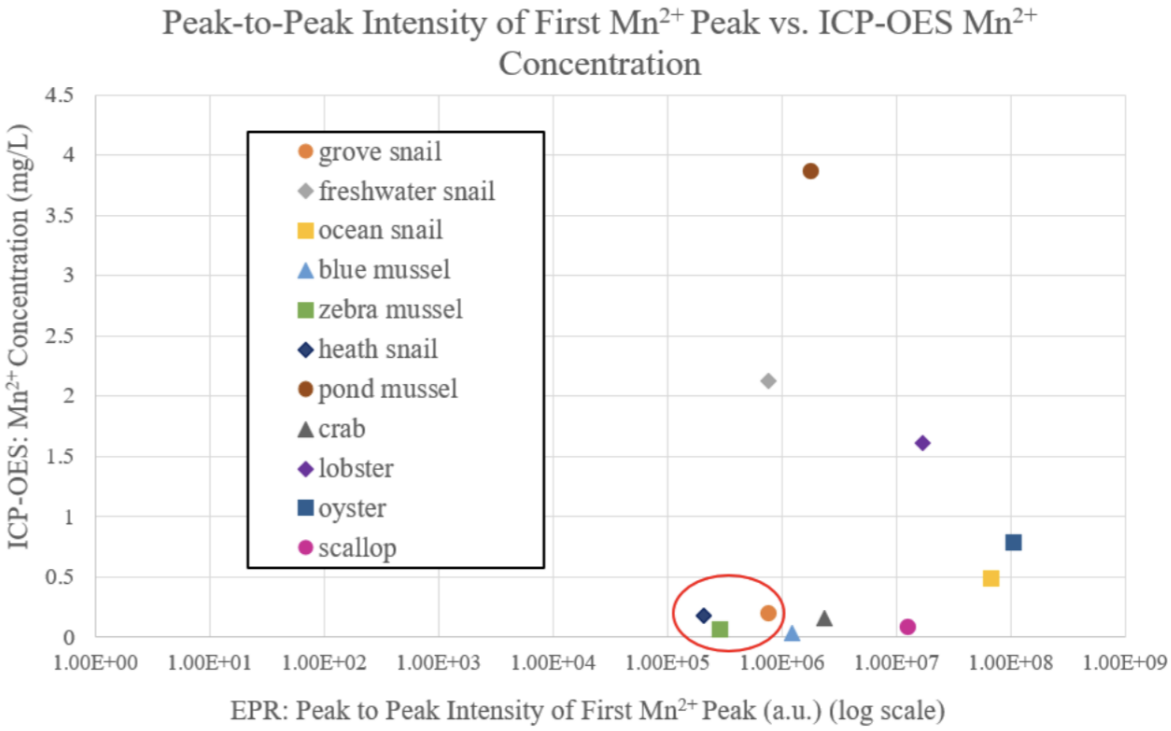

FIGURE 4.1: The comparative results of the Mn^{2+} investigation. The samples circled in red have the lowest Mn^{2+} concentrations and Mn^{2+} peaks.

On the other hand, the samples showing the highest Mn^{2+} peaks and concentrations

are the lobster, oyster, and pond mussel shells. A. Hassan's investigation into the dose-response of these three species concluded that the EPR spectra for none of those samples showed a dose-response at a dose of 10 Gy [21]. Blue mussel shells were also irradiated in that investigation and showed no dose-response at 10 Gy. The ultimate goal of developing and testing this methodology for Mn^{2+} investigations in shelled species was to identify if it can be used as a tool for selecting shelled species for EPR dose analysis in the future.

It must be noted that this is a preliminary investigation into this novel Mn^{2+} investigation methodology. Repeated experiments following the same methodology would need to be conducted to confirm the technique's validity. Future ICP-OES experiments should also include more than one sample per species to achieve statistically significant results and track digestion efficiency. A spiked sample can also be run through the process to track analyte recovery.

Chapter 5

Results and Discussion - Irradiation Experiments

This chapter discusses the results from the shell irradiation experiments detailed in Chapter 3. The results from the irradiation experiments on terrestrial grove snails (*Cepaea nemoralis*) and heath snail (*Xerolenta obvia*) shells will be presented, and the suitability of these shells for retrospective EPR dosimetry will be discussed. The results from the turtle shell irradiation experiment will also be discussed. Based on the results from Chapter 4, heath snail and grove snail shells both had low Mn^{2+} concentrations and low-intensity Mn^{2+} peaks in their EPR spectra. As such, it was deemed necessary to investigate the dose-response of these shells to verify the applicability of ICP-OES manganese(2+) detection and comparison with EPR spectra as a method for selecting suitable species for low-dose EPR dosimetry.

5.1 Grove Snail Shell Dose Response

In addition to verifying the dose-response of grove snail shells, another goal of this experiment was to generate a refined dose-response curve for this species based on recommendations from previous work by A. Hassan.

To make the grove snail (*Cepaea nemoralis*) calibration curve, grove snail shell samples were irradiated at doses of 1.5, 2, 3, 5, 7, and 10 Gy. Each dose group consisted of ten shell samples ground to grain sizes between 0.5 to 0.1 mm, and one alanine dosimeter was included for reference dosimetry purposes. The methods used to generate the dose-response curve are detailed in Section 3.4.3.

The EPR spectra of terrestrial grove snails were measured first with a sweep width of 800 G, as per the parameters in Table 3.2. Figure 5.1 shows the EPR spectra of the unirradiated background spectrum and 10 Gy irradiated spectrum of the GS10-2 sample.

As expected, at a magnetic field value of 3490 G, a central native peak was observed, and at 3500 G (g-value = 2.0016) a radiation-induced signal was observed. The six characteristic Mn^{2+} peaks were also observed.

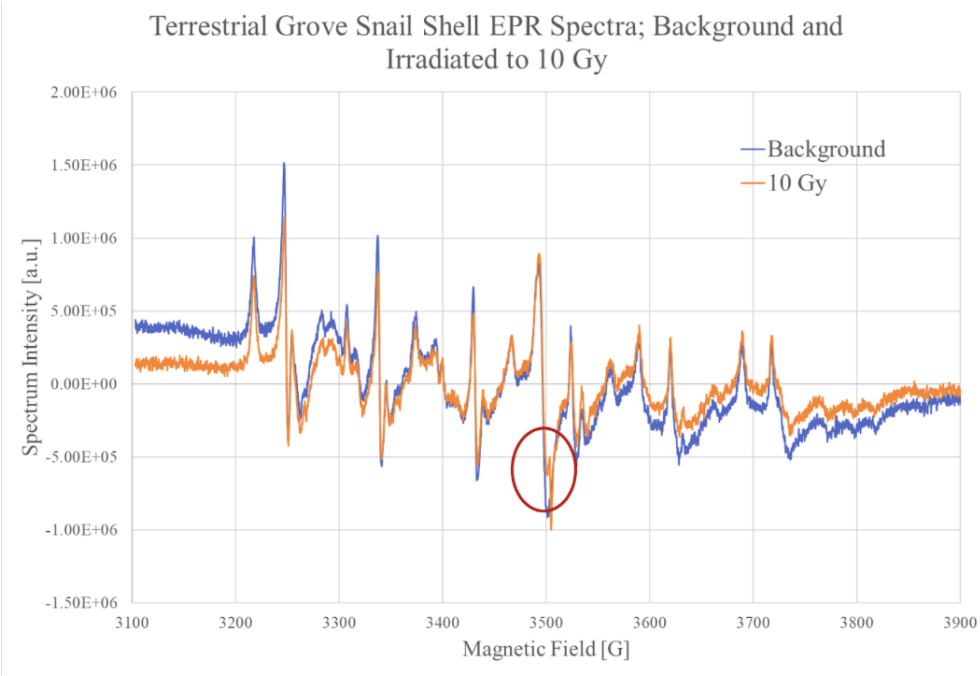

FIGURE 5.1: Spectra for a grove snail shell sample at 0 Gy and 10 Gy. The radiation-induced peak is circled in red and is at g=2.0016.

As the radiation-induced peak was difficult to observe over a sweep width of 800 G, all shell samples were analyzed using a smaller sweep width of 50 G to better identify the increase in the radiation-induced peak. The peak-to-peak intensity of this peak is measured for dose-response analysis. Figure 5.2 shows an example of the increase in intensity of the radiation-induced peak in the spectra of samples GS2-2, GS3-2, GS5-2, GS7-2 and GS10-2. A clear increase in this peak is observed as the dose increases.

The peak-to-peak heights of the radiation-induced signals were density normalized for all terrestrial snail shell samples following the process in Section 5.4. Density normalization was necessary to account for mass differences between each sample. Since every sample in each dose group was measured three times, the average intensity of the radiation-induced peak was first calculated. This average intensity was then used in calculating the density-normalized intensity for every spectrum. The density-normalized radiation-induced signal intensities for each sample in every dose group were averaged and plotted against the measured doses. The resulting dose-response curve is seen in Figure

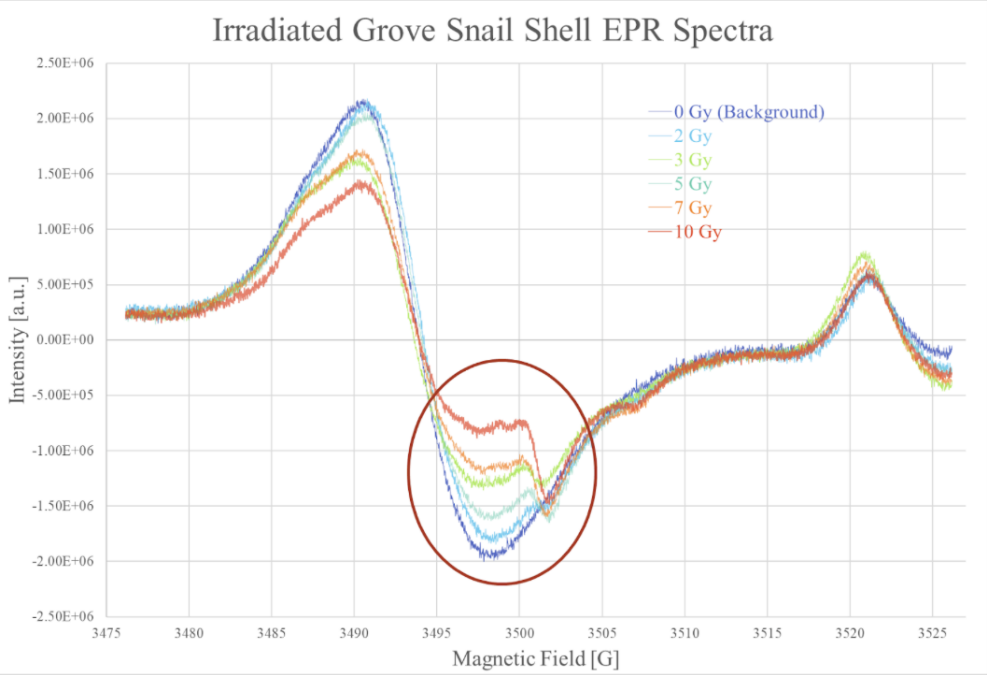

FIGURE 5.2: Spectra for a grove snail shell samples irradiated to 2, 3, 5, 7, and 10 Gy. The radiation-induced peak is circled in red and it is seen to increase with dose.

5.3, and Table 5.1 presents the data used to generate the plot. The EPR signal intensity increases linearly with dose from 2 to 10 Gy. A linear function was fitted to the data and is shown in Figure 5.3, along with the coefficient of determination (R^2). The coefficient of determination is above 0.99, indicating a high degree of linearity within the dose range. The error bars represent the standard deviation of the peak-to-peak intensities of the ten samples in each dose group. Relative errors for each sample range from about 0.3 to 1%.

TABLE 5.1: The density normalized peak-to-peak height data for all terrestrial grove snail shell samples.

Measured Dose [Gy]	Average p-p Height [a.u.]	Standard Deviation [a.u.]
2.11	1.14×10^6	1.65×10^5
3.22	2.21×10^6	1.72×10^5
4.94	3.47×10^6	1.06×10^5
6.87	5.32×10^6	1.97×10^5
9.93	7.83×10^6	2.30×10^5

The linear relationship between the signal height and dose-response between 2 Gy to

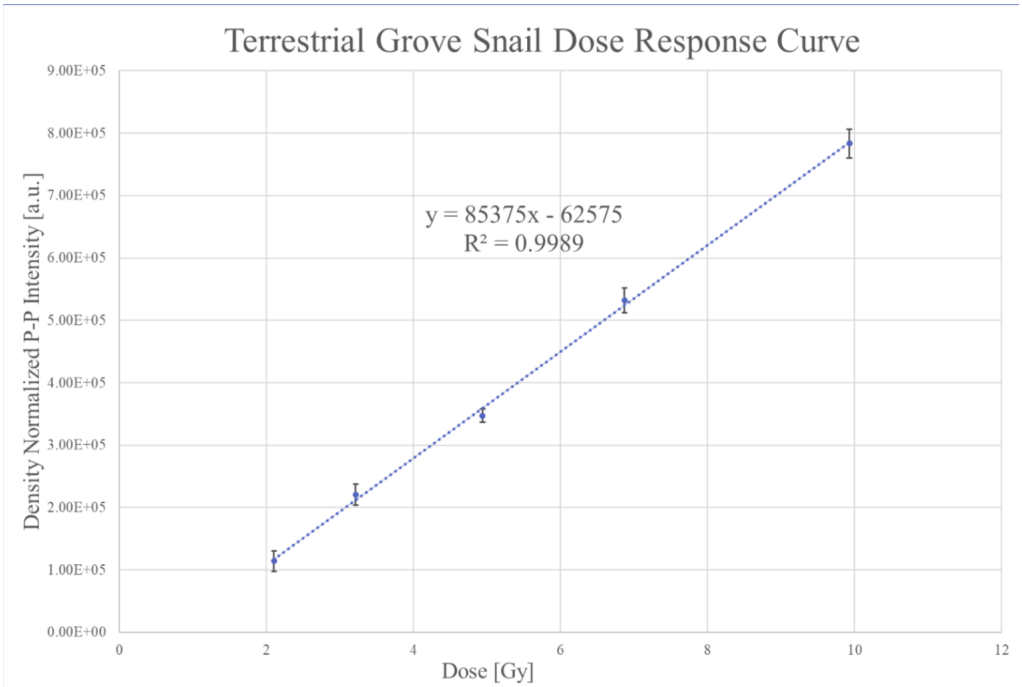

FIGURE 5.3: The density-normalized dose-response curve generated for irradiated grove snail shells from 2 to 10 Gy.

10 Gy indicates the suitability of this species for EPR dose detection within that dose range. A dose lower than 2 Gy was not able to be resolved. The samples irradiated to 1.5 Gy were also measured using EPR using the same methodologies and parameters as all the other grove snail shell samples, but no radiation-induced signals were seen/able to be resolved at this dose. This concludes that using this methodology and the selected parameters, 2 Gy is the lowest detectable dose.

5.2 Heath Snail Shell Dose Response

To quantify the dose-response of the terrestrial heath snail, shell samples were irradiated to doses of 2, 3, 5, 7 and 10 Gy. Each dose group consisted of 2 shell samples ground to grain sizes between 0.5 mm to 0.1 mm and one alanine dosimeter included for reference dosimetry purposes. The methods used to generate the dose-response curve are detailed in Section 3.4.3.

The background and irradiated spectrum of the HS10-1 sample using a sweep width of 800 G is shown in Figure 5.4. Similar to the grove snail spectrum, a native peak is identified at 3490 G and the radiation-induced signal attributed to the CO_2^- radical is

seen at 3500 G. The peak seen at 3550 G is the internal standard marker. The increase in intensity of the internal standard marker is not due to irradiation, but rather having the internal standard at different positions during both scans. Six Mn^{2+} peaks were also identified on the spectra. As with the grove snails, the radiation-induced peak is difficult to analyze at a sweep width of 800 G, and as such, the samples were all analyzed using a sweep width of 50 G.

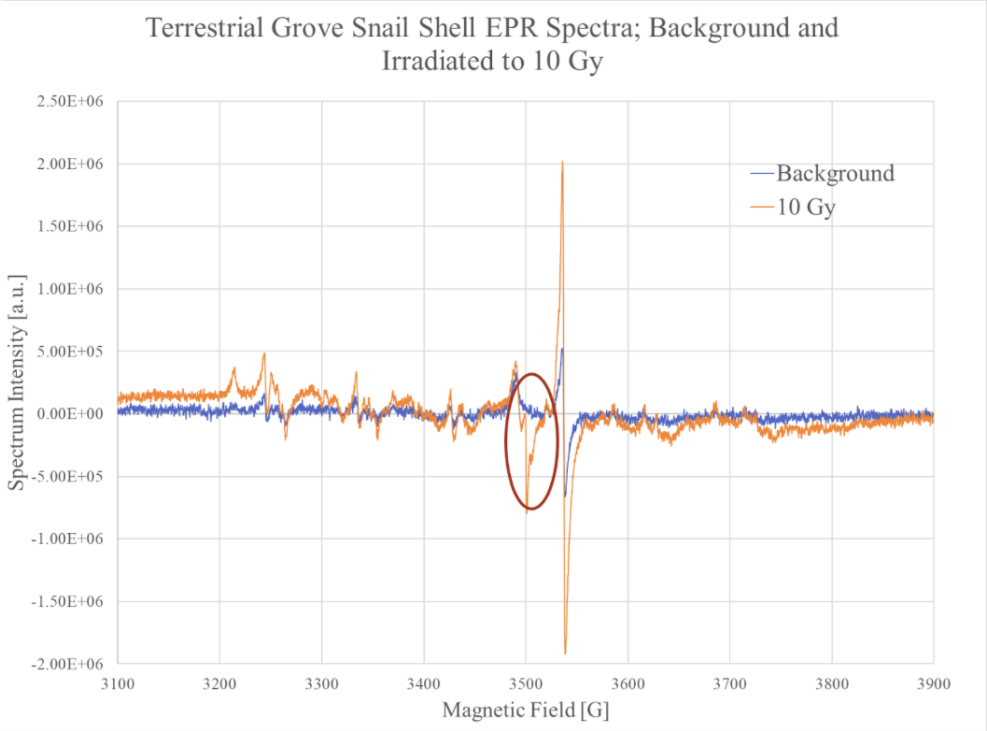

FIGURE 5.4: Spectra for a heath snail shell sample at 0 Gy and 10 Gy. The radiation-induced peak is circled in red and is at g=2.0016.

Figure 5.5 shows an example of the increase in intensity of the radiation-induced signal in the spectra of samples HS2-3, HS3-3, HS5-3, HS7-3 and HS10-3. A clear increase in this peak is seen as the dose increases.

The intensities of the radiation-induced signals for every sample were density normalized following the process in Section 5.4. Every sample was measured three times, so the average intensity of the three measurements was used in density normalization calculations. The calculated signal intensities were plotted against the measured dose using the data shown in Table 5.2, and the resulting dose-response curve is seen in Figure 5.6. The radiation-induced signal intensity is seen to increase linearly from 2 Gy to 10 Gy, and the

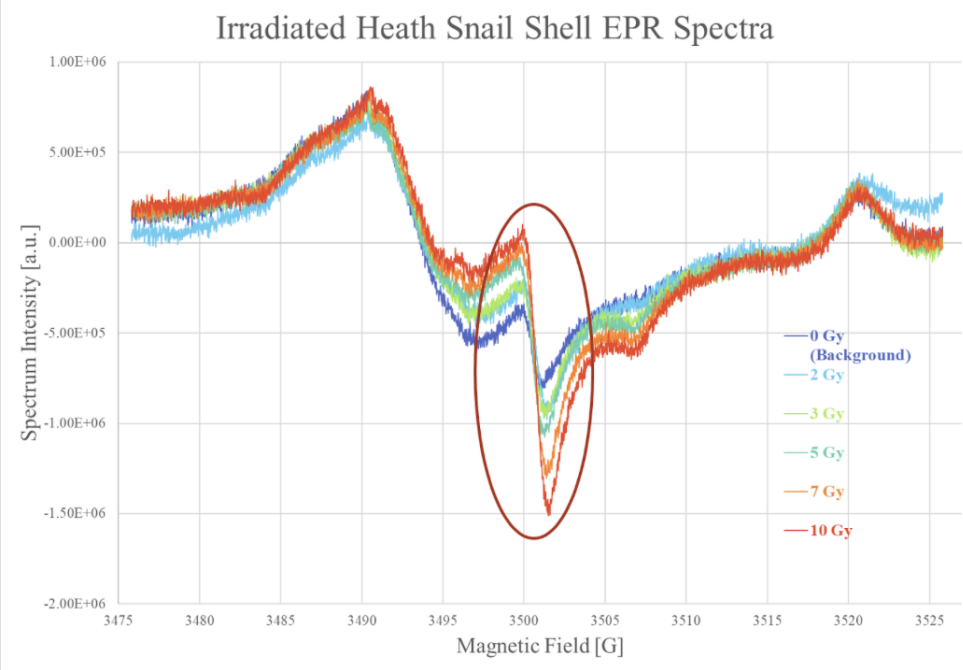

FIGURE 5.5: Spectra for a heath snail shell samples irradiated to 2, 3, 5, 7, and 10 Gy. The radiation-induced peak is circled in red and it is seen to increase with dose.

linear equation fitted to the data is shown on the plot. The coefficient of determination is 0.9892, indicating good linearity of the dose-response. The error bars represent the standard deviation of the signal intensities of the two samples in each dose group.

TABLE 5.2: The density normalized peak-to-peak height data for all terrestrial heath snail shell samples.

Measured Dose [Gy]	Average p-p Height [a.u.]	Standard Deviation [a.u.]
2.32	7.59×10^6	2.12×10^5
3.45	8.07×10^6	5.87×10^5
5.66	1.04×10^7	4.05×10^5
7.95	1.31×10^7	1.16×10^5
11.11	1.54×10^7	9.50×10^5

The linearity of the dose-response indicates that heath snail shells may be suitable for EPR dose detection within the 2 to 10 Gy dose range. To confirm this suitability, the dose group sample sizes should be increased from two samples to ten samples.

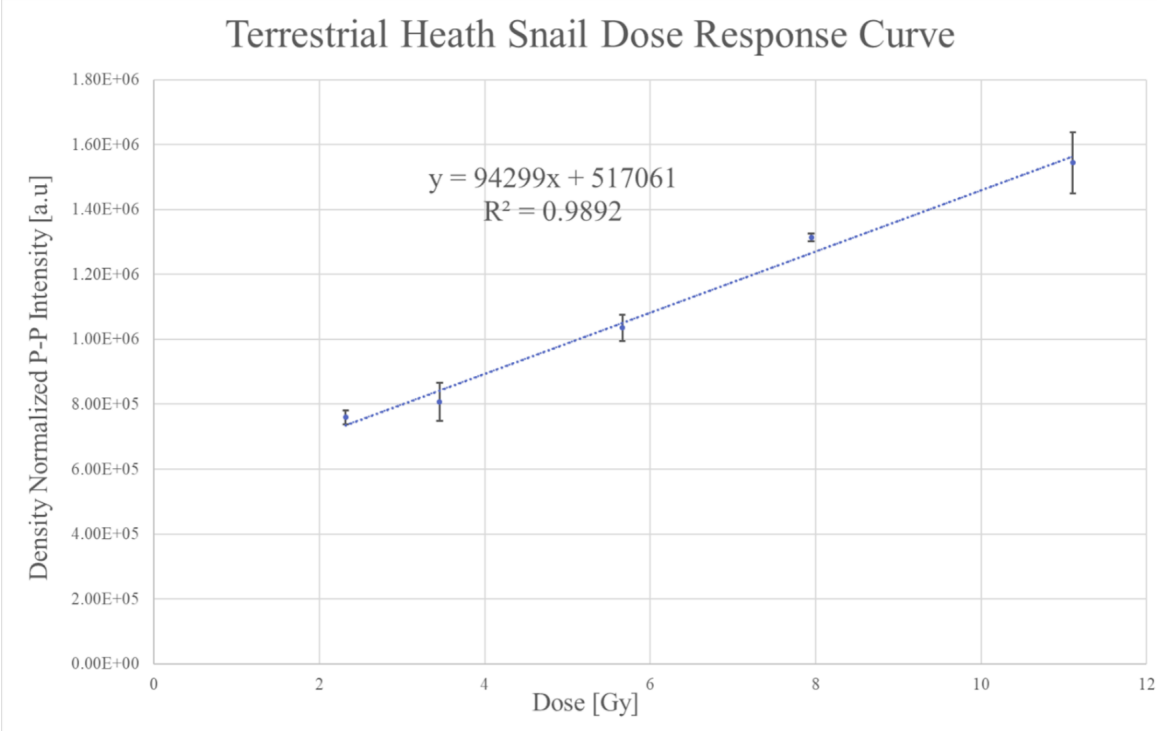

FIGURE 5.6: The density-normalized dose-response curve generated for irradiated heath snail shells from 2 to 10 Gy.

Summary

Both snail samples analyzed in this work display the characteristic Mn^{2+} sextet, a dose-dependent radiation-induced peak at a g-value of 2.0016, and dose-detection limits of about 2 Gy. Based on these detection limits, and the detection limit of 2 Gy reported in the literature for the terrestrial snail (*Cepaea homoralis*), it can be hypothesized that the dose-detection limits of other terrestrial snail species would be around 2 Gy. Further experiments on more terrestrial snail shell species must be conducted to confirm this assumption.

Grove snail, zebra mussel, and heath snail shells were all identified as having the lowest Mn^{2+} concentrations and EPR peak intensities. All of these species showed a dose-response and dose dependence. Both snail shell samples had minimum detectable doses at 2 Gy, and M. Tzivaki reported zebra mussel shells to have a minimum detectable dose at 0.2 Gy. These dose-response results, in conjunction with the conclusion that heath snail, grove snail, and zebra mussel shells had low Mn^{2+} peaks and low EPR intensities, confirms that the Mn^{2+} investigation method could be used as a tool for selecting suitable

species for EPR analysis.

5.3 Turtle Shell Dose Response Measurements

The carcass of a midland painted turtle (*Chrysemis picta marginata*) was cleaned using the methodology described in Section 3.1. The samples were prepared for EPR measurements and measured following the protocols outlined in Sections 3.2 and 3.3. As detailed in Section 3.4.4, various sample parameters were tested, and background measurements were taken using the various sets of parameters detailed in Table 3.5.

To determine if there was a dose-response in turtle shells, samples were additively irradiated to doses of 2, 3, 6, 9.5, and 19 Gy, and every sample was measured after each irradiation using all four parameter sets. No dose-response was identified at any dose using any parameter set. The irradiated spectra were identical to the background spectra seen in Figure 3.21. Due to the presence of hydroxyapatite in the turtle shell's mineral structure, it was hypothesized that carbonate free radicals would be formed during irradiation [125]. Radiation-induced peaks at g-values of 2.0035 and 2.0015 were expected if a dose-response were to be identified [161]. The lack of dose-response in the spectra at doses of 19 Gy was unexpected. It is possible that the doses used were not high enough. The literature has noted that many spectra of irradiated calcified tissues that show a dose-response have been irradiated to doses in the kGy range. It is possible that a dose-response would be seen in the spectra at doses in the kGys, however doses that high are not applicable in the context of low-dose radiation detection. As such, the shell of the painted turtle was not deemed an adequate sample for EPR dose detection at low doses. Interestingly, no manganese(2+) peaks were identified in the EPR spectra of the turtle shells either. It is unknown why no Mn^{2+} peaks were visible in the spectra since turtles are semi-aquatic freshwater species, and inhabit similar environments to many of the other shelled species identified in this work, which all show Mn^{2+} EPR peaks. The absence of peaks could be due to the differences in shell formation and composition between turtles and other species. An investigation into the composition of the turtle shell and an elemental analysis would be required in order to understand these unexpected results better.

5.4 Density Normalization and Measurement Error

Although each sample was filled in the EPR tube to the approximate same height, it was necessary to normalize every EPR measurement as the amount of sample in each EPR tube varies from sample to sample. This normalization was done according to

the packing density of each sample in the EPR tube. The methods below for density normalizing measurements were developed by A. Hassan and M. Tzivaki [29] [21].

First, the volume of the sample is calculated. The outer and inner diameters of the EPR tubes are 5 mm and 4 mm respectively. Following this, the thickness, t, of the glass is 0.5 mm, and the inner radius of the tube, r_i, is 2 mm. The height of the sample is measured from the bottom of the tube. Due to this, the actual sample height is $h_s = h_{measured} - 1mm$, where 1 mm is the thickness of glass at the bottom of the tube. The tube volume comprises of a semi-sphere and a cylinder:

$$V_{cylinder} = \pi r^2 h_s \tag{5.1}$$

$$V_{semi-sphere} = \frac{1}{2} \cdot \frac{4}{3} \pi {r_i}^3 \tag{5.2}$$

$$V_{sample} = V_{cylinder} + V_{semi-sphere} \tag{5.3}$$

The sample density is calculated by dividing the mass by the volume:

$$\rho = \frac{m_{sample}}{V_{sample}} \tag{5.4}$$

The EPR peak-to-peak amplitude, $I_{measured}$ results are then normalized by dividing the measured result by the density:

$$I_{norm} = \frac{I_{measured}}{\rho} \tag{5.5}$$

The following equations were used to perform error analysis on the grove snail samples. First, the sample height standard deviation is calculated to be 0.12 mm using Equation 5.6. The sample height standard deviation was determined to be 0.32 mm after measuring each sample from the 2 Gy grove snail sample group seven times each.

$$\Delta h = \frac{\text{sample standard deviation}}{\sqrt{\text{number of measurements}}} = \frac{0.32mm}{\sqrt{7}} = 0.12 \tag{5.6}$$

The uncertainty of the mass measurements, Δ m, is 1 mg. The thickness of the glass in the EPR tubes is 0.5 mm.

The sample volume error is:

$$\Delta V_{sample} = \Delta h r_i^2 \pi \tag{5.7}$$

The density uncertainty can be calculated using the following equation:

$$\Delta\rho = \sqrt{(\frac{\Delta V_{sample}}{V_{sample}})^2 + (\frac{\Delta m}{m})^2}\rho \tag{5.8}$$

Lastly, the density normalized intensity error is found as follows:

$$\Delta I_{norm} = \frac{\Delta\rho}{\rho} I_{norm} \tag{5.9}$$

Chapter 6

Conclusions and Future Work

6.1 Summary of Work

This work aims to assess manganese(2+) concentrations in the calcified tissues of shelled species in the context of retrospective electron paramagnetic resonance (EPR) dosimetry. This work is motivated by growing interest in the radiological protection of the natural environment in light of the rapid progression of the nuclear industry. When an unplanned radiological release occurs, it can cause an increase in radioactive material in the environment. It is imperative to assess the dose to the environment to understand the impact of the release and inform the response and remediation measures taken. When conventional dosimeters are not on hand, assessments of the dose are conducted through the use of materials from the environment. This work investigates the suitability and limitations of calcified tissues, particularly mollusc and crustacean shells, as natural dosimeters.

EPR is a retrospective dosimetry technique commonly used for determining doses to a sample from an environment affected by a radiological release. This is done by analyzing radiation-induced free electrons formed in the typically crystalline structure of a material. A shell's crystalline calcium carbonate structure can trap electrons in its crystal lattice proportional to the radiation dose, making shells a suitable material for retrospective dosimetry studies. There are, however, some limitations to using shells as dosimeters, one being the presence of Mn^{2+} within the shell structure. Specifically, when conducting a dose reconstruction of the samples using EPR, high-intensity Mn^{2+} peaks in the EPR spectra can obstruct the radiation-induced signals, making it impossible to resolve low doses.

As such, this work investigates the many factors that affect the incorporation of Mn^{2+} into the crystalline structure of mollusc and crustacean shells in order to select suitable species from the environment for EPR dosimetry. The main calcium carbonate polymorph and the species' habitats were identified as the main factors affecting Mn^{2+}

concentrations in shells. The shells of fourteen different species from diverse habitats (freshwater, marine, and terrestrial) were selected to compare the effects of habitat and shell structure on Mn^{2+} concentrations between various species.

To quantify the amount of Mn^{2+} in each shell, inductively coupled plasma-optical emission spectroscopy (ICP-OES) was used as an elemental analysis technique. EPR was used to measure the intensity of the Mn^{2+} peaks in the spectra of each shell sample. Methodologies for preparing and measuring samples using EPR and ICP-OES were developed.

The results of the ICP-OES and EPR experiments were reviewed. The Mn^{2+} concentrations determined from the ICP-OES experiment revealed that in general, shells coming from freshwater environments generally had the highest Mn^{2+} concentrations, while shells of terrestrial gastropods, and shells presumed to be from farmed molluscs had the lowest. Results from the EPR investigation revealed that shells composed of calcite had the highest intensity Mn^{2+} peaks. A quantitative comparison between the Mn^{2+} concentrations and Mn^{2+} EPR peak intensities revealed that terrestrial grove snail (*Cepaea nemoralis*), heath snail (*Xerolenta obvia*), and zebra mussel (*Dreissena polymorpha*) had the lowest Mn^{2+} concentrations and lowest Mn^{2+} peaks. Confirming a dose-response in those three shell samples was the next step in confirming the validity of this technique for selecting species for low-dose studies.

Following the Mn^{2+} investigation, irradiation experiments were carried out on the *Cepaea nemoralis* and *Xerolenta obvia* shells. Irradiations were performed using a cesium-137 gamma source. Shell samples for both species were irradiated to doses of 2, 3, 5, 7 and 10 Gy and then analyzed using EPR dosimetry. A dose-response was identified, and the minimum detectable dose determined for both terrestrial gastropod samples was 2 Gy. At the same time, the literature indicated that the minimum detectable dose in zebra mussels was 0.2 Gy. Additionally, a refined dose-response curve from 2 to 10 Gy was developed for the *Cepaea nemoralis* and a novel dose-response curve from 2 to 10 Gy was developed for *Xerolenta obvia*. Both curves showed strong linearity. The main calcium carbonate polymorph in all three shell samples was aragonite, which may indicate that shells composed of aragonite are better suited for low-dose EPR studies than shells composed of calcite. These results also indicate that terrestrial gastropods are well-suited for retrospective dose assessments. These doses could not be resolved into the defined 'low-dose' range (<100 mGy), which limits the practical applications of these shells in the case of a low-level release into the environment. This preliminary work on an ICP-OES method of manganese detection and comparison with EPR spectra may be used as a tool to select suitable species for low-dose EPR dosimetry. Further investigations must be

done to determine the feasibility of this technique conclusively.

A novel investigation was also conducted into the potential dose-response in turtle shells. A midland painted turtle (*Chrysemys picta marginata*) was obtained. Sample preparation methodologies for shell grinding and EPR analysis were developed. Different sets of EPR parameters were tested. The shell samples were irradiated to doses of 2, 3, 6, 9.5 and 19 Gy. No dose-response was identified at any dose using any parameter set. This result was surprising, given that turtle shells have a crystalline structure and are composed of hydroxyapatite and calcium carbonate, similar to other materials that have been successfully used as dosimeters. It was assumed that the dose to the sample was too low and that a dose-response may be seen at higher doses. There was also no Mn^{2+} signal in the EPR spectra of these shells, which was surprising given the similarity in a midland painted turtle's habitat to other shelled species investigated in this work. The reason for the lack of Mn^{2+} signals is unknown at this time. Future work surrounding turtle shells will be discussed in the next section.

The above conclusions can be summarized as follows:

1. A quantitative comparison between the Mn^{2+} concentrations and EPR peak intensities in various shelled species revealed that terrestrial grove snail (*Cepaea nemoralis*), heath snail (*Xerolenta obvia*) and zebra mussel (*Dreissena polymorpha*) shells had the lowest Mn^{2+} concentrations and lowest intensity Mn^{2+} peaks. These shells may have been particularly effective due to a combination of factors, including their crystalline structure and environmental exposure to Mn^{2+}. The results indicate that gastropod species with aragonitic shells living in terrestrial environments could be particularly good candidates for reference dosimetry.

2. An EPR dose-respone was confirmed in terrestrial grove snail and heath snail shells. Dose detection limits of 2 Gy were identified for both terrestrial gastropod species, and a limit of 0.2 Gy in zebra mussels is known from the literature, which confirms their suitability as dosimetric materials. These dose-response results, in conjunction with the conclusion that heath snail, grove snail, and zebra mussel shells had low Mn^{2+} concentrations and EPR intensities, confirms that the Mn^{2+} investigation method could be used as a tool for selecting suitable species for EPR analysis.

3. No dose-response or Mn^{2+} peaks were identified in the EPR spectra of irradiated midland painted turtle (*Chrysemys picta marginata*) shells.

6.2 Improvements and Future Work

This work primarily investigates the factors causing Mn^{2+} quantities in shelled species and develops a practical method of determining the Mn^{2+} concentrations in shells to detect their suitability for EPR dose investigations.

As the ICP-OES method of detecting Mn^{2+} concentrations was a preliminary study, many improvements can be made to the methodology. Repeated experiments following the same methodology should be conducted to confirm the technique's validity and the significance of the results. One ICP-OES sample was prepared per species for this analysis. For future ICP-OES analyses, it would be good practice to include at least two samples per species to track digestion efficiency and achieve more accurate results. As some measurements were outside the calibrated range, dose spiking should be considered to enhance weak signals and track analyte recovery. During sample preparation, many shell samples did not fully dissolve during open vessel digestion, reducing the amount of analyte in the samples. For dissolving future shell samples, microwave vessel digestion should be considered as an alternative to open-vessel digestion as it produces higher digestion efficiency.

In the dose-response experiments, no investigation was done into the effects of signal fading and temperature, which according to the literature, can affect the reproducibility and intensity of EPR spectra. In the future, it is recommended to remeasure the samples at different times post-irradiation to determine signal fading. Irradiated samples should also be stored at different temperatures to observe the effects of temperature on signal fading and spectrum intensity. Additionally, the number of samples per dose group should be increased for studying the *Xerolenta obvia* shells. Only two samples per dose group were prepared in this work. Further irradiation experiments should be conducted using the snail shells with more samples per group to achieve more statistically significant results. The dose-response of additional terrestrial gastropods should also be examined to confirm if more species in this group have limits of detection around 2 Gy.

Based on the results of the Mn^{2+} investigation, it is essential to know the habitat from which shelled species were procured. Some species' unexpectedly low Mn^{2+} concentrations emphasize the importance of knowing where the animal was collected from. Additionally, secondary ICP-OES measurements of the soil, sediment, and water in the species' habitat could clarify the primary sources of Mn^{2+}. Furthermore, confirming the dominant calcium carbonate polymorph and proportions of aragonite and calcite within the shells would allow a better understanding of which polymorphic form of $CaCO_3$ is better suited for radiation studies. As such, it would be prudent to analyze the shells

using X-ray diffraction (XRD) or even a synchrotron to analyze the local coordination of the molecules within the shell, the different minerals present, and the radiation interaction with the mineralogy of the shell.

Regarding the investigation into the dose-response of turtle shells, it would be pertinent to analyze the shell using different analytical methods to gather information on their microstructure and elemental composition. A deeper understanding of the shell microstructure could help explain why no Mn^{2+} peaks were present and why no radiation-induced peaks at a dose of 19 Gy were observed using EPR.

Combining the results from this thesis with information about the microstructure and local coordination within a shell can provide the basis for developing a framework that can be used for selecting shelled species suitable for retrospective EPR dose assessments. It should include the species' habitats, primary calcium carbonate polymorph, diet, procurement location, and shell composition, thickness, and colour. Using a more refined approach to identifying suitable species will enable a more swift and efficient selection in the event of an unplanned release to the environment.

Appendix A

Grove Snail Breeding and Snail Farm

To gain a deeper understanding of the pathways through which Mn^{2+} incorporates into shelled species, a side project that involved breeding snails and fabricating snail farms was initiated. Terrestrial grove snails were specifically used in this experiment as their shells displayed good dose-response characteristics as discussed in Chapter 5. The goal of this project was to construct snail farms with controlled concentrations of Mn^{2+}, and to study grove snail shells using elemental analysis techniques to understand the pathways of Mn^{2+} incorporation into the shells. An additional goal of this project was to eventually establish snail farms on-site at various nuclear power plants in Ontario, with the purpose of having a control group of non-human biota that could be used for EPR dosimetry studies. The snail farm environments would be constructed and maintained using the factors that contribute to the least amount of Mn^{2+} uptake in the snail shells.

As summarized in Chapter 3, manganese can be incorporated into shells via many pathways including through water, soil, and food [68] [69]. The goal of a snail breeding experiment was to create different environments for snails to inhabit and limiting the Mn^{2+} exposure in each controlled environment. Every snail enclosure would include soil, water, leaves, sticks, rocks and other objects common in snail habitats, as well as food. Each controlled environment would be made by introducing known, limited quantities of manganese to the snails. The different potential control environments could include:

- Manganese incorporated via diet only
- Manganese incorporated via the environment only
- Manganese incorporated via diet and the environment

To incorporate manganese via the environment, extra manganese would be added to the soil via the addition of a manganese standard solution. To incorporate manganese via the snail's diet, it would be fed a diet of vegetables containing manganese (such as carrots). The purpose of this experiment was to determine which combination of environmental and dietary factors contribute to the least amount of manganese uptake into grove snails possible. Knowing this, if a snail farm is created, the environment and food can be controlled to limit the snails' exposure to Mn^{2+} and subsequently minimize the Mn^{2+} interferences in EPR spectra.

To begin the process of breeding snails, live snails first had to be collected from the natural environment. Grove snails were collected from the Ontario Tech University campus (Figure A.1), in May 2022 and placed in an enclosure (Figure A.2). To prepare the snail enclosures, soil was sourced from the environment where the snails were collected and placed in a clear plastic bin, with approximate dimensions of 37 by 29 by 17 cm. The collected soil was sieved through by hand to ensure no bugs, worms, or other organisms were transferred to the enclosure. About 4 cm of soil were layered on the bottom of the plastic bin. Grove snails prefer being in dark, damp environments, so leaves, grass, and sticks from the environment were placed in as well. Small clay gardening pots were carefully broken into smaller pieces and placed in the soil to provide the snails with some shade. Snails were transferred into the enclosures. A maximum of 20 snails were placed in the bins to avoid overcrowding. The snail enclosure was sprayed twice daily (once in the morning and once in the evening) with water from a spray bottle set to the fine mist setting. The enclosure was wiped down with a damp paper towel every few days to remove feces accumulation. Small holes were punctured in the top of the plastic bin to allow air to enter the enclosure. When puncturing small holes in the lid, it was imperative that the holes be punctured from the inside of the lid to the outside, as the protruded plastic surrounding the hole can be sharp and harm the snails.

FIGURE A.1: Live grove snails found at Ontario Tech University.

FIGURE A.2: Grove snails in an enclosure.

The grove snails were fed a diet of fresh vegetables. They also required food high in calcium to grow strong shells. Cuttlefish bone is one food that can provide calcium to snails and small pieces of it were placed in the snail enclosures. The fresh vegetables were also switched out every 2 days to avoid mould growth. As grove snails are hermaphrodites, there was no need to identify male and female snails for breeding purposes. In early June 2022, many eggs were laid in the snail enclosures (Figure A.3), and around two weeks later the eggs hatched. As the snails required nearly daily care, maintaining the snail farms until the snails reached maturity was not sustainable. As such, the project was

terminated. This work does however prove that collecting and breeding grove snails in captivity is not a difficult task, and this project can be restarted at a later date.

FIGURE A.3: Grove snail eggs.

Bibliography

[1] ICRP, "Environmental protection - the concept and use of reference animals and plants," *ICRP Publication 108*, vol. Ann. ICRP 38, 2008.

[2] *Radiation Protection of the Public and the Environment* (General Safety Guides GSG-8). Vienna: International Atomic Energy Agency, 2018, ISBN: 978-92-0-102517-3.

[3] CNSC, *REGDOC-2.7.1, Radiation Protection.*

[4] IAEA, *Improving external dosimetry for terrestrial animals and plants*, 2018.

[5] UN, *The Sustainable Development Goals Report.* 2022.

[6] UNSCEAR, *Sources and effects of ionzing radiation.* 2000, vol. 1.

[7] J.-F. Barquinero, P. Fattibene, V. Chumak, *et al.*, "Lessons from past radiation accidents: Critical review of methods addressed to individual dose assessment of potentially exposed people and integration with medical assessment," *Environment International*, vol. 146, Jan. 2020.

[8] E. A. Ainsbury, E. Bakhanova, J. F. Barquinero, *et al.*, "Review of retrospective dosimetry techniques for external ionising radiation exposures," *Radiation Protection Dosimetry*, vol. 147, no. 4, 573–592, 2010.

[9] C.-C. Lu, H.-H. Lin, C.-H. Hsu, F.-N. Wang, J.-P. Lin, and L.-H. Lai, "Potential use of environmental biological samples for retrospective electron paramagnetic resonance dosimetry of radiation accidents," *Applied Sciences*, vol. 10, no. 19, p. 6867, 2020.

[10] J. Sadło, J. Michalik, W. Stachowicz, G. Strzelczak, A. Dziedzic-Gocławska, and K. Ostrowski, "Epr study on biominerals as materials for retrospective dosimetry," *Nukleonika*, vol. 51, 2006.

[11] IAEA, *Protection of the Environment from Ionising Radiation; The Development and Application of a System of Radiation Protection for the Environment.* 2003.

[12] E. Smolders, "Plant uptake of radiocaesium: A review of mechanisms, regulation and application," *Journal of experimental botany*, vol. 51, pp. 1635–45, Nov. 2000.

[13] M. Iammarino, D. dell'Oro, N. Bortone, and E. Chiaravalle, "Strontium-90 accumulation in animal bones: Radiochemical determination by liquid scintillation counting (lsc)," Oct. 2014.

[14] IAEA, *Environmental Consequences of the Chernobyl Accident and their Remediation: Twenty Years of Experience*. 2006.

[15] A. Alberti, E. Chiaravalle, P. Fuochi, *et al.*, "Irradiated bivalve mollusks: Use of epr spectroscopy for identification and dosimetry," *Radiation Physics and Chemistry*, vol. 80, pp. 1363–1370, Dec. 2011.

[16] C. Clement, P. Strand, N. Beresford, *et al.*, "Environmental protection: Transfer parameters for reference animals and plants," *Annals of the ICRP*, vol. 39, no. 6, 1–111, 2009.

[17] M. Brustolon and G. Giamello, *Electron Paramagnetic Resonance: A practitioner's Toolkit*. Wiley, 2009.

[18] K. Mahmoud and H. Taleb, "Fresh water snails as bioindicator for some heavy metals in the aquatic environment," *African Journal of Ecology*, vol. 51, Jun. 2013.

[19] J. Liu, L. Cao, and S. Dou, "Bioaccumulation of heavy metals and health risk assessment in three benthic bivalves along the coast of laizhou bay, china," *Marine Pollution Bulletin*, vol. 117, Feb. 2017.

[20] M. Dar, A. Belal, and A. Madkour, "The differential abilities of some molluscs to accumulate heavy metals within their shells in the timsah and the great bitter lakes, suez canal, egypt," *Egyptian Journal of Aquatic Research*, vol. 44, Dec. 2018.

[21] A. Hassan, "Towards low dose retrospective dosimetry on shelled species," M.S. thesis, 2020.

[22] M. Desrosiers and D. A. Schauer, "Electron paramagnetic resonance (epr) biodosimetry," *Nuclear Instruments and Methods in Physics Research Section B: Beam Interactions with Materials and Atoms*, vol. 184, no. 1-2, 219–228, 2001.

[23] K. E. Prosser and C. J. Walsby, "Electron paramagnetic resonance as a tool for studying the mechanisms of paramagnetic anticancer metallodrugs," *European Journal of Inorganic Chemistry*, vol. 2017, no. 12, 1573–1585, 2016.

[24] R. T. Weber, *Xenon user's guide*, 2011.

[25] A. Maghraby, "Ionizing radiation induced radicals," *Current Topics in Ionizing Radiation Research*, 649–682, 2012.

[26] D. Mesterházy, M. Osvay, A. Kovács, and A. Kelemen, "Accidental and retrospective dosimetry using tl method," *Radiation Physics and Chemistry*, vol. 81, no. 9, 1525–1527, 2012.

[27] R. B. Hayes, "Electron paramagnetic resonance dosimetry: Methodology and material characterization," Ph.D. dissertation, 1999.

[28] F. Trompier, C. Bassinet, A. Wieser, C. De Angelis, D. Viscomi, and P. Fattibene, "Radiation-induced signals analysed by EPR spectrometry applied to fortuitous dosimetry," *Annali dell'Istituto superiore di sanità*, vol. 45, pp. 287–96, Jan. 2009.

[29] M. Tzivaki, "Electron paramagnetic resonance for dosimetry in freshwater aquatic environments," Ph.D. dissertation, 2020.

[30] E. Seletchi and O. Duliu, "Comparative study of esr spectra of carbonates," *Romanian Journal of Physics*, vol. 72, pp. 744 –763, Jan. 2007.

[31] "Use of electron paramagnetic resonance dosimetry with tooth enamel for retrospective dose assessment," International Atomic Energy Agency, Tech. Rep., 2002.

[32] M. F. Desrosiers, J. M. Publ, and S. L. Cooper, "An absorbed-dose/dose-rate dependence for the alanine-epr dosimetry system and its implications in high-dose ionizing radiation metrology," *Journal of Research of the National Institute of Standards and Technology*, vol. 113, no. 2, 79–95, 2008.

[33] P. Levêque, C. Desmet, A. M. Dos Santos-Goncalvez, *et al.*, "Influence of free radicals signal from dental resins on the radio-induced signal in teeth in epr retrospective dosimetry," *PLoS ONE*, vol. 8, no. 5, 2013.

[34] P. J. Ebert, K. A. Hardy, and D. G. Cadena, "Energy dependence of free radical production in alanine," *Radiation Research*, vol. 26, no. 2, 178–197, 1965.

[35] D. Regulla, "Alanine dosimetry – a versatile dosimetric tool," in Jan. 2010, vol. 25, pp. 478–481, ISBN: 978-3-642-03901-0.

[36] D. A. Schauer, A. Iwasaki, A. A. Romanyukha, H. M. Swartz, and S. Onori, "Electron paramagnetic resonance (epr) in medical dosimetry," *Radiation Measurements*, vol. 41, 2006.

[37] P. Fattibene and F. Callens, "Epr dosimetry with tooth enamel: A review," *Applied radiation and isotopes : including data, instrumentation and methods for use in agriculture, industry and medicine*, vol. 68, pp. 2033–116, Nov. 2010.

[38] S. S. Eaton and G. R. Eaton, "Electron paramagnetic resonance spectroscopy," *ChemInform*, vol. 35, no. 49, 2004. DOI: 10.1002/chin.200449280.

[39] Y. E. Nesmelov, A. Gopinath, and D. D. Thomas, "Aqueous sample in an epr cavity: Sensitivity considerations," *Journal of Magnetic Resonance*, vol. 167, no. 1, 138–146, 2004.

[40] M. Zdybel and B. Pilawa, "Application of electron paramagnetic resonance spectroscopy in ophthalmology," *Ophthalmology - Current Clinical and Research Updates*, 2014.

[41] D. Ovhal, B. Samant, N. Dhoble, D. Mohabey, and S. J. Dhoble, "Study of thermoluminescence in turtle shell fossils using radiation dosimetry," *Luminescence*, vol. 35, Nov. 2019.

[42] V. Pagonis, G. Kitis, and C. Furetta, "Numerical and practical exercises in thermoluminescence," *Numerical and Practical Exercises in Thermoluminescence*, pp. 1–208, Jan. 2006.

[43] M. Discher, C. Woda, D. Ekendahl, C. Rojas-Palma, and F. Steinhäusler, "Evaluation of physical retrospective dosimetry methods in a realistic accident scenario: Results of a field test," *Radiation Measurements*, vol. 142, p. 106 544, Feb. 2021.

[44] C. Bassinet, N. Pirault, M. Baumann, and I. Clairand, "Radiation accident dosimetry: Tl properties of mobile phone screen glass," *Radiation Measurements*, vol. 71, pp. 461–465, 2014, ISSN: 1350-4487.

[45] H. Kim, M. C. Kim, J. Lee, *et al.*, "Characterization of thermoluminescence of chip cards for emergency dosimetry," *Radiation Measurements*, vol. 134, p. 106 321, 2020.

[46] D. Ekendahl and L. Judas, "Osl and tl retrospective dosimetry with leucite glass-based dental ceramics," *Radiation Measurements*, vol. 104, pp. 1–7, 2017, ISSN: 1350-4487.

[47] S. Yasmin, M. U. Khandaker, S. N. M. Nawi, *et al.*, "The effectiveness of ornamental building materials (tiles) for retrospective thermoluminescence dosimetry," *Applied Radiation and Isotopes*, vol. 184, p. 110 218, 2022.

[48] C. Boronat, V. Correcher, M. Virgos, and J. Garcia-Guinea, "Ionising radiation effect on the luminescence emission of inorganic and biogenic calcium carbonates," *Nuclear Instruments and Methods in Physics Research Section B: Beam Interactions with Materials and Atoms*, vol. 401, pp. 1–7, 2017.

[49] H. Göksu and I. Bailiff, "Luminescence dosimetry using building materials and personal objects," *Radiation protection dosimetry*, vol. 119, pp. 413–20, Feb. 2006.

[50] A. Sawakuchi, F. Rodrigues, T. Mineli, *et al.*, "Optically stimulated luminescence sensitivity of quartz for provenance analysis," *Methods and Protocols*, vol. 3, p. 6, Jan. 2020.

[51] J. Lee, H. Kim, J. Kim, *et al.*, "Thermoluminescence of chip inductors and resistors in new generation mobile phones for retrospective accident dosimetry," *Radiation Measurements*, vol. 105, pp. 26–32, 2017.

[52] A. almeida, S. Tatumi, A. Soares, and R. Barbosa, "Tl and osl analysis of natural orange calcite crystal," *Brazilian Journal of Radiation Sciences*, vol. 10, Jul. 2022.

[53] P. D. Howe, S. Dobson, and H. M. Malcolm, *Manganese and its compounds: Environmental aspects*. World Health Organization, 2004.

[54] W. H. Organization, "Manganese in drinking-water; background document for development of who guidelines for drinking-water quality," Tech. Rep., 2021.

[55] B. J. Presley, R. R. Brooks, and I. R. Kaplan, "Manganese and related elements in the interstitial water of marine sediments," *Science*, vol. 158, no. 3803, 906–910, 1967.

[56] A. L. Soldati, D. E. Jacob, P. Glatzel, J. C. Swarbrick, and J. Geck, "Element substitution by living organisms: The case of manganese in mollusc shell aragonite," *Scientific Reports*, vol. 6, no. 1, 2016.

[57] D. Mierzwa, "Chemical composition of shells of cepaea vindobonensis (férussac, 1821) (gastropoda: Pulmonata: Helicidae) from localities with different substrata," *Folia Malacologica*, vol. 19, no. 2, p. 97, Jun. 2011.

[58] S. Owuamanam and D. Cree, "Progress of bio-calcium carbonate waste eggshell and seashell fillers in polymer composites: A review," *Journal of Composites Science*, vol. 4, p. 70, Jun. 2020.

[59] R. L. WHISTLER, "Chapter 22 - chitin," in *Industrial Gums (Third Edition)*, R. L. WHISTLER and J. N. BEMILLER, Eds., Third Edition, London: Academic Press, 1993, pp. 601–604.

[60] K. SIMKISS, "Variations in the crystalline form of calcium carbonate precipitated from artificial sea water," *Nature*, vol. 201, no. 4918, 492–493, 1964.

[61] R. Roer and R. DILLAMAN, "The structure and calcification of the crustacean cuticle," *Integrative and Comparative Biology - INTEGR COMP BIOL*, vol. 24, pp. 893–909, Nov. 1984.

[62] K. Narasimhulu and J. Rao, "Epr and ir spectral studies of the sea water mussel mytilus conradinus shells," *Spectrochimica acta. Part A, Molecular and biomolecular spectroscopy*, vol. 56A, pp. 1345–53, Jul. 2000.

[63] A. Soldati, D. Jacob, B. Schöne, M. Bianchi, and A. Hajduk, "Seasonal periodicity of growth and composition in valves of diplodon chilensis patagonicus (d'orbigny, 1835)," *Journal of Molluscan Studies*, vol. 75, pp. 75–85, Oct. 2008.

[64] J. R. Dodd, "Paleoecological implications of shell mineralogy in two pelecypod species," *The Journal of Geology*, vol. 71, no. 1, 1–11, 1963.

[65] E. Bullard, I. Torres, T. Ren, O. Graeve, and K. Roy, "Shell mineralogy of a foundational marine species, mytilus californianus , over half a century in a changing ocean," *Proceedings of the National Academy of Sciences*, vol. 118, e2004769118, Jan. 2021.

[66] T. Geeza, D. Gillikin, D. Goodwin, S. Evans, T. Watters, and N. Warner, "Controls on magnesium, manganese, strontium, and barium concentrations recorded in freshwater mussel shells from ohio," *Chemical Geology*, vol. 526, Jan. 2018.

[67] S. Baden and S. Eriksson, "Role, routes and effects of manganese in crustaceans," *Oceanography and marine biology*, vol. 44, pp. 61–83, Jun. 2006.

[68] D.-M. Bordean, D. Nica, M. Harmanescu, I. Banatean-Dunea, and I. Gergen, "Soil manganese enrichment from industrial inputs: A gastropod perspective," *PloS one*, vol. 9, e85384, Jan. 2014.

[69] K. Kesavan, M. Arumugam, V. Vellathi, and B. Kumar, "Heavy metal accumulation in molluscs and sediment from uppanar estuary, southeast coast of india," *Thalassas*, vol. 29, pp. 15–21, Jan. 2013.

[70] L. Ojwang, M. Swaleh, RenisonRuwa, *et al.*, "Heavy metals bioaccumulation in edible marine bivalve mollusks of tudor creek mombasa kenya," *IOSR Journal of Environmental Science, Toxicology and Food Technology*, vol. 10, Aug. 2016.

[71] F. Nekvapil, I.-V. Ganea, A. Ciorîță, *et al.*, "Wasted biomaterials from crustaceans as a compliant natural product regarding microbiological, antibacterial properties and heavy metal content for reuse in blue bioeconomy: A preliminary study," *Materials*, vol. 14, p. 4558, Aug. 2021.

[72] C. Richardson, "Molluscs as archives of environmental change," *Oceanography and marine biology*, vol. 39, pp. 103–164, Jan. 2001.

[73] B. Berger and R. Dallinger, "Terrestrial snails as quantitative indicators of environmental metal pollution," *Environmental monitoring and assessment*, vol. 25, pp. 65–84, Mar. 1993.

[74] M. Brito Gomes, L. Oliveira, B. Cortez, *et al.*, "Epr dating of shells from malhada marsh, rio de janeiro, brazil," *Annals of Marine Science*, vol. 4, pp. 008–013, Jan. 2020.

[75] X. Sheng, J. Chen, J. Ji, and Y. Sui, "An epr study on mollusk shells from loess-paleosol sequences in the loess plateau, central china," *Geochemical Journal - GEOCHEM J*, vol. 39, pp. 61–67, Jan. 2005.

[76] J. Kónya and N. M. Nagy, "2 - basic concepts," in *Nuclear and Radiochemistry*, J. Kónya and N. M. Nagy, Eds., Oxford: Elsevier, 2012, pp. 13–26.

[77] L. Douifi, J. Raffi, P. Stocker, and F. Dole, "A point about electron paramagnetic resonance detection of irradiated foodstuffs," *Spectrochimica Acta Part A: Molecular and Biomolecular Spectroscopy*, vol. 54, no. 14, pp. 2403–2412, 1998.

[78] R. Köseoğlu and F. Köksal, "Detection of free radicals in -irradiated seasnail hard tissues by electron paramagnetic resonance," *Applied Radiation and Isotopes*, vol. 59, no. 1, pp. 73–77, 2003.

[79] S. Della Monaca, P. Fattibene, C. Boniglia, R. Gargiulo, and E. Bortolin, "Identification of irradiated oysters by epr measurements on shells," *Radiation Measurements*, vol. 46, no. 9, pp. 816–821, 2011.

[80] N. Yordanov and B. Mladenova Kattnig, "Epr studies on gamma-irradiated snails hard tissues," *Radiation Physics and Chemistry - RADIAT PHYS CHEM*, vol. 60, pp. 191–193, Feb. 2001.

[81] J. Raffi, C. Hasbany, G. Lesgards, and D. Ochin, "Esr detection of irradiated seashells," *Applied Radiation and Isotopes*, vol. 47, no. 11, pp. 1633–1636, 1996.

[82] E. M. Stewart, "The use of esr spectroscopy for the detection of irradiated crustacea with particular reference to nephrops norvegicus (norway lobster)," Ph.D. dissertation, 1993.

[83] S. Smith, N. Udomkan, P. Winotai, and Y. Chaimanee, "Electron spin resonance studies of mn2+ in freshwater snail shells," *International Journal of Modern Physics B - IJMPB*, vol. 18, pp. 3419–3428, Oct. 2004.

[84] P. Fattibene, D. Aragno, and S. Onori, "Effectiveness of chemical etching for background electron paramagnetic resonance signal reduction in tooth enamel," *Health Physics*, vol. 75, no. 5, 500–505, 1998.

[85] A. Negron, C. Raya, V. Gomez, R. Uribe, and S. Bernal, "Effects of temperature during the irradiation of calcium carbonate," *Applied Radiation and Isotopes*, vol. 111, Feb. 2016.

[86] R. Koseoglu, F. Koksal, and M. Birey, "Electron paramagnetic resonance study of defects in -irradiated marine mussel (mytilus galloprovincialis) and scallop (pecten jacobaeus) shells," *Zeitschrift für Naturforschung A*, vol. 59, Jun. 2014.

[87] D. U. Schramm, M. M. Cattani, N. L. Del Mastro, and A. M. Rossi, "Electron spin resonance (esr) of gamma-irradiated oyster shells," 1997.

[88] F. Callens, G. Vanhaelewyn, P. Matthys, and E. Boesman, "Epr of carbonate derived radicals: Applications in dosimetry, dating and detection of irradiated food," *Applied Magnetic Resonance*, vol. 14, no. 2-3, 235–254, 1998.

[89] A. Molodkov, "Esr-dating of non-marine mollusc shells," *Applied Radiation and Isotopes*, vol. 44, Feb. 1993.

[90] T. Vichaidid, U. Youngchuay, and P. Limsuwan, "Dating of aragonite fossil shell by esr for paramagnetic species assignment of mae moh basin," *Nuclear Instruments and Methods in Physics Research Section B: Beam Interactions with Materials and Atoms*, vol. 262, pp. 323–328, Sep. 2007.

[91] A. Maghraby, "Identification of irradiated crab using epr," *Radiation Measurements*, vol. 42, pp. 220 –224, Aug. 2006.

[92] A. Checa, "Physical and biological determinants of the fabrication of molluscan shell microstructures," *Frontiers in Marine Science*, vol. 5, Sep. 2018.

[93] C. Prasuna, K. Narasimhulu, N. Gopal, J. Rao, and T. Rao, "The microstructures of biomineralized surfaces: A spectroscopic study on the exoskeletons of fresh water (apple) snail, pila globosa," *Spectrochimica Acta Part A: Molecular and Biomolecular Spectroscopy*, vol. 60, no. 10, 2305–2314, 2004.

[94] J. Huang and R. Zhang, "The mineralization of molluscan shells: Some unsolved problems and special considerations," *Frontiers in Marine Science*, vol. 9, p. 874 534, Jun. 2022.

[95] F. Marin and G. Luquet, "Molluscan shell proteins," *Comptes Rendus Palevol*, vol. 3, pp. 469–492, Oct. 2004.

[96] S. Abdel Gawad, "Concentrations of heavy metals in water, sediment and mollusk gastropod, lanistes carinatus from lake manzala, egypt," Jun. 2018.

[97] S. Parveen, A. Chakraborty, D. Chanda, S. Pramanik, A. Barik, and G. Aditya, "Microstructure analysis and chemical and mechanical characterization of the shells of three freshwater snails," *ACS Omega*, Sep. 2020.

[98] J. Rech, J. Pigati, K. Springer, S. Bosch, J. Nekola, and Y. Yanes, "Oxygen isotopes in terrestrial gastropod shells track quaternary climate change in the american southwest," *Quaternary Research*, vol. 104, pp. 1–11, May 2021.

[99] D. Mierzwa-Szymkowiak, "Chemical composition and structure of the shell of cepaea vindobonensis (férussac, 1821) (gastropoda: Pulmonata: Helicidae)," *Folia Malacologica*, vol. 16, pp. 17–20, Mar. 2009.

[100] J. Leung, S. Connell, I. Nagelkerken, and B. Russell, "Impacts of near-future ocean acidification and warming on the shell mechanical and geochemical properties of gastropods from intertidal to subtidal zones," *Environmental Science Technology*, vol. 51, Oct. 2017.

[101] C. Brönmark, "Interactions between epiphytes, macrophytes and freshwater snails: A review," *Journal of Molluscan Studies*, vol. 55, May 1989.

[102] B. Speiser, "Food and feeding behaviour.," *The biology of terrestrial molluscs*, 259–288, 2001.

[103] S. Boyer, S. Wratten, A. Holyoake, J. Abdelkrim, and R. Cruickshank, "Using next-generation sequencing to analyse the diet of a highly endangered land snail (powelliphanta augusta) feeding on endemic earthworms," *PloS one*, vol. 8, e75962, Sep. 2013.

[104] D. L. Hawksworth and A. T. Bull, "Marine, freshwater, and wetlands biodiversity conservation," 2006.

[105] J. Ziętek, M. Ziomek, M. MAĆKOWIAK-DRYKA, A. Wilczyńska, S. SAJDAK, and L. Adaszek, "Determination of selected biochemical parameters of the haemolymph of free-living cepaea nemoralis (l.) snails. preliminary study," *Medycyna Weterynaryjna*, vol. 78, pp. 6679–2022, Jan. 2022.

[106] P. Williamson and R. Cameron, "Natural diet of the landsnail cepaea nemoralis," *Oikos*, vol. 27, p. 493, Jan. 1976.

[107] P. F. Brussard, "Geographic variation in north american colonies of cepaea nemoralis," *Evolution*, vol. 29, no. 3, p. 402, 1975.

[108] P. Singh and S. Gupta, "Molluscs as biomonitors of heavy metal pollution: A review," pp. 35–42, Jan. 2021.

[109] S. Yoshioka and M. Terai, "Manganese accumulation in freshwater bivalves," in *Mechanisms and Phylogeny of Mineralization in Biological Systems*, S. Suga and H. Nakahara, Eds., Tokyo: Springer Japan, 1991, pp. 321–325.

[110] B. Stewart, S. Jenkins, C. Boig, *et al.*, "Metal pollution as a potential threat to shell strength and survival in marine bivalves," *Science of The Total Environment*, vol. 755, Oct. 2020.

[111] M. Kannan, T. Muralisankar, R. Jayakumar, and C. Gandhi, "A study on structural comparisons of -chitin extracted from marine crustacean shell waste," *Carbohydrate Polymer Technologies and Applications*, vol. 2, p. 100 037, Dec. 2021.

[112] H. Nagasawa, "The crustacean cuticle: Structure, composition and mineralization," *Frontiers in bioscience (Elite edition)*, vol. 4, pp. 711–20, Jan. 2012.

[113] R. L. WHISTLER, "Chitin," *Industrial Gums*, 601–604, 1993.

[114] G. Luquet, "Biomineralizations: Insights and prospects from crustaceans," *ZooKeys*, vol. 176, pp. 103–21, Mar. 2012.

[115] C. Chou, L. Paon, J. Moffatt, and T. King, "Selection of bioindicators for monitoring marine environmental quality in the bay of fundy, atlantic canada," *Marine Pollution Bulletin*, vol. 46, no. 6, 756–762, 2003.

[116] M Zaaboub, N. Ayas, R. Ms, and M. V. Martins, "Crabs as bioindicators of trace element accumulation in mediterranean lagoon," Jan. 2018.

[117] A. Ochs, J. Shields, G. Rice, and M. Unger, "Acute and long-term manganese exposure and subsequent accumulation in relation to idiopathic blindness in the american lobster, homarus americanus," *Aquatic Toxicology*, vol. 219, p. 105 379, Dec. 2019.

[118] K. A. Keteles, "Metal partitioning among tissues and exoskeleton of palaemonetes pugio and its role in depuration and trophic transfer," Ph.D. dissertation, 2001.

[119] M. F. Desrosiers, ".gamma.-irradiated seafoods: Identification and dosimetry by electron paramagnetic resonance spectroscopy," *Journal of Agricultural and Food Chemistry*, vol. 37, no. 1, 96–100, 1989.

[120] T. Kampouris, A. Asimaki, D. Klaoudatos, A. Exadactylos, I. Karapanagiotidis, and I. Batjakas, "Nutritional quality of the european spiny lobster palinurus elephas (j.c. fabricius, 1787) (achelata, palinuridae) and the non-indigenous northern brown shrimp penaeus aztecus ives, 1891 (dendrobranchiata, penaeidae)," *Foods*, vol. 10, p. 2480, Oct. 2021.

[121] L. M. Tsang, C. Schubart, S. Ahyong, *et al.*, "Evolutionary history of true crabs (crustacea: Decapoda: Brachyura) and the origin of freshwater crabs," *Molecular biology and evolution*, vol. 48, Feb. 2014.

[122] T. Buck, G. Breed, S. Pennings, M. Chase, M. Zimmer, and T. Carefoot, "Diet choice in an omnivorous salt-marsh crab: Different food types, body size, and habitat complexity," *Journal of Experimental Marine Biology and Ecology*, vol. 292, pp. 103–116, Jul. 2003.

[123] S. Abdou and N. El-Faramawy, "Response detection of irradiated crab portions using epr technique," *Radiation Effects and Defects in Solids*, vol. 174, pp. 1–12, Apr. 2019.

[124] J. Moustakas-Verho and G. Cherepanov, "The integumental appendages of the turtle shell: An evo-devo perspective," *Journal of experimental zoology. Part B, Molecular and developmental evolution*, vol. 324, pp. 221–9, May 2015.

[125] S. J. Warburton and D. C. Jackson, "Turtle (chrysemys picta bellii) shell mineral content is altered by exposure to prolonged anoxia," *Physiological Zoology*, vol. 68, no. 5, 783–798, 1995.

[126] B. Cosentino, R. Schooley, and C. Phillips, "Wetland hydrology, area, and isolation influence occupancy and spatial turnover of the painted turtle, chrysemys picta," *Landscape Ecology*, vol. 25, pp. 1589–1600, Dec. 2010.

[127] J. Bau, A.-H. Emwas, and M. Rueping, "An overview of solid-state epr for artificial fuel reactions," *iScience*, vol. 25, p. 105 360, Oct. 2022.

[128] D. Hong and K. Lee, "Grain size effect of tooth enamel to electron paramagnetic resonance spectrum," vol. 41, pp. 200–202, Mar. 2004.

[129] C.-R. Liu, G.-M. Yin, and F. Han, "Effects of grain size on quartz esr dating of ti–li center in fluvial and lacustrine sediments," *Quaternary Geochronology*, vol. 30, Feb. 2015.

[130] M. Guardia and S. Armenta, "Multianalyte determination versus one-at-a-time methodologies," *Comprehensive Analytical Chemistry*, vol. 57, pp. 121–156, Dec. 2011.

[131] C. Schoenfeld and T. Michel, "An open-vessel microwave digestion system for preparing large samples of volatile or heterogeneous materials," *American laboratory*, vol. 38, pp. 14–16, Feb. 2006.

[132] L. Zhu, C. Xiao, X. Teng, M. Xu, and L. Yin, "An inductively coupled plasma mass spectrometry method for the determination of elemental impurities in calcium carbonate mineral medicine," *Spectrochimica Acta Part B: Atomic Spectroscopy*, vol. 192, p. 106 429, Apr. 2022.

[133] I. Rodushkin, T. Ruth, and Huhtasaari, "Comparison of two digestion methods for elemental determinations in plant material by icp techniques," *Analytica Chimica Acta*, vol. 378, pp. 191–200, Jan. 1999.

[134] B. Schöne, Z. Zhang, D. Gillikin, *et al.*, "Effect of organic matrices on the determination of minor elements (mg, sr) and mg/ca and sr/ca ratios of aragonitic bivalve shells (arctica islandica) – comparison of icp-oes and la-icp-ms data," *Geochemical journal GJ*, vol. 44, pp. 23–37, Jan. 2010.

[135] N. Oleszczuk, J. Castro, M. Silva, M. D. G. Korn, B. Welz, and M. Vale, "Method development for the determination of manganese, cobalt and copper in green coffee comparing direct solid sampling electrothermal atomic absorption spectrometry and inductively coupled plasma optical emission spectrometry," *Talanta*, vol. 73, pp. 862–9, Nov. 2007.

[136] A. Mohammad, A. Thamer, M. Al-Hamdany, K. Al Azzam, and G. Talk, "Characterization and screening of metals, metalloids and biomarkers in crude oil by icp-ms/oes, and gc-ms techniques after digestion by microwave-induced combustion," *Biomedical Chromatography*, vol. 33, e4481, Jan. 2019.

[137] M. A. Farrukh, "Atomic absorption spectroscopy," 2012.

[138] S. Mohammadi, T. Shamspur, and Y. Baghelani, "Determination of copper, nickel, manganese and cadmium ions in aqueous samples by flame atomic absorption spectrometry after simultaneous coprecipitation with co(oh)2," *Arabian Journal of Chemistry*, vol. 5, Dec. 2014.

[139] S. Wilschefski and M. Baxter, "Inductively coupled plasma mass spectrometry: Introduction to analytical aspects," *The Clinical biochemist. Reviews*, vol. 40, pp. 115–133, Aug. 2019.

[140] T. Nham, "Typical detection limits for an icp-ms," *American laboratory*, vol. 30, 17A–17D, Aug. 1998.

[141] L. A. Hamidatou, "Overview of neutron activation analysis," *Advanced Technologies and Applications of Neutron Activation Analysis*, 2019.

[142] M. Nandy, "Neutron activation analysis: Application in geology and medicine," *Advanced Technologies and Applications of Neutron Activation Analysis*, 2019.

[143] Y. Liu, D. Rolle-McFarland, F. Mostafaei, *et al.*, "In vivo neutron activation analysis of bone manganese in workers," *Physiological Measurement*, vol. 39, Jan. 2018.

[144] IAEA, *In situ applications of X ray fluorescence techniques*. 2005.

[145] B. Beckhoff, *Handbook of practical X-ray fluorescence analysis*. Springer, 2006.

[146] A. Specht, X. Zhang, A. Young, *et al.*, "Validation of in vivo toenail measurements of manganese and mercury using a portable x-ray fluorescence device," *Journal of Exposure Science Environmental Epidemiology*, vol. 32, pp. 1–7, May 2022.

[147] D. Barr, S. S. Eaton, and G. R. Eaton, *Workshop on Quantitative EPR*. 2008.

[148] E. H. Haskell, "Retrospective dosimetry using epr and tl techniques: A status report," 1996.

[149] IAEA, "Calibration of reference dosimeters for external beam radiotherapy," Tech. Rep., 2009.

[150] W. L. McLaughlin, "Esr dosimetry," *Radiation Protection Dosimetry*, vol. 47, 255–262, 1993.

[151] R. Chu, W. McLaughlin, A. Miller, and P. Sharpe, "5. dosimetry systems," *Journal of the ICRU*, vol. 8, pp. 29–70, Dec. 2008.

[152] A. Hassan, M. Tzivaki, L. Felner, and E. Waller, "A practical method for epr dosimetry using alanine powder," *Health Physics*, May 2022.

[153] L. Ghimire and E. Waller, "Methodology and instrumentation for electron paramagnetic resonance dosimetry with tooth enamel," *Journal of Nuclear Engineering and Radiation Science*, vol. 9, no. 1, 2022.

[154] P. Levêque, Q. Godechal, A. Bol, F. Trompier, and B. Gallez, "X-band epr imaging as a tool for gradient dose reconstruction in irradiated bones," *Medical Physics*, vol. 36, no. 9Part1, 4223–4229, 2009.

[155] H. B. Stenzel, "Aragonite and calcite as constituents of adult oyster shells," *Science*, vol. 142, no. 3589, pp. 232–233, 1963.

[156] J. Murphy, C. Schneider, L. Mailänder, Q. Lepillet, K. Hawboldt, and F. Kerton, "Wealth from waste: Blue mussels (mylitus edulis) offer up a sustainable source of natural and synthetic nacre," *Green Chemistry*, vol. 21, Jun. 2019.

[157] H. Findlay, H. Wood, M. Kendall, J. Spicer, R. Twitchett, and S. Widdicombe, "Calcification, a physiological process to be considered in the context of the whole organism," *Biogeosciences Discussions*, vol. 6, Feb. 2009.

[158] F. P. Andreasson, B. Schmitz, and E. Jonsson, "Surface-water seasonality from stable isotope profiles of littorina littorea shells: Implications for paleoenvironmental reconstructions of coastal areas," *PALAIOS*, vol. 14, no. 3, p. 273, 1999.

[159] R. Filgueira, L. Peteiro, U. Labarta, and M.-J. Fernández-Reiriz, "Assessment of spat collector ropes in galician mussel farming," *Aquacultural Engineering*, vol. 37, pp. 195–201, Nov. 2007.

[160] M. Kwan, L. Chan, and Y. De Lafontaine, "Metal contamination in zebra mussels (dreissena polymorpha) along the st. lawrence river," *Environmental monitoring and assessment*, vol. 88, pp. 193–219, Oct. 2003.

[161] M. Vidotto, T. Grego, B. Petrović, *et al.*, "A comparative epr study of non-substituted and mg-substituted hydroxyapatite behaviour in model media and during accelerated ageing," *Crystals*, vol. 12, p. 297, Feb. 2022.